RADIATION EFFECTS IN CRYSTALLINE SiO_2: STRUCTURE OF THE E" CENTERS

By

MAHENDRAKUMAR G. JANI

Bachelor of Science
Gujarat University
Ahmedabad, India
January, 1976

Master of Science
Oklahoma State University
Stillwater, Oklahoma
1979

Submitted to the Faculty of the Graduate College
of the Oklahoma State University
in partial fulfillment of the requirements
for the Degree of
DOCTOR OF PHILOSOPHY
May, 1982

DEDICATION

to

MY PARENTS, RAHUL, PRAGNA, SHAILESH

AND MANDAKINI

RADIATION EFFECTS IN CRYSTALLINE SiO_2: STRUCTURE OF THE E" CENTERS

Thesis Approved:

Larry E. Halliburton
Thesis Adviser

W. A. Sibley

[signature]

[signature]

Norman N. Durham
Dean of the Graduate College

ACKNOWLEDGMENTS

Special thanks are extended to Dr. Larry E. Halliburton for his guidance, support and friendship through all phases of my graduate study. I wish to thank Dr. W. A. Sibley, Dr. E. E. Kohnke, and Dr. M. G. Rockley for serving on my committee and providing helpful suggestions. The discussions and help from Dr. J. J. Martin, and Dr. R. Bossoli are also gratefully appreciated.

I wish to thank Mr. Heinz Hall and the staff of the Instrument Shop for their help. The excellent work done by Mrs. Janet Sallee in typing this thesis is gratefully appreciated. I also wish to thank Ms. Sauwanee Senusu for her love, affection, and moral support.

Financial support from the Physics Department at Oklahoma State University and the U.S. Air Force under Contract Number F 19628-77-C-0171 is gratefully acknowledged. Appreciation is also expressed to Toyo Communications Company for kindly providing the quartz samples used in this study.

TABLE OF CONTENTS

LIST OF TABLES

LIST OF FIGURES

CHAPTER I

INTRODUCTION

Background

Radiation-induced defects in insulating (i.e., wide band gap) materials have been widely studied in the last fifty years. Much of the interest has arisen because of their fundamental properties and also because of their technological potential. Optical and magnetic resonance techniques have been primarily used in these investigations and a number of sophisticated combinations of these techniques have evolved. Point defects in insulators are generally known as color centers because they usually have two or more electronic states lying within the band gap between which optical transitions are possible. A vast amount of research has been done on color centers in alkali halides and much of this work has been described in depth by Fowler (1). A similar large amount of work on defects in alkaline-earth oxides has been reviewed by Henderson and Wertz (2).

In more recent years, researchers have focused their attention on piezoelectric materials such as quartz, $LiNbO_3$, $LiTaO_3$, and berlinite ($AlPO_4$) because of the many applications in precision frequency control and surface acoustic wave (SAW) devices. Since many of these latter materials have complex crystal structures, a much wider variety of defect configurations are possible and, as a result, it is very difficult

to determine precise models for defects or to disentangle the observed kinetic behavior of defects. However, because of the vast amount of work previously done on point defects in the simpler materials such as alkali halides and alkaline-earth oxides, researchers today have a base of information which allows progress to be made more rapidly in the studies of the more complex, but more useful, materials.

Since its discovery by E. Zavoisky in 1945 (3), the electron spin resonance (ESR) technique has been widely used in different branches of the physical and biological sciences. In solid state physics, ESR is a very powerful technique making it possible to obtain an exact knowledge of the electronic structure and the local environment of a defect. Also, it has been used to study the influence of external stress and the effects of electric fields upon the properties of color centers and their interactions, and it can measure concentrations of these defects.

Magnetic resonance is an experimental technique that can be applied to the study of materials containing permanent magnetic dipole moments. Both electrons and nuclei have permanent magnetic moments. Let's consider a spin system consisting of non-interacting electron spins. The magnetic moment $\vec{\mu}$ of an electron is related to the spin angular momentum $\vec{S}$ as follows

$$\vec{\mu} = -g_e \beta \vec{S}$$

where β is the Bohr magneton ($\beta = \frac{e\hbar}{2mc} = 9.2741 \times 10^{-21}$ erg/gauss) and g_e is the free spin g factor. The energy of a magnetic dipole of moment $\vec{\mu}$ in a magnetic field $\vec{H}$ is

$$W = -\vec{\mu} \cdot \vec{H} .$$

From the above two equations, the Hamiltonian can be written as

$$\mathcal{H} = g_e \beta \vec{S} \cdot \vec{H} .$$

If the electron spin is quantized along the direction of the magnetic field (taken to be Z) then

$$\mathcal{H} = g_e \beta H \hat{S}_z$$

where $\hat{S}_z$ is a spin operator.

The energy is given by

$$E = \langle M_s | \mathcal{H} | M_s \rangle$$

which reduces to the following

$$E = g_e \beta H M_s .$$

There are two values for M_s, +1/2 and -1/2. This gives us two energy levels

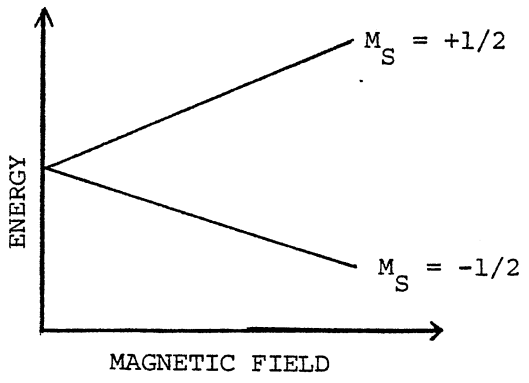

The separation in energy is

$$\Delta E = E_{+1/2} - E_{-1/2} = g_e \beta H$$

Transitions between the two energy levels can be induced by an electromagnetic field of the appropriate frequency ν, if the photon energy $h\nu$ matches the energy-level separation ΔE. Then

$$h\nu = g\beta H_r$$

where H_r is the magnetic field at which the resonance condition is met. Further details of the magnetic resonance techniques have been well reviewed in the literature (4-7).

Defects in Quartz

Structural and radiation-induced defects in quartz have been studied extensively over the last twenty-five years because of the wide application of this material in precision frequency control devices; one example being in crystal-controlled oscillators in communication satellites that are continuously bombarded by high-energy radiation. It is now well-known that defects in the quartz crystals play an important role in determining the performance of these oscillators. One of the first radiation-induced defects in quartz to be studied by ESR was reported by Weeks (8) in 1956. It is an oxygen-vacancy-associated trapped electron center and is known as the E_1' center. Since the mid-1950s, many people have reported studies of defects in quartz. Some of the more pertinent of these studies are discussed briefly in the following paragraphs.

Weeks and Nelson (9) investigated radiation-induced defects in quartz and fused silica using optical and magnetic resonance techniques.

Evidence was presented showing a correlation of the observed optical absorption band at 210 nm with the E_1' center and a correlation of the 230 nm band with the E_2' center, in both quartz and fused silica. For crystalline quartz it was observed that the E_2' band was more easily produced than the E_1' band, and the E_2' band could be bleached easily at 78K using an ultraviolet lamp. Heating treatments between 250-300^{o}C revealed an increase in the E_1' optical absorption band and the ESR absorption associated with this center. In contrast to the behaviour of crystalline quartz, the E_1' optical absorption band in high purity fused silica seemed to decrease in intensity upon heating above the room temperature. Another optical absorption band at 260 nm was observed in irradiated fused silica, which annealed in the same manner as the E_1' optical band. This band was not associated with any of the defects observed by ESR. Models for the E_1', E_2', and E_1'' centers were proposed. [The E" notation used in this dissertation is different from their notation.] These workers have suggested that the E_1' center is an oxygen vacancy with one trapped electron at the vacancy and the E_1'' center is an oxygen vacancy with two electrons (S=O). They proposed that the E_2' center is an oxygen vacancy with a trapped electron in an unsaturated silicon bond.

Silsbee (10) reported a detailed ESR study of the E_1' center which followed the initial work by Weeks (8). Neutron irradiation of the quartz crystals at room temperature was used to produce the E_1' centers. The optical rotation and etch patterns indicated that the crystal was left-handed quartz. The observed ESR spectrum was interpreted as being due to a single unpaired electron interacting strongly with one ^{29}Si nucleus and weakly with two other ^{29}Si nuclei. The $\vec{g}$, $\vec{A}_{^{29}Si}$

(strong hfs) and $\vec{A}_{^{29}Si}$ (I,II) (weak hfs) matrix parameters were obtained. On the basis of experimental results and calculations, it was suggested that possibly the E_1' center is an oxygen vacancy with the electron in a nonbonding sp^3 hybrid orbital localized primarily on one silicon. But this model could not explain the observed weak hyperfine ESR spectrum.

Further work on the E_1' center has been reported by Feigl et al. (11) and Yip and Fowler (12). A linear combination of localized orbital-molecular orbital (LCLO-MO) cluster method was used to calculate the electronic structure of the E_1' center in α-quartz. As a result of their calculations, it was suggested that the E_1' center is an O^- vacancy with a highly asymetric relaxation of the two silicons adjacent to the O^- vacancy. The unpaired electron is strongly localized in the nonbonding sp^3 hybrid orbital centered on the closest silicon and oriented along the Si-O short bond direction toward the oxygen vacancy as shown in Figure 1.

The E_2' center in α-quartz was studied in detail by Weeks (13) using ESR. The observed ESR spectrum when the magnetic field is along the c-axis consisted of two primary lines separated by 0.4G at 300K. From the ESR measurements at 24 GHz it was decided that the two-line spectrum was due to an unpaired electron (S = 1/2) at the defect interacting with a single 100% abundant nuclear spin I = 1/2. In addition to the primary lines, additional pairs of weak lines, one pair at high field and one pair at low field, separated by 412.0G were observed in the c-axis spectrum. The separation within these pairs of lines was the same as the primary doublet, 0.4G. The ratio of the intensities of each of these lines to each component of the primary lines was 0.03. No additional weak pairs of lines with 7G and 8G splittings were observed for the E_2'

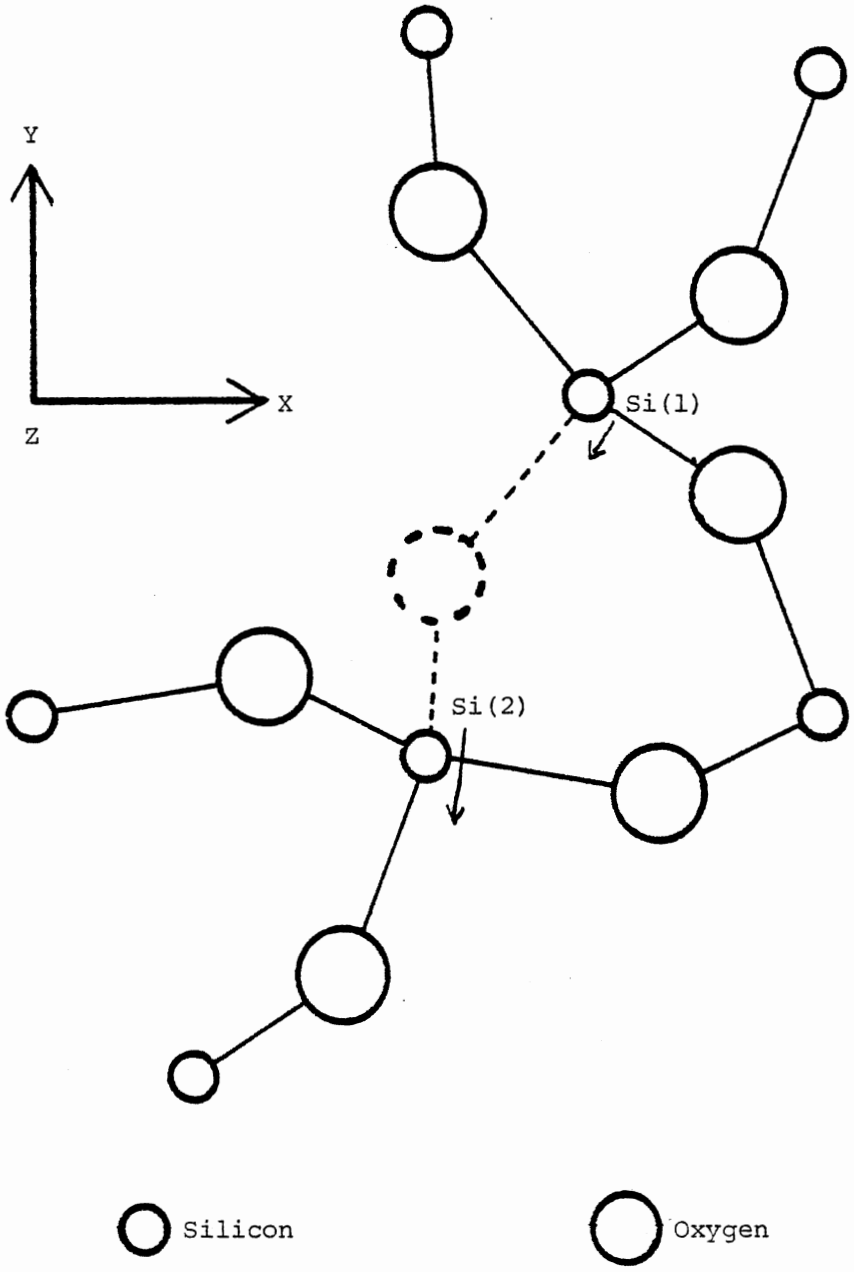

Figure 1. Proposed Model for the E_1' Center (Yip and Fowler Ref). The Arrows Indicate the Assymetric Relaxation of the Two Silicon Positions. The Unpaired Electron is Located on Si(O) (i.e., the Short-Bond Side)

center, in contrast to the E_1' center (10). From the comparison of the crystals grown in H_2O with one grown in D_2O, it was determined that the doublet structure of the E_2' center is due to a hyperfine interaction of the unpaired electron with a nearby proton. The weak (0.03 intensity), but widely separated, pairs of hyperfine interactions were interpreted as arising from an interaction of the defect electron with a ^{29}Si nucleus. Since only one pair of such lines and no additional weak interactions were observed, Weeks proposed that the E_2' center is an electron trapped in a nonbonding sp^3 hybrid orbital on a silicon with an oxygen and the next neighbor silicon missing, as shown in Figure 2. The excess charge due to the remaining oxygen ions around the silicon vacancy are compensated by the monovalent and divalent cation impurities present in the crystal. The nearby proton associated with the E_2' center is one of these impurities. Considering the weak hyperfine interaction of the E_1' center with two nearby ^{29}Si, the proposed model by Weeks is an oxygen divacancy shown in Figure 2. In this model the weak hyperfine interaction arises from the two nearest-neighbor silicons through the oxygen vacancies. Such a defect could trap four or two electrons in a nonparamagnetic state, and such a nonparamagnetic state has been observed indirectly according to Weeks and Nelson (9).

In support of the models proposed by Weeks (13) for the E_1' and E_2' center, Castle et al. (14), measured the spin-lattice relaxation time T_1 by the inversion-recovery technique for these centers over a wide temperature range. The data were interpreted in terms of cross relaxation, direct processes, and Raman processes. The theory of spin-lattice relaxation was extended to account for the modification of strain at a defect site due to a lattice wave. A detailed comparison

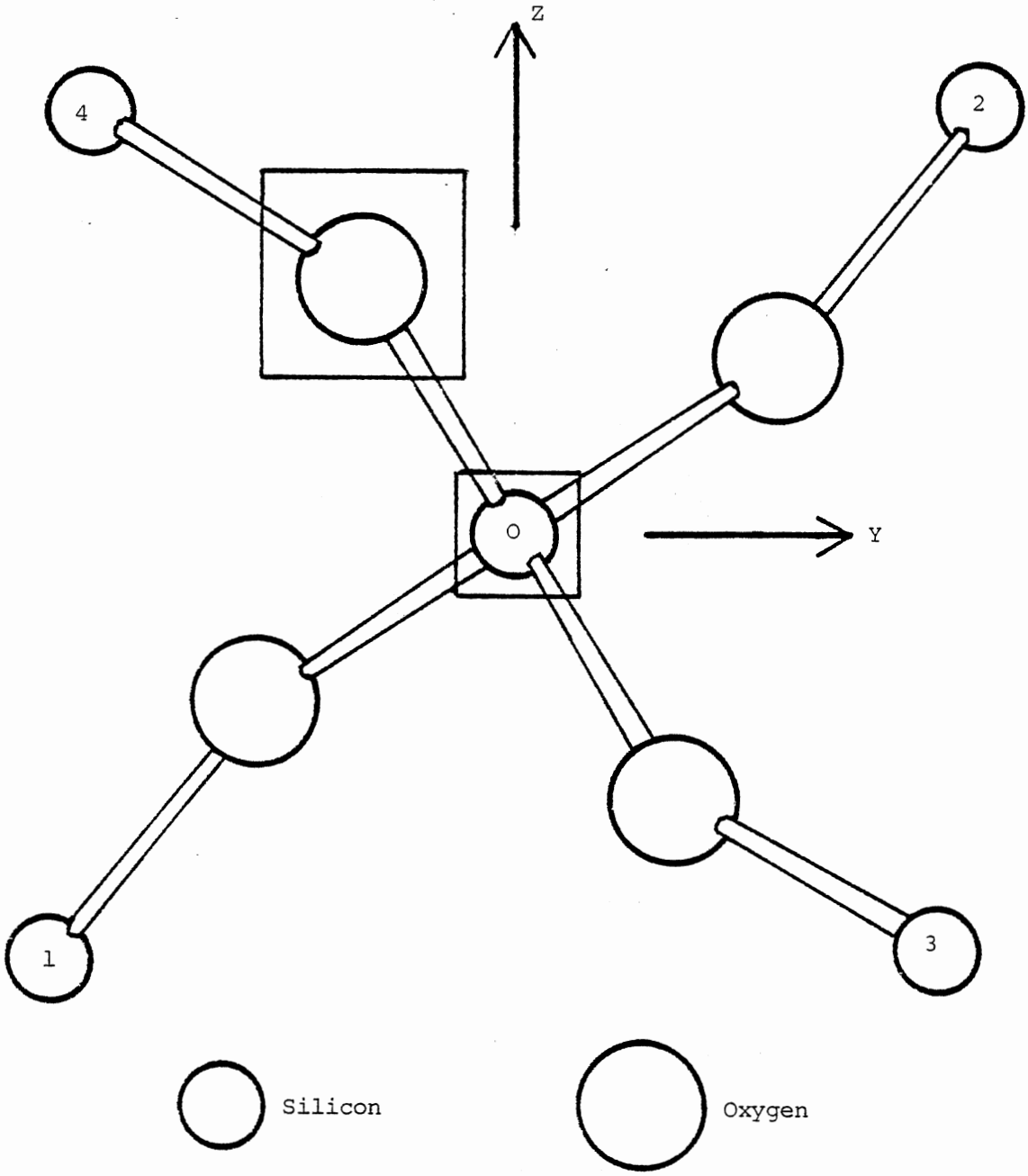

Proposed model for the E_2' center. Location of nearby proton is not specified. The unpaired electron is located on Si(4).

Figure 2. Models for the E_1' and E_2' Center as Proposed by R. A. Weeks (13)

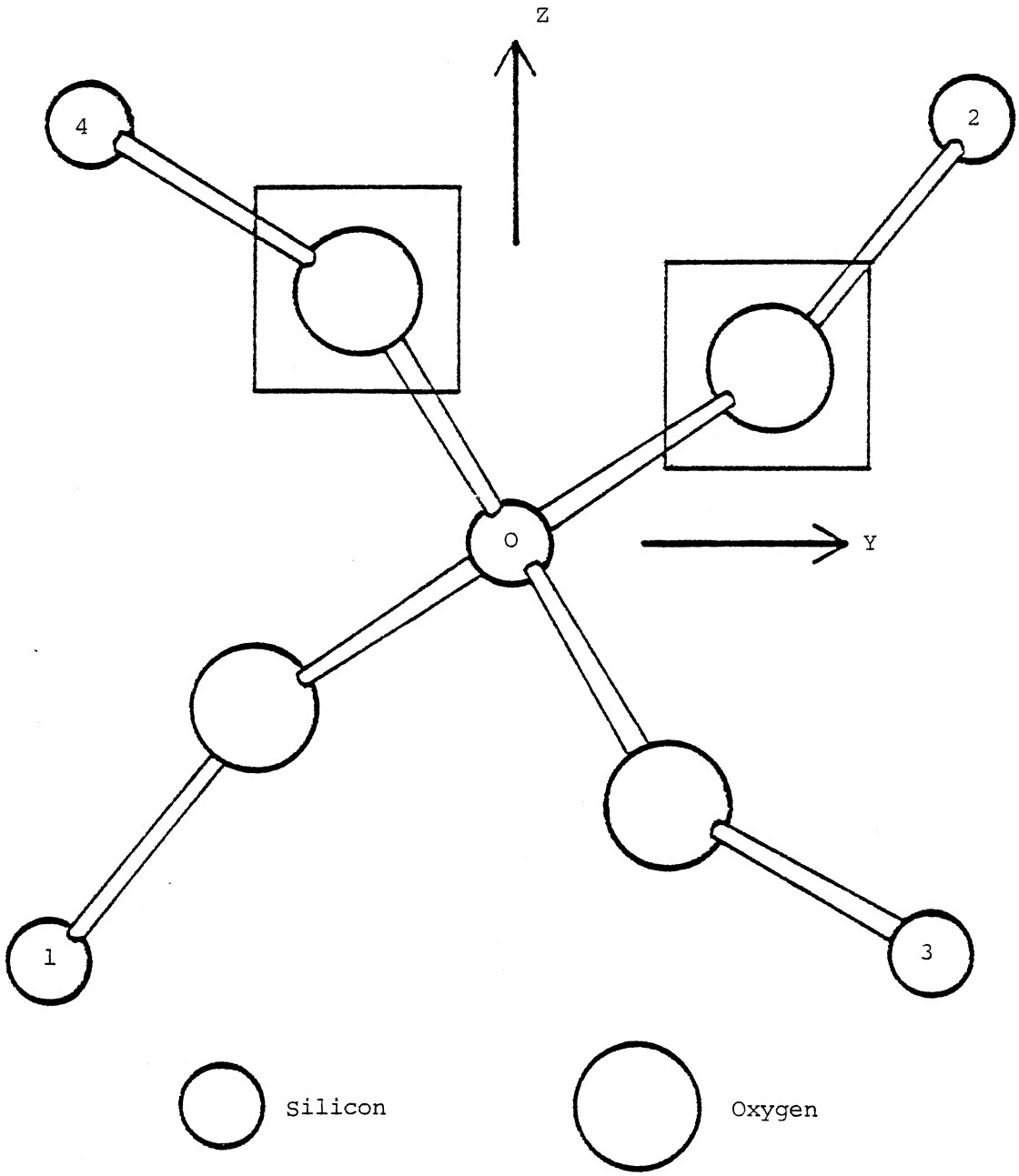

Proposed model for the E_1' center. The unpaired electron is located on Si(O).

Figure 2 (Continued)

with theory of the relaxation rates observed for the two E' centers suggested that each center had two characteristic frequencies or temperatures θ_i. For the E_2' center, one of these was ascribed to the vibration of a neighboring impurity ion, probably a proton. The authors proposed that the E_1' center is an electron trapped at a silicon ion located in an oxygen divacancy, which is similar to the model proposed by Weeks (13).

Feigl and Anderson (15) used ESR to study paramagnetic defects produced by low energy ionizing radiation in crystalline quartz doped with germanium. Their analysis indicated that these defects are similar to the E_1' and E_2' centers in pure crystalline quartz with a germanium ion substituted for the central silicon ion in the E'-defect structures. Two distinct but similar spectra of the E_1'-type associated with Ge impurities were observed, each characteristic of a specific irradiation and heating treatment. In contrast to the proposed divacancy model of Weeks (8), a single-oxygen-vacancy model for the E_1'(Ge) center was proposed where the unpaired electron occupies a non-bonding sp^3 orbital strongly localized on the Ge impurity.

Another oxygen-vacancy center, the E_4' center, first reported by Weeks and Nelson (9), has been studied in more detail by Isoya et al. (16) using ESR. Weeks and Nelson (5) suggested that the ESR spectrum of this center, which consisted of four equally spaced and equally lines, was a result of an electron (S = 1/2) interacting with an alkali ion (I = 3/2) present in the crystal as a charge compensating impurity. Isoya et al. (16) observed that for low microwave power levels, the intensity ratio of the outer pair of lines to the inner pair is approximately 1.2:1 at 9.85 GHz. This is not consistent with an S = 1/2 and

I = 3/2 system. In a detailed angular dependence study of the E_4' spectrum at X-band, it was observed that as the separation of the inner pairs of lines decreases, the intensities of these inner lines increases and remain equal while the intensities of the outer pair of lines correspondingly decrease and remain equal. Further, as the splitting between the inner pair of lines approached zero, the outer pairs of lines were separated by 10.5G, which is very nearly twice the proton Larmor frequency. Therefore, they concluded that the E_4' center has S = 1/2 and the hyperfine structure arises from interaction with a proton (I = 1/2) in a situation permitting observation of all $2S(2I+1)^2$ possible ESR transitions. The near equality of the amplitudes and spacings of the four primary absorption lines observed at X-band were not found when the spectrum was taken at 20.4 GHz (K-band) with the magnetic field parallel to the c-axis. Also, to a first-order approximation, the separation of the outer pair of lines scaled with the magnetic field and thus with the proton Larmor frequency. This additional work at K-band confirmed their conclusion that the E_4' center is an S = 1/2, I = 1/2 spin system. The spin Hamiltonian parameter matrices $\vec{g}$, $\vec{A}_{1H}$, $\vec{A}_{^{29}Si}$ (1,2) have been measured. A proposed model of the E_4' center, consisting of an O^- vacancy between Si(1) and Si(2) with a hydride ion bonded to Si(1), is shown in Figure 3. Ab initio SCF-MO calculations for a 15-atom cluster using the Gaussian 70 quantum chemistry computer program allowed them to obtain the minimum energy configuration for this cluster. The results of this calculation supported the model and gave good agreement with the experimental ESR data.

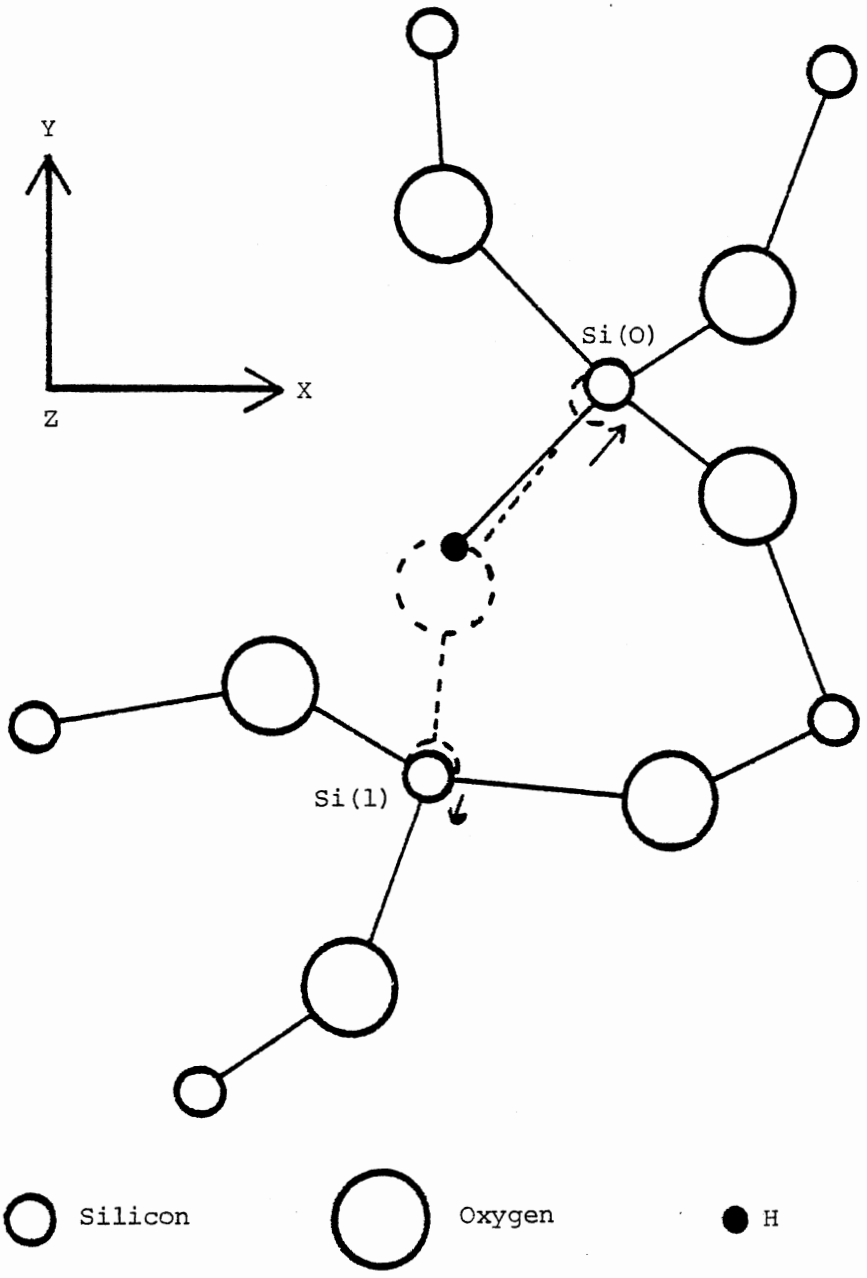

Figure 3. Model for the E_4' Center as Proposed by Isoya et al. (16). The Unpaired Electron is Unequally Shared Between Si(O) and Si(1)

Present Study

Additional new oxygen-vacancy centers, other than the E_1', E_2' and E_4' centers, have been observed in α-quartz following electron irradiation at room temperature. In the past, lengthy electron irradiations at room temperature had raised the sample temperature during the process and thus thermally annealed these new defects as soon as they were formed. Reduction of radiation times minimized the sample heating effects and allowed the new defects to be monitored in subsequent ESR measurements. After recognizing the heating problem during irradiations, the samples were irradiated at $0^{\circ}C$ by immersing them in ice water.

These three new centers, labeled as E_1'', E_2'', and E_3'' centers, were observed along with the E_2' and E_4' centers. The ESR linewidths for these centers are 0.05 G. The c-axis doublet separations for the E_1'', E_2'' and E_3'' centers are 5.00 G, 11.00 G and 17.87 G, respectively. Initial efforts were concentrated on the most intense E_1'' center spectrum. Preliminary angular dependence showed that the doublet separation varied from approximately 5.00 G to 192.00 G. Such a large angular dependence of the splitting effectively eliminated the proton as a cause of the splitting. A half-field line, characteristic of S = 1 spin systems, was observed for this center. The double primes represent the number of unpaired electrons in the centers, in contrast to the double primes denoting a diamagnetic center as proposed by Weeks and Nelson (9). Centers similar to the present E" defects have been reported by Weeks and Abraham (17,18) and Solntsev et al. (19). However, complete analyses were not presented in the above three-referenced papers.

In this study, an analysis of the main line spectra for the E_1''

and E_3'' centers has been presented along with an analysis of the hyperfine interactions for the E_1'' center. From the parameters obtained for the $\vec{g}$, $\vec{D}$ and $\vec{A}$ matrices, models will be proposed for the E_1'' and E_3'' centers.

CHAPTER II

EXPERIMENTAL PROCEDURE

All the ESR spectra reported in this dissertation were obtained using a Varian 4502 ESR spectrometer. The block diagram of this homodyne X-band (9-10 GHz) spectrometer is shown in Figure 4.

Microwave power was supplied by a VA153C klystron and the microwave frequency was stabilized by an automatic frequency control system in which the klystron was locked to the sample cavity. This AFC used 10 kHz frequency modulation of the klystron, via the reflector voltage, to create an error signal. A home-built microwave bridge having both a bias and sample arm was substituted for the less-versatile Varian bridge. The sample arm contained a precision attenuator (0-60 db) to control the level of microwave power incident on the sample. The bias arm contained a phase shifter and an attenuator to vary the detector bias. A self-locking HP 5340A frequency counter was used to measure the microwave frequency.

A home-made TE_{102} rectangular cavity was used to measure the angular dependence of the main-line spectra, whereas a V-4531 rectangular cavity was used for the hyperfine spectra measurements. The static magnetic field was amplitude modulated at 100 kHz, with the modulation coils mounted on the outside of the TE_{102} home-made rectangular cavity and within the wall of the Varian cavity. A GaAs FET solid state microwave amplifier (Narda N62445-37) was incorporated in the sample arm to

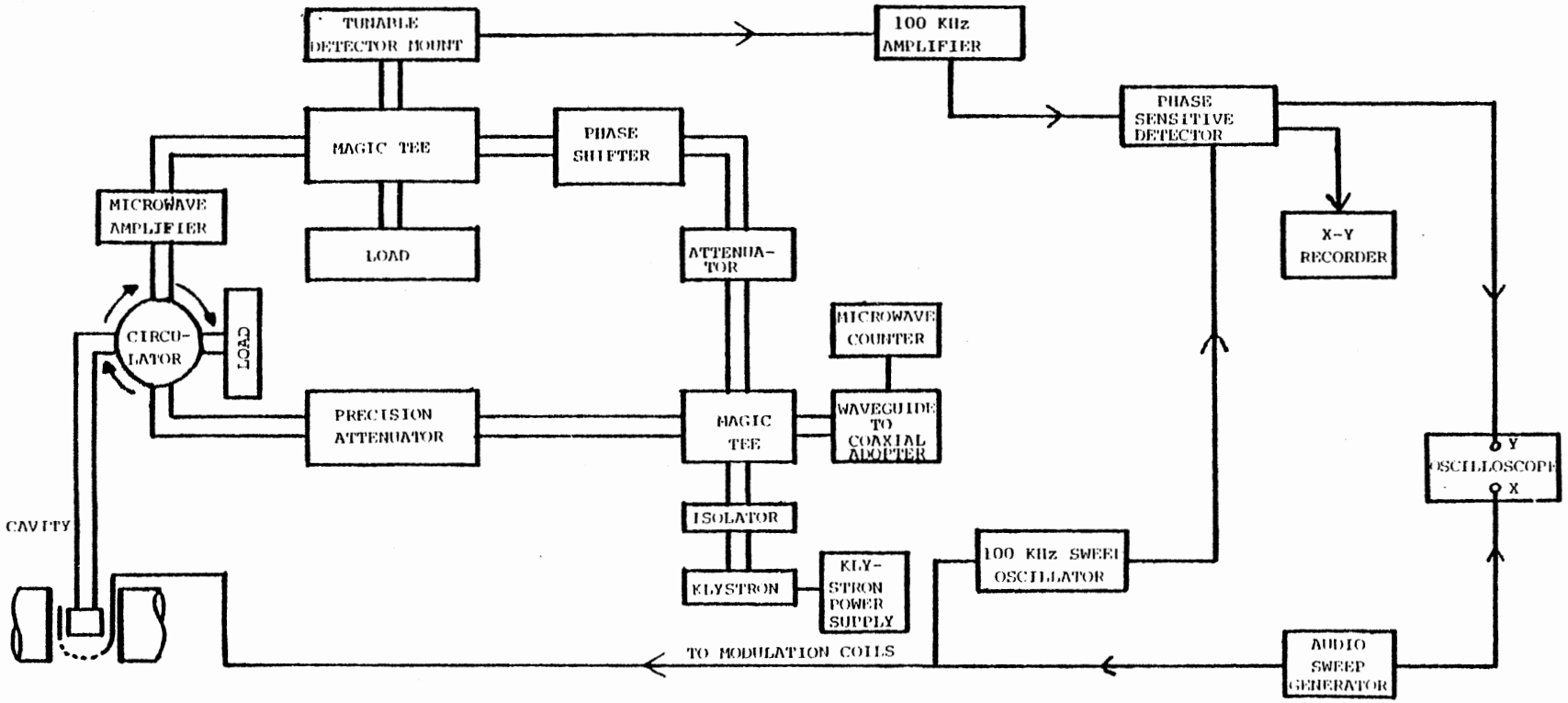

Figure 4. Block Diagram of the ESR Spectrometer

increase sensitivity especially at lower microwave power. The output from the amplifier was detected using a properly-biased low noise Schottky barrier diode (MA40075). This resulting signal from the diode was then amplified and fed to a phase-sensitive detector. The output from the phase-sensitive detector was fed to an oscilloscope and to a Houston Instruments (Model 2000) x-y recorder.

A Varian 12-inch fieldial-regulated electromagnet was used to produce the static magnetic field. Stabilization of the magnetic field was achieved by use of a Hall probe, mounted on one of the pole caps, and its associated error-feedback circuitry. The Hall probe supplied a signal proportional to the magnetic field, which was compared to a reference in order to obtain an error signal. This error signal was then used to adjust the magnet current and maintain a fixed magnetic field. All the magnetic field values reported in this dissertation were measured using a self-tracking Varian E-500 digital Gaussmeter.

Samples used in this investigation were obtained from Toyo Communications Company and from Western Electric and all were unswept. The angular dependence of the main ESR spectra for the E_1'' and E_3'' centers were measured using sample SQA-10(2.1x8.7x25.0 mm^3), an X-plate cut from a pure Z growth bar of Toyo Supreme Q quartz. The ^{29}Si hyperfine angular dependence data for the E_1'' center were obtained from Sample WEA-1, a Z-plate (2.72x10x13 mm^3) cut from the X-growth region of a Western Electric synthetic quartz stone.

Crystal Structure

There are three well-known polymorphic crystalline forms of silica: Quartz, Tridymite and Cristobalite (20). Quartz is the most common and

important of these three forms of silica. The structure of all forms of crystalline silica consists of SiO_4 tetrahedra sharing each of their corners with other tetrahedra in a continuous three-dimensional network. Quartz occurs in two distinct forms, a low-temperature form called low-quartz (or α-quartz) and a high temperature form called high-quartz (or β-quartz). The transition from one form to the other occurs at about 846K and can take place reversibly; although cooling through the α-β transition temperature nearly always results in an electrically twinned crystal. Both high and low quartz can exist in two enantiamorphous forms, right-handed and left-handed crystals, which are mirror images of one another.

Quartz has a hexagonal unit cell which consists of 3 formulas with $a_o = 4.9157\text{Å}$ and $Co = 5.406\text{Å}$ (21). The space group for right-handed quartz is $P3_221$. Symmetry elements for quartz consist of a threefold axis ($\vec{c}$) and three twofold axes ($\vec{a}_1$,$\vec{a}_2$ and $\vec{a}_3$). A projection of right-handed α-quartz in a plane perpendicular to the c-axis is shown in Figure 5. The crystallographic coordinate system is formed from two axes $\vec{a}_1$ and $\vec{a}_2$, making an angle of 120° with each other, and a third axis $\vec{c}$.

The atomic position coordinates are evaluated in terms of these three axes ($\vec{a}_1$, $\vec{a}_2$, $\vec{c}$) by Wyckoff (22) using fractions of the unit cell dimensions.

Si1:$(\bar{u},\bar{u},1/3)$ Si2:(u,o,o) Si3:(o,u,2/3) O1:(x,y,z)

O2:$(y-x,\bar{x},z+1/3)$ O3:$(\bar{y},x-y,z+2/3)$ O4:$(x-y,\bar{y},\bar{z})$

O5:(y,x,2/3-z) O6:$(\bar{x},y-x,1/3-z)$

The position parameters x,y,z and u at room temperature have been reported by Lepage and Donnay (23) using cell dimensions measured at 298K

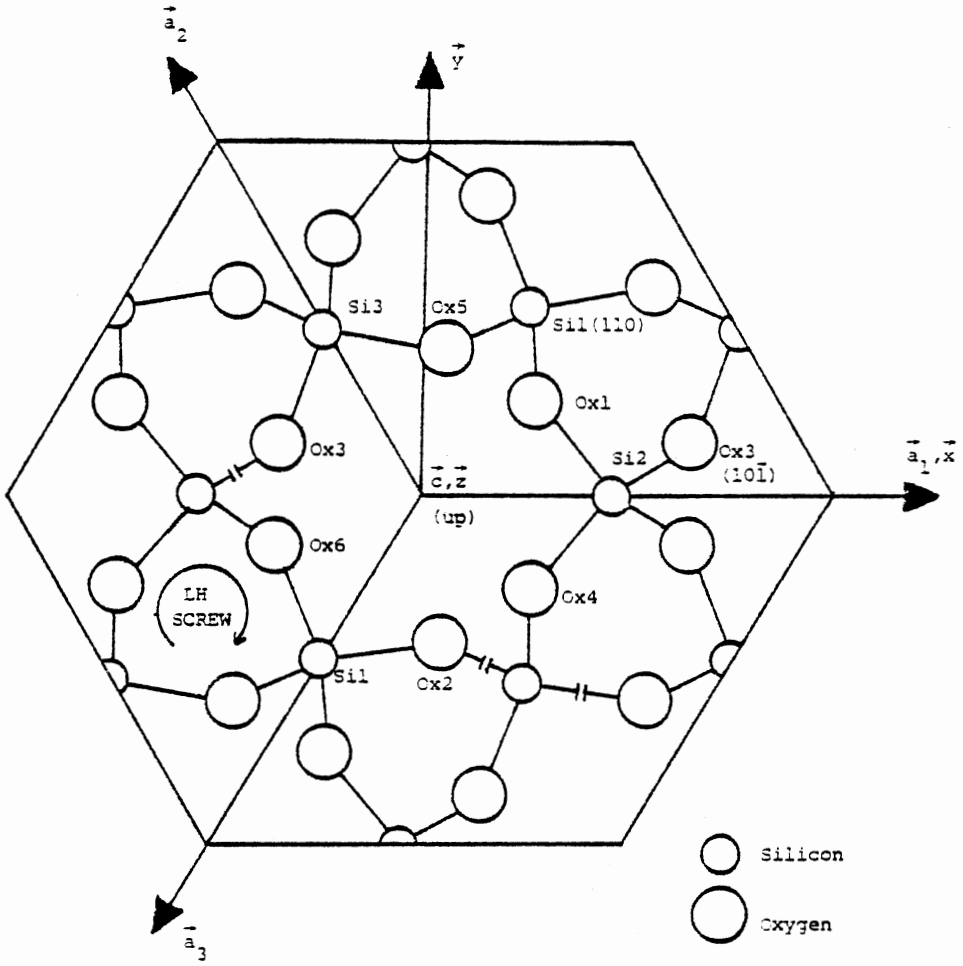

Figure 5. Projection of Atomic Positions in Right Quartz Onto [001] Plane, Showing Co-ordinate System Conventions Used in This Dissertation. Wyckoff's Atomic Positions are Labeled

by Cohen and Summer (21). These parameters are as follows.

$$x = 0.41372\mathring{A} \qquad y = 0.26769\mathring{A}, \qquad z = 0.11880\mathring{A}$$

and

$$u = 0.46981\mathring{A}$$

Quartz exhibits a piezoelectric effect and the positive end of the x-axis (or a-axis) is defined as the side developing a negative charge during compression of the crystal along that axis (24). A projection of quartz on the plane perpendicular to the x-axis is shown in Figure 6. One can generate every atomic position in the quartz lattice by lattice translations along $\vec{a}_1$, $\vec{a}_2$ and $\vec{c}$ from one of the nine positions specified by Wyckoff. The nomeclature used to specify any atom position in the lattice is A(i,j,k), where A represents one of the Wyckoff atoms and i,j and k are integers representing the numbers of lattice translation along $\vec{a}_1$, $\vec{a}_2$ and $\vec{c}$, respectively.

The SiO_4 groups which form the quartz lattice are not perfect tetrahedra and local symmetry at a silicon site is C_2. Thus, there are two types of Si-O bonds, slightly different in bond lengths from each other. The equilibrium bond lengths for these two types are $1.611\mathring{A}$ and $1.607\mathring{A}$ at room temperature (23). Consequently, when considering the environment of a particular silicon the neighboring oxygens are in general referred to as long-bonded and short-bonded oxygens. For our discussion, a shorter nomenclature for atoms surrounding Si2(0,0,0) is introduced in Table I and Figure 6. As an example, Ox[0,2] represents the oxygen bonded between Si(0) and Si(2). The x,y,z coordinates, separation distances, and bond directions for the set of atoms in Table I are listed in Tables II and III.

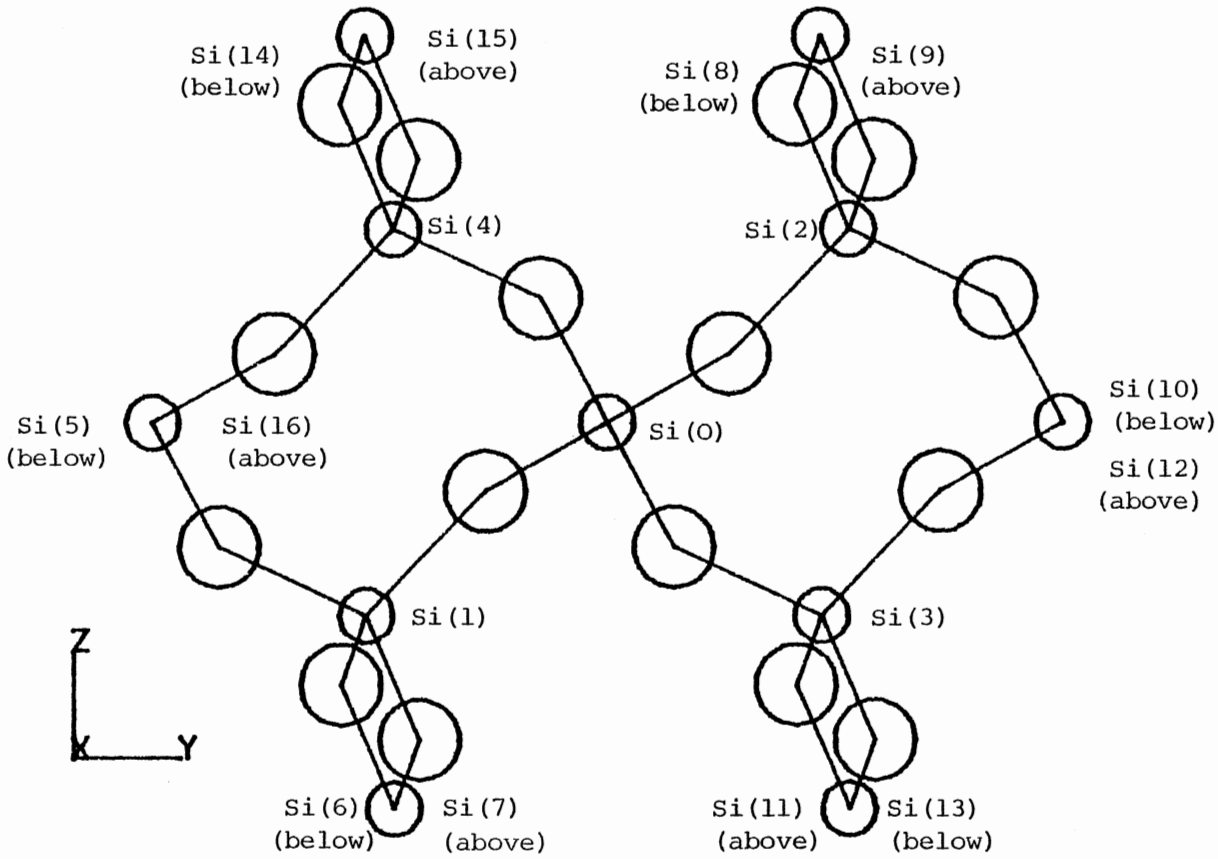

Figure 6. A Thirty-three Atom Projection of Right Quartz on the Plane Perpendicular to the X-axis. The Six Outer Silicons Actually Represent Two Silicon Sites Each, One Above the Other

TABLE I

RELATION BETWEEN FULL SPECIFICATION AND SHORT FORM NOMENCLATURE

Full Specifications	Short Form	Full Specifications	Short Form
Si2(0,0,0)	Si(0)	04(0,0,0)	0[1,0]
Si3(0,$\bar{1}$,$\bar{1}$)	Si(1)	03(0,$\bar{1}$,$\bar{1}$)	0[1,5]
Si1(1,1,0)	Si(2)	02(0,0,$\bar{1}$)	0[1,6]
Si3(1,0,$\bar{1}$)	Si(3)	05(0,$\bar{1}$,$\bar{1}$)	0[1,7]
Si1(1,0,0)	Si(4)	01(0,0,0)	0[2,0]
Si2($\bar{1}$,$\bar{1}$,0)	Si(5)	05(0,0,0)	0[2,8]
Si1(0,0,$\bar{1}$)	Si(6)	02(1,1,0)	0[2,9]
Si1(1,0,$\bar{1}$)	Si(7)	06(1,1,0)	0[2,10]
Si3(0,0,0)	Si(8)	03(1,0,$\bar{1}$)	0[3,0]
Si3(1,0,0)	Si(9)	05(1,0,$\bar{1}$)	0[3,11]
Si2(0,1,0)	Si(10)	04(1,1,0)	0[3,12]
Si1(2,1,$\bar{1}$)	Si(11)	02(1,1,$\bar{1}$)	0[3,13]
Si2(1,1,0)	Si(12)	06(1,0,0)	0[4,0]
Si1(1,1,$\bar{1}$)	Si(13)	05(0,$\bar{1}$,0)	0[4,14]
Si3(0,$\bar{1}$,0)	Si(14)	02(1,0,0)	0[4,15]
Si3(1,$\bar{1}$,0)	Si(15)	01(0,$\bar{1}$,0)	0[4,16]
Si2(0,$\bar{1}$,0)	Si(16)		

TABLE II

ATOMIC POSITION CO-ORDINATES OF ATOMS IN QUARTZ AT 300K

Short Form	x	y	z
Si(0)	2.30944	0.0	0.0
Si(1)	1.30313	-2.25708	-1.80206
Si(2)	1.30313	2.25708	1.80206
Si(3)	3.76097	2.00004	-1.80206
Si(4)	3.76097	-2.00004	1.80206
Si(5)	-0.14840	-4.25712	0.0
Si(6)	-1.15472	-2.00004	-3.60413
Si(7)	3.76097	-2.00004	-3.60413
Si(8)	-1.15472	2.00004	3.60413
Si(9)	3.76097	2.00004	3.60413
Si(10)	-0.14840	4.25712	0.0
Si(11)	6.21882	2.25708	-3.60413
Si(12)	4.76729	4.25712	0.0
Si(13)	1.30313	2.25708	-3.60413
Si(14)	1.30313	-2.25708	3.60413
Si(15)	6.21883	-2.25708	3.60413
Si(16)	4.76729	-4.25712	0.0
O[1,0]	1.37578	-1.13958	-0.64226
O[1,5]	0.78305	-3.63545	-1.15981
O[1,6]	0.29902	-1.76125	-2.06187
O[1,7]	2.75687	-2.49586	-2.44432
O[2,0]	1.37578	1.13958	0.64226
O[2,8]	0.29902	1.76125	2.96187

TABLE II (Continued)

Short Form	x	y	z
O[2,9]	2.75687	2.49586	2.44432
O[2,10]	0.78305	3.63545	1.15981
O[3,0]	3.24089	0.62166	-1.15981
O[3,11]	5.21472	1.76125	-2.44432
O[3,12]	3.83363	3.11753	-0.64226
O[3,13]	2.75687	2.49586	-2.96187
O[4,0]	3.24089	-0.62166	1.15981
O[4,14]	2.75687	-2.49586	2.96187
O[4,15]	5.21472	-1.76125	2.44432
O[4,16]	3.83363	-3.117529	0.64226

TABLE III

INTERATOMIC DISTANCES AND BOND DIRECTIONS BETWEEN ATOMS IN QUARTZ AT 300K

Atoms	Distance in Å	Direction	
		θ	φ
Si(0) - Si(1)	3.0585	126.1°	245.0°
Si(0) - Si(2)	3.0585	53.9°	114.0°
Si(0) - Si(3)	3.0585	126.1°	54.0°
Si(0) - Si(4)	3.0585	53.9°	306.0°
Si(1) - Si(2)	5.7764	51.39°	90.0°
Si(1) - Si(0)	3.0585	53.9°	65.97°
Si(8) - Si(7)	9.598	138.7°	320.9°
Si(0) - Ox[1,0]	1.6071	113.5°	230.7°
Si(0) - Ox[2,0]	1.6071	66.4°	129.3°
Si(0) - Ox[3,0]	1.6122	136.0°	33.7°
Si(0) - Ox[4,0]	1.6122	44.0°	326.3°
Si(1) - Ox[1,0]	1.6122	49.0°	86.3°
Si(8) - Ox[1,0]	5.8559	136.5°	308.9°
Si(8) - Ox[2,0]	3.9895	137.9°	341.2°
Ox[2,0] - Si(2)	1.6122	44.0°	93.7°
Ox[1,0] - Si(2)	4.1853	54.3°	91.2°

All the results reported in this work are for right-handed α-quartz using a right-handed coordinate system. The $\bar{x}$ axis is parallel to a twofold axis having the same sense, as determined by the piezoelectric response on compression of the crystal. The proper point group governing the symmetry-related properties of most defects is D_3. There are six equivalent symmetry sites for defects containing an oxygen site, all of which can be obtained from a particular site by using the proper transformation matrices for point group D_3.

CHAPTER III

THEORETICAL ANALYSIS

The spin Hamiltonian describing an S = 1 system (two unpaired electrons) interacting with one magnetic nucleus is given, in general by

$$H = \beta \vec{H}\cdot\overleftrightarrow{g}\cdot\vec{S} + \vec{S}\cdot\overleftrightarrow{D}\cdot\vec{S} + \vec{I}\cdot\overleftrightarrow{A}\cdot\vec{S} - g_N\beta_N \vec{H}\cdot\vec{I}$$

where the first term represents the electron Zeeman interaction, the second term represents the dipolar and/or exchange interaction (fine structure) between the two unpaired electrons, and the third term represensts the hyperfine interaction due to the magnetic nucleus. The last term is the nuclear Zeeman interaction.

The following coordinate systems are used in converting this spin Hamiltonian to a suitable form for computer manipulation.

x,y,z: magnetic coordinate system chosen such that the magnetic field is along the z direction.

x_c,y_c,z_c: Crystal coordinate system.

x_g,y_g,z_g: Principal axes of the g-matrix.

x_1,y_1,z_1: Principal axes of the D-matrix.

x_2,y_2,z_2: Principal axes of the hyperfine matrix $\vec{A}$.

Rewriting the Hamiltonian in terms of these different coordinate systems, we have

$$H = \beta[S_{x_g} g_x H_{x_g} + S_{y_g} g_y H_{y_g} + S_{z_g} g_z H_{z_g}]$$

$$+ S_{x_1} D_x S_{x_1} + S_{y_1} D_y S_{y_1} + S_{z_1} D_z S_{z_1}$$

$$+ S_{x_2} A_x I_{x_2} + S_{y_2} A_y I_{y_2} + S_{z_2} A_z I_{z_2}$$

$$- g_N \beta_N H I_{z_2}$$

The relationships between the different coordinate systems are

$$\begin{bmatrix} x_g \\ y_g \\ z_g \end{bmatrix} = [TG] \begin{bmatrix} x \\ y \\ z \end{bmatrix},$$

$$\begin{bmatrix} x_1 \\ y_1 \\ z_1 \end{bmatrix} = [TH] \begin{bmatrix} x \\ y \\ z \end{bmatrix},$$

and

$$\begin{bmatrix} x_2 \\ y_2 \\ z_2 \end{bmatrix} = [TZ] \begin{bmatrix} x \\ y \\ z \end{bmatrix}$$

where [TG], [TH], and [TZ] are rotation matrices transforming the principal axes coordinate systems of the $\overleftrightarrow{g}$, $\overleftrightarrow{D}$, and $\overleftrightarrow{A}$ matrices to the magnetic field coordinate system. The spin vectors and magnetic field transform in the same manner, i.e.,

$$\begin{bmatrix} S_{x_g} \\ S_{y_g} \\ S_{z_g} \end{bmatrix} = [TG] \begin{bmatrix} S_x \\ S_y \\ S_z \end{bmatrix} , \quad \begin{bmatrix} H_{x_g} \\ H_{y_g} \\ H_{z_g} \end{bmatrix} = [TG] \begin{bmatrix} O \\ O \\ H \end{bmatrix} ,$$

etc. Similar expressions are used for the (x_1,y_1,z_1) and (x_2,y_2,z_2) coordinate systems when [TH] and [TZ], respectively, replace [TG].

Using the above transformations, the Hamiltonian is written only in terms of the magnetic field coordinate system (x,y,z), as follows:

$$\begin{aligned} H = {} & W1\, S_x + W2\, S_y + W3\, S_z + W4\, S_x^2 + W5\, S_y^2 + W6\, S_z^2 \\ & + W7\, S_y S_x + W7\, S_x S_y + W8\, S_x S_z + W8\, S_z S_x \\ & + W9\, S_z S_y + W9\, S_y S_z + W10\, S_x I_x + W11\, S_x I_y + W11\, S_y I_x \\ & + W12\, S_x I_z + W12\, S_z I_x + W13\, S_y I_y + W14\, S_z I_y + W14\, S_y I_z \\ & + W15\, S_z I_z - (g_N \beta_N) H I_z \end{aligned}$$

where the W's are:

$$W1 = H\beta\left[TG(1,1)TG(1,3)\, g_x + TG(2,1)TG(2,3)\, g_y + TG(3,1)TG(3,3)\, g_2\right]$$

$$W2 = H\beta\left[TG(1,2)TG(1,3)\, g_x + TG(2,2)TG(2,3)\, g_y + TG(3,2)TG(3,3)\, g_z\right]$$

$$W3 = H\beta\left[TG(1,3)TG(1,3)\, g_x + TG(2,3)TG(2,3)\, g_y + TG(3,3)TG(3,3)\, g_z\right]$$

$$W4 = TH(1,1)TH(1,1)D_x + TH(2,1)TH(2,1)D_y + TH(3,1)TH(3,1)D_z$$

$$W5 = TH(1,2)TH(1,2)D_x + TH(2,2)TH(2,2)D_y + TH(3,2)TH(3,2)D_z$$

$$W6 = TH(1,3)TH(1,3)D_x + TH(2,3)TH(2,3)D_y + TH(3,3)TH(3,3)D_z$$

$$W7 = TH(1,1)TH(1,2)D_x + TH(2,1)TH(2,2)D_y + TH(3,1)TH(3,2)D_z$$

$$W8 = TH(1,1)TH(1,3)D_x + TH(2,1)TH(2,3)D_y + TH(3,1)TH(3,3)D_z$$

$$W9 = TH(1,2)TH(1,3)D_x + TH(2,2)TH(2,3)D_y + TH(3,2)TH(3,3)D_z$$

$$W10 = TZ(1,1)TZ(1,1)A_x + TZ(2,1)TZ(2,1)A_y + TZ(3,1)TZ(3,1)A_z$$

$$W11 = TZ(1,1)TZ(1,2)A_x + TZ(2,1)TZ(2,2)A_y + TZ(3,1)TZ(3,2)A_z$$

$$W12 = TZ(1,1)TZ(1,3)A_x + TZ(2,1)TZ(2,3)A_y + TZ(3,1)TZ(3,3)A_z$$

$$W13 = TZ(1,2)TZ(1,2)A_x + TZ(2,2)TZ(2,2)A_y + TZ(3,2)TZ(3,2)A_z$$

$$W14 = TZ(1,2)TZ(1,3)A_x + TZ(2,2)TZ(2,3)A_y + TZ(3,2)TZ(3,3)A_z$$

$$W15 = TZ(1,3)TZ(1,3)A_x + TZ(2,3)TZ(2,3)A_y + TZ(3,3)TZ(3,3)A_z$$

Using the raising and the lowering operators

$$S_+ = S_x + iS_y,\ S_- = S_x - iS_y,$$

$$I_+ = I_x + iI_y, \text{ and } I_- = I_x - iI_y,$$

we can write the Hamiltonian in the following form,

$$\begin{aligned} H = {} & W3S_z + Q1^*S_+ + Q1\,S_- + Q_2^*S_z^2 + Q2\,S_-^2 \\ & + W6\,S_z^2 + Q3\,S_+S_- + Q3\,S_-S_+ \\ & + Q4^*\,S_+S_Z + Q4\,S_-S_Z + Q4^*\,S_ZS_+ \\ & + Q4\,S_ZS_- + Q5^*\,I_+S_+ + Q6\,I_+S_- \\ & + Q6\,I_-S_+ + Q5\,I_+S_- + Q7\,I_ZS_- \\ & + Q7\,I_-S_Z + Q7^*\,I_ZS_+ + Q7^*I_+S_Z \\ & + W15\,I_ZS_Z - g_N\beta_N HI_Z\ . \end{aligned}$$

where

$$Q1 = 1/2(W1 + iW2)$$

$$Q2 = 1/4(W4-W5+2iW7)$$

$$Q3 = 1/4(W4+W5)$$

$$Q4 = 1/2(W8+iW9)$$

$Q5 = 1/4(W10+2iW11-W13)$

$Q6 = 1/4(W10+W13)$

$Q7 = 1/2(W12+iW14)$.

Since we are concerned with an S=1 electron spin system and a ^{29}Si nucleus which has I = 1/2, the basis set chosen is $|M_S M_I>$ where M_S can be +1, 0, or -1 and M_I can be + 1/2 or - 1/2. This basis set consists of six eigen vectors, which allows one to write the Hamiltonian in a 6x6 matrix form. The Hamiltonian must be hermitian and the lower half of the matrix elements are sufficient to calculate the energy eigenvalues. The notation for the lower half of the matrix elements is presented in Table IV and the resulting energy level scheme, upon diagonalization of the 6x6 matrix, is shown in Figure 7. The non-zero elements of the energy matrix are given as follows:

$$A(1,1) = W3 + W6 + W15/2 + 2Q3 - \frac{g_N\beta_N H}{2}$$

$$A(2,1) = Q7$$

$$A(2,2) = W3+W6 + 2Q3 - \frac{W15}{2} + \frac{g_N\beta_N H}{2}$$

$$A(3,1) = \sqrt{2}\ (Q1 + Q4 + \frac{Q7}{2})$$

$$A(3,2) = \sqrt{2}\ Q6$$

$$A(3,3) = 4Q3 - \frac{g_N\beta_N H}{2}$$

$$A(4,1) = \sqrt{2}\ Q5$$

$$A(4,2) = \sqrt{2}\ (Q1+Q4 - \frac{Q7}{2})$$

$$A(4,4) = 4Q3 + \frac{g_N\beta_N H}{2}$$

$$A(5,1) = 2Q2$$

$$A(5,3) = \sqrt{2}\ (Q1 - Q4 + \frac{Q7}{2})$$

$$A(5,4) = \sqrt{2}\ Q6$$

TABLE IV

LOWER HALF OF THE SPIN HAMILTONIAN MATRIX FOR AN S=1, I=1/2 SPIN SYSTEM

	$\|+1, +1/2\rangle$	$\|+1 - 1/2\rangle$	$\|0, +1/2\rangle$	$\|0, -1/2\rangle$	$\|-1, +1/2\rangle$	$\|-1, -1/2\rangle$
$\langle +1, +1/2\|$	A(1,1)					
$\langle +1, -1/2\|$	A(2,1)	A(2,2)				
$\langle 0, +1/2\|$	A(3,1)	A(3,2)	A(3,3)			
$\langle 0, -1/2\|$	A(4,1)	A(4,2)	A(4,3)	A(4,4)		
$\langle -1, +1/2\|$	A(5,1)	A(5,2)	A(5,3)	A(5,4)	A(5,5)	
$\langle -1, -1/2\|$	A(6,1)	A(6,2)	A(6,3)	A(6,4)	A(6,5)	A(6,6)

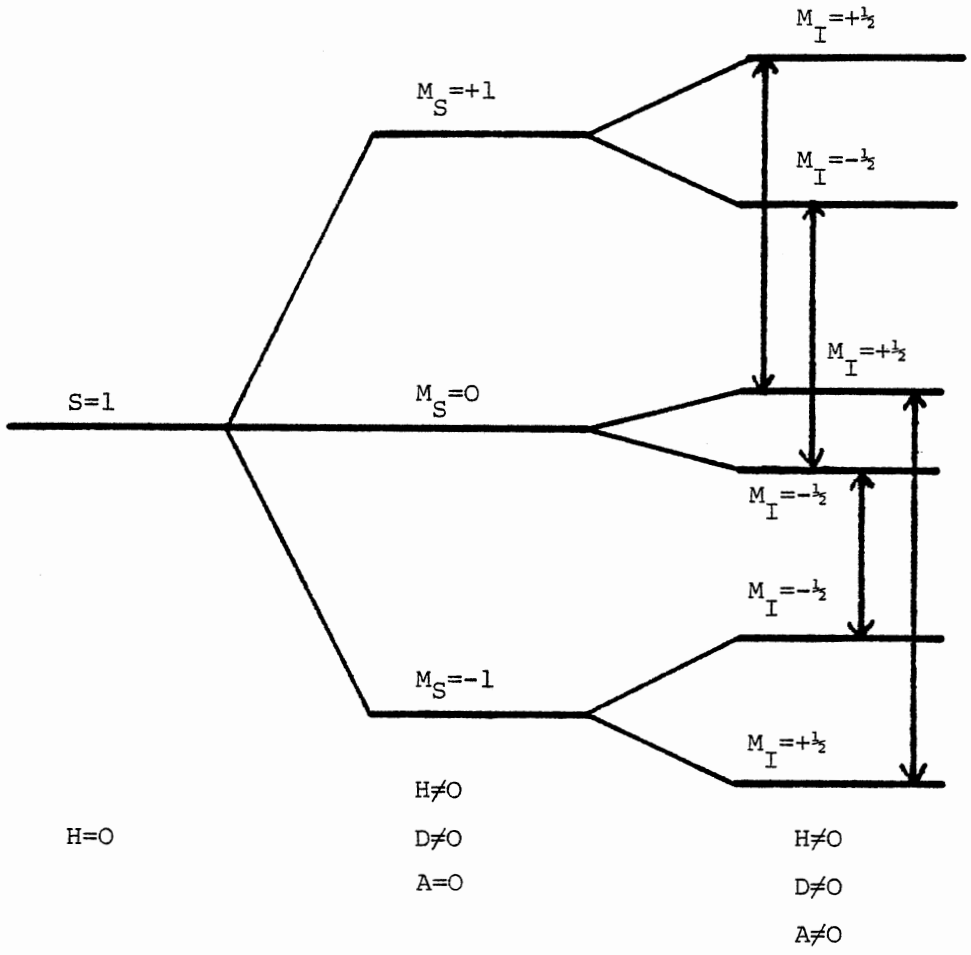

Figure 7. Energy Level Diagram for an S=1, I=½ Spin System

$$A(5,5) = W6 - W3 - \frac{W15}{2} + 2Q3 - \frac{g_N \beta_N H}{2}$$

$$A(6,2) = 2Q2$$

$$A(6,3) = \sqrt{2}\, Q5$$

$$A(6,4) = \sqrt{2}\, (Q1 - Q4 - Q7/2)$$

$$A(6,5) = - Q7$$

$$A(6,6) = W6 + \frac{W15}{2} + 2Q3 - W3 + \frac{g_N \beta_N H}{2}$$

For the analysis of only the $\overleftrightarrow{g}$ and $\overleftrightarrow{D}$ tensors, the Hamiltonian can be simplified by setting the $\overleftrightarrow{A}$ tensor and the nuclear Zeeman term equal to zero. In this case, the basis set of vectors chosen is $|M_S>$, where M_S can be +1, 0, or -1. This allows one to obtain the 3x3 energy matrix shown in Table V. Three energy eigenvalues are calculated for this matrix and the corresponding energy level diagram is shown in Figure 8.

TABLE V

LOWER HALF OF THE SPIN HAMILTONIAN MATRIX
FOR AN S=1 SPIN SYSTEM

	$\|+1\rangle$	$\|0\rangle$	$\|-1\rangle$
$\langle+1\|$	A(1,1)		
$\langle0\|$	A(2,1)	A(2,2)	
$\langle-1\|$	A(3,1)	A(3,2)	A(3,3)

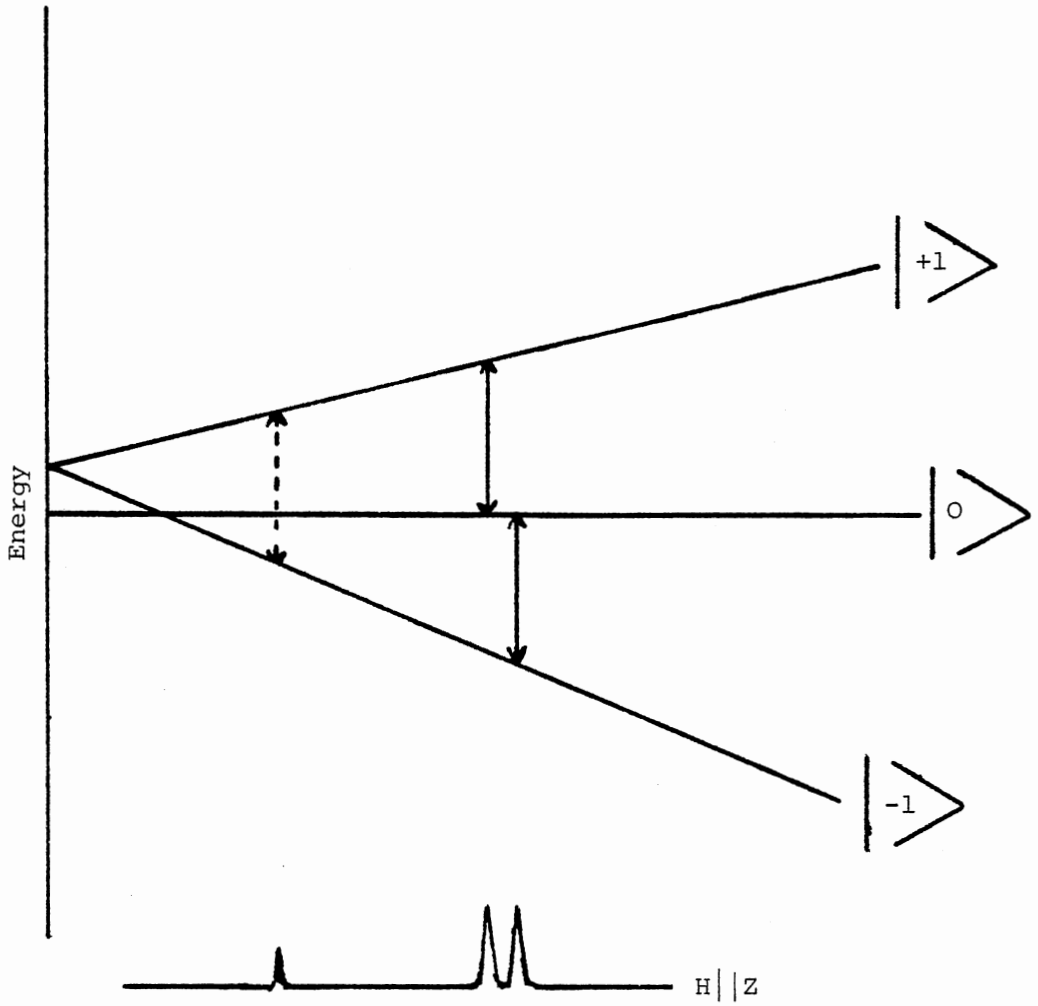

Figure 8. Energy Level Diagram for an S=1 Spin System. The Two Allowed $\Delta M_S = \pm 1$ Transitions are Shown Along With the Semi-forbidden $\Delta M_S = \pm 2$ (Half-Field) Transition

CHAPTER IV

EXPERIMENTAL RESULTS

When high quality synthetic quartz was irradiated at 300K, followed by a short 77K electron irradiation, the ESR spectrum shown in Figure 9 was observed at 300K for the magnetic field H parallel to the [001] direction. This c-axis primary-line spectrum consists of three doublets with 5.00G, 11.00G, and 17.87G separations and intensity ratios of approximately 3:2:1, respectively.

The doublet with 11.00G separation annealed in about 6 hours at the room temperature and the doublet with 5.00G separation annealed in a few days. The ESR spectrum taken after the sample had been sitting at room temperature for a few days consi-ted of only the doublet with 17.87G. Hence it was concluded that the three doublets were due to three different centers. These doublets have been assigned the labels of E_1'', E_2'', and E_3'' centers, respectively. Since the ESR linewidths were extremely narrow (=0.05G) and the lines were easily power saturated because of long spin-lattice relaxation times, the phase of the 100kHz modulation unit was adjusted out-of-phase to optimize the intensity of the lines and to prevent modulation "sidebands" from appearing and giving distorted ESR line shapes. All the ESR spectra presented in this chapter (except for the half-field line discussed in the next paragraph) were recorded with the phase adjusted in this manner.

In principle, a doublet ESR spectrum can either result from an interaction between an unpaired electron (S=1/2) and a nuclear spin I=1/2 or

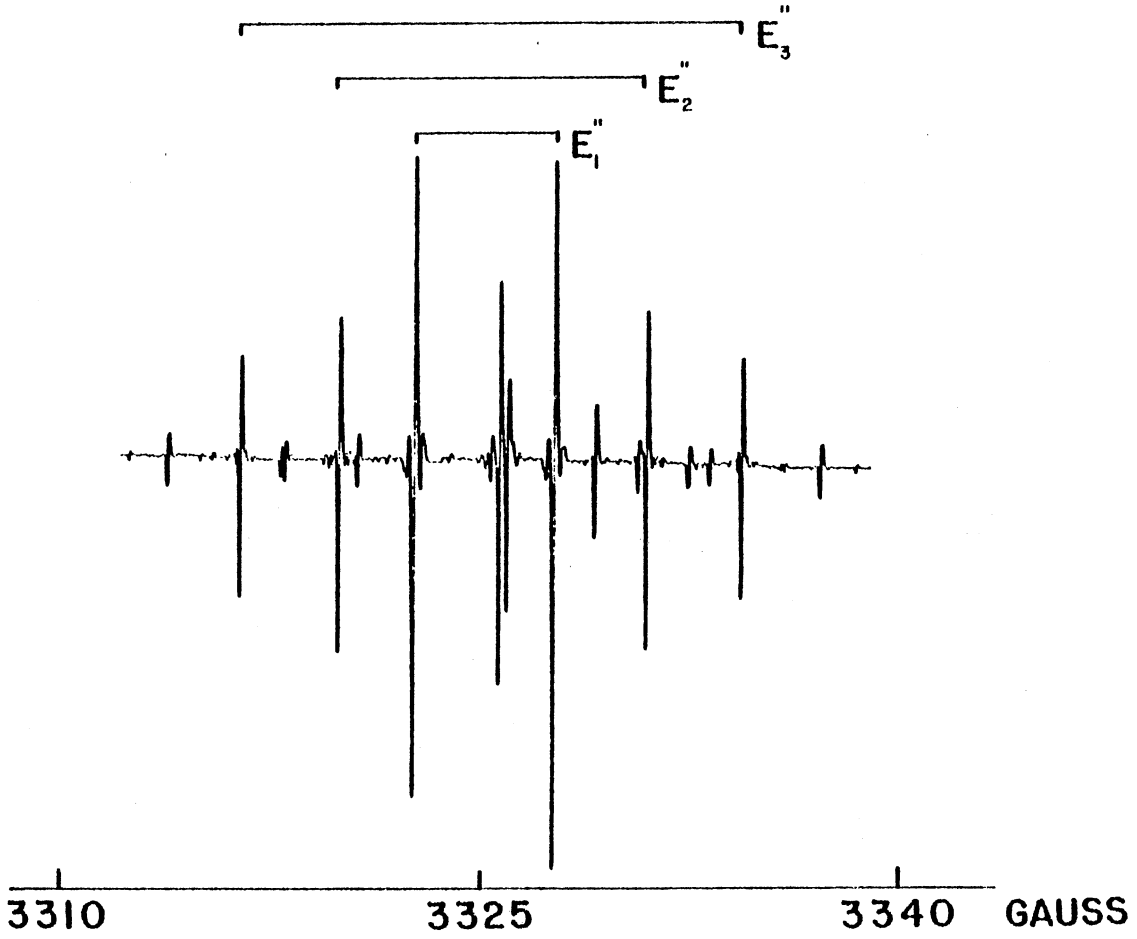

Figure 9. ESR Trace Showing the E" Centers at 300K When $\vec{H}$ is Along the C-Axis. Many of the Weak Lines are Unidentified. The Microwave Frequency is 9.31412 GHZ

from a triplet system (S=1) with no hyperfine as shown in Figure 8 in Chapter III. The definitive evidence for the triplet nature of a center is the presence of the semi-forbidden transition ($M_S = +1 \leftrightarrow M_S = -1$) at half the magnetic field of the allowed transitions. Such a half-field line was observed for the E" centers and it is shown in Figure 10. Since the three centers have nearly identical g_c values, the three half-field lines overlap and only one line was observed when the magnetic field was along the c-axis. This spectrum was recorded at higher microwave power, higher gain, and in-phase relative to the primary lines.

An angular dependence study of the E_1'' center was carried out using sample SQA-10. This allowed the $\overleftrightarrow{g}$ and $\overleftrightarrow{D}$ matrix principal values and directions to be determined. The magnetic field was rotated about a twofold crystal axis (i.e., the x axis) and ESR spectra were recorded at 20°, 40°, 60°, and 70° on each side of the [001] direction. Spectra beyond the 70° angle were not obtained because the signal intensity was dropping rapidly. This is because the microwave field component perpendicular to the static magnetic field is proportional to $\cos^2\beta$ for the orientation of the rectangular cavity being used where β is the angle between the static field and the crystal's c-axis. The magnetic field values and corresponding microwave frequencies are listed in Table VI for each measured ESR line. Since the gaussmeter probe was not located at exactly the same place as the sample, a standard sample $MgO:Cr^{3+}$ (having a known g value of 1.9799) was placed in the cavity and correction factors determined for the different orientations of the magnetic field. These are listed in Table VII.

The best sets of parameters for the $\vec{g}$ and $\vec{D}$ matrices were obtained using the two computer programs listed in Appendix A and B. The first

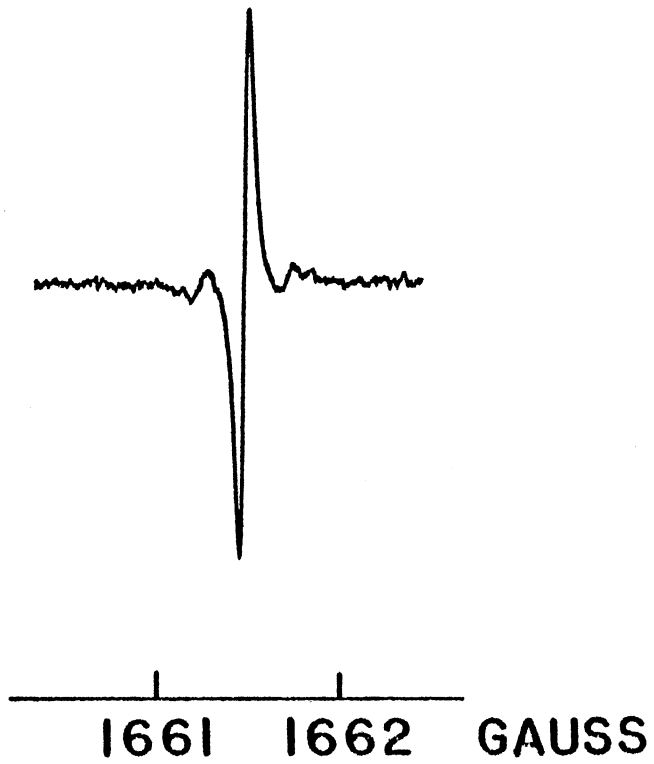

Figure 10. Half-Field Transition of the E" Centers When $\vec{H}$ is Along the C-Axis. The Microwave Frequency is 9.31412 GHZ, and the Temperature is 300K

TABLE VI

ORIGINAL DATA FOR THE PRIMARY LINES OF THE E_1'' CENTER

Angle	Uncorrected Field in Gauss	Corrected Field in Gauss	Calculated Field in Gauss	Microwave Frequency in GHz
-70°	3185.1	3185.51	3185.44	9.1151497
(-69.70°)	3202.46	3202.90	3202.84	9.1151451
	3239.82	3240.26	3240.21	9.1151460
	3268.23	3268.68	3268.61	9.1151423
	3306.04	3306.50	3306.45	9.1151389
	3321.89	3322.34	3322.30	9.1151377
-60°	3173.42	3173.94	3173.81	9.1145077
(-59.76°)	3211.31	3211.84	3211.72	9.1145028
	3217.71	3218.24	3218.13	9.1145014
	3290.34	3290.88	3290.76	9.1145014
	3296.54	3297.09	3296.97	9.1145016
	3333.04	3333.59	3333.49	9.1144987
-40°	3175.36	3175.73	3175.74	9.1145658
(-39.86°)	3195.38	3195.75	3195.75	9.1145661
	3232.00	3232.38	3232.38	9.1145609
	3275.75	3276.12	3276.13	9.1145617
	3313.48	3313.86	3313.89	9.1145598
	3331.36	3331.74	3331.76	9.1145571
-20°	3207.98	3208.27	3208.38	9.1146018
(-19.92°)	3208.58	3208.88	3208.96	9.1146014
	3247.84	3248.14	3248.19	9.1145992
	3259.91	3260.21	3260.26	9.1145946
	3299.12	3299.42	3299.42	9.1145944
	3300.08	3300.39	3300.42	9.1145959
0°	3251.38	3251.58	3251.72	9.1146036
	3256.38	3256.68	3256.75	9.1146013
$+20^\circ$	3203.26	3203.60	3203.59	9.1152273
(19.94°)	3210.71	3211.05	3211.04	9.1152218
	3241.24	3241.58	3241.56	9.1152224
	3267.12	3267.46	3267.43	9.1152201
	3298.42	3298.77	3298.73	9.1152169
	3304.35	3304.70	3304.65	9.1152175
$+40^\circ$	3164.94	3165.32	3165.27	9.1151215
(39.88°)	3195.46	3195.84	3195.82	9.1151183
	3221.75	3222.13	3222.08	9.1151099
	3286.64	3287.03	3287.02	9.1151012
	3313.85	3314.24	3314.18	9.1151003
	3342.35	3342.74	3342.70	9.115097

TABLE VI (Continued)

Angle	Uncorrected Field in Gauss	Corrected Field in Gauss	Calculated Field in Gauss	Microwave Frequency in GHz
$+60^{\circ}$	3159.21	3159.53	3159.59	9.1150115
(59.76°)	3202.26	3202.59	3202.64	9.1150053
	3212.81	3213.13	3212.17	9.1150000
	3295.72	3296.06	3296.10	9.1149937
	3306.23	3306.57	3306.60	9.1149901
	3347.85	3348.19	3348.22	9.1149850
$+70^{\circ}$	3170.09	3170.36	3170.47	9.1149567
(69.76°)	3195.43	3195.70	3195.83	9.1149560
	3231.83	3232.11	3232.23	9.1149549
	3276.12	3276.40	3276.51	9.1149545
	3313.10	3313.39	3313.50	9.1149530
	3336.85	3337.14	3337.27	9.1149541

TABLE VII

FIELD-CORRECTION FACTORS AS DETERMINED FROM STANDARD MgO:Cr^{3+} SAMPLE

Degrees	$(H_{Cr^{3+}})$	Microwave Frequency (GHZ)	ΔH
0°	3300.87	9.1478600	0.308
-20°	3300.88	9.1478843	0.307
-40°	3300.80	9.1478717	0.381
-60°	3300.61	9.1478134	0.543
-70°	3300.69	9.1477849	0.453
$+20^{\circ}$	3300.79	9.1477551	0.349
$+40^{\circ}$	3300.75	9.1477739	0.391
$+60^{\circ}$	3300.82	9.1477996	0.337
$+70^{\circ}$	3300.87	9.1477980	0.284

$$\Delta H = (H_{sample})_{Cr^{3+}} - (H_{Cr^{3+}})_{Gaussmeter}$$

$$(H_{sample})_{Cr^{3+}} = \frac{h\nu}{g\beta} = \frac{6.6262 \times 10^{-27} \times \nu_{Cr^{3+}}}{9.2741 \times 10^{-21} \times 1.9799}$$

program, listed in Appendix A, was used to predict line positions (i.e., magnetic field values) for different orientations of the magnetic field when given a set of spin Hamiltonian parameters and a microwave frequency. The second program calculates the final set of parameters when the microwave frequencies and experimental ESR line positions are provided as input data.

In the first program, it was assumed that the parameters for the $\vec{g}$ and $\vec{D}$ matrices were known. Then the magnetic field values associated with different ESR resonance lines were predicted by an iteration scheme. The direction of the magnetic field relative to the crystal axes was specified by the angles alpha(α) and beta(β) as shown in Figure 11. For each set of these angles there were two transitions per inequivalent defect site according to the spin selection rules $\Delta M_S = \pm 1$. These possible transitions for one site are shown in Figure 8 in Chapter III and were determined by the following procedure. First, an initial value of magnetic field, H, was assigned. Then the 3x3 matrix shown in Table V was diagonalized by the computer and three energy eigenvalues D(I) given in order of ascending values were obtained. The microwave frequency necessary for a transition is the difference between the appropriate eigenvalues. The assigned magnetic field was then varied systematically and the microwave frequency corresponding to a particular transition was recalculated and compared with the experimental microwave frequency for each assigned magnetic field value. The iteration continues until the calculated microwave frequency lies within 0.1 MHz of the experimental frequency, the last value of the magnetic field was taken to be the particular line position.

The values of the different spin Hamiltonian parameters were systematically varied in the second program, listed in Appendix B, until

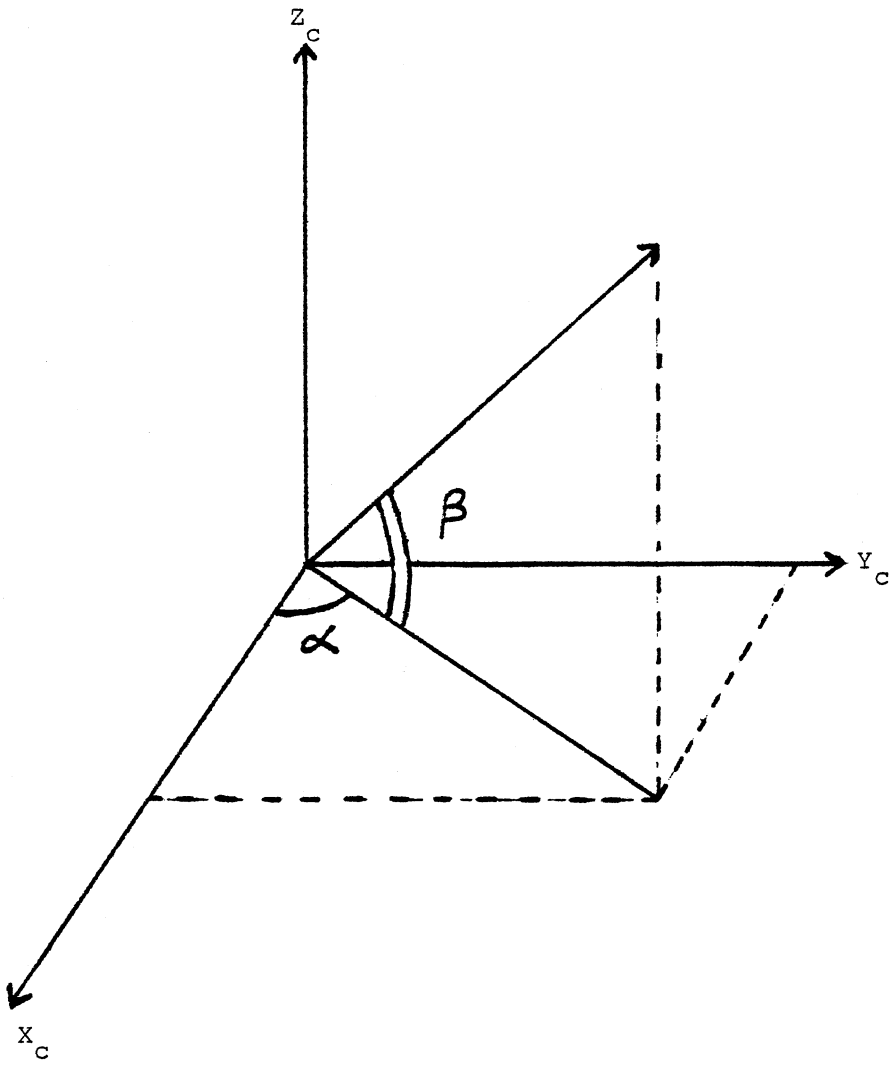

Figure 11. Definition of Angles Alpha (α) and Beta (β)

good agreement between the calculated and experimental microwave frequency for each experimental transition was obtained. The program essentially uses a least-squares-fit method. An initial set of parameters was assumed and the magnetic field positions for different orientation of the magnetic field were provided as experimental data. Using this information the energy eigenvalues were obtained as in the first program and the microwave frequency associated with each resonance was calculated.

Since the assumed set of parameters was most likely not the correct one, the calculated microwave frequency was not the same as the experimental value. Hence a quantity called SUM

$$\text{SUM} = \sum_{i=1} [\nu_i^{exp} - \nu_i^{cal}]^2$$

was calculated where the summation is over all measured ESR lines. In each iteration, one of the parameters was increased by a pre-determined amount and a new set of microwave frequencies were obtained. The new value of SUM thus obtained was compared against the previous value of SUM. If the new value of SUM was greater than the previous value, then the value of that parameter (which had just been increased) was decreased by twice the specified increment. All the microwave frequencies were recalculated and the new value of SUM was obtained. This SUM was again compared with the initial value of SUM and the value of this parameter which gave the smallest SUM was retained. This procedure was repeated for all the other parameters. The final set of parameters correspond to the case when any variation in any of the parameters failed to lower the value of SUM.

The above discussed procedure was used to fit the experimental

field values and microwave frequencies for different transitions at various magnetic field directions of the E_1'' center in the y-z plane. The final set of parameters as determined from these computations is listed in Table VIII. This set of parameters was used in the first (i.e., line position) program to predict the angular dependence for the main line spectrum, shown in Figure 12. The O's represent the magnetic field values used as experimental data in the fitting program. The calculated magnetic field values for different lines are listed in Table VI for comparison with the measured field values. Angles listed in the first column of Table VI were also varied as parameters in the fitting program since the angular scale on the magnet seemed to be very slightly in error. The best values of the angles obtained from the program are listed in parenthesis (in the first column of Table VI).

Similar analysis was done for the E_3'' center using the two programs discussed above. The measured values of the magnetic field and microwave frequency for different line positions are listed in Table IX. The best set of parameters for the E_3'' center is presented in Table X. The predicted angular dependence for the E_3'' center is shown in Figure 13. The O's represent the magnetic field values used as experimental data in the fitting program.

TABLE VIII

SPIN-HAMILTONIAN PARAMETERS FOR THE E_1'' CENTER AS DETERMINED AT ROOM TEMPERATURE

		θ	ϕ
g_x	2.0004	32.3°	246.0°
g_y	2.0006	91.8°	333.1°
g_z	2.0014	57.8°	61.9°
D_x	110.0 MHZ	34.2°	234.9°
D_y	117.6 MHZ	86.0°	330.8°
D_z	-227.6 MHZ	56.0°	63.5°

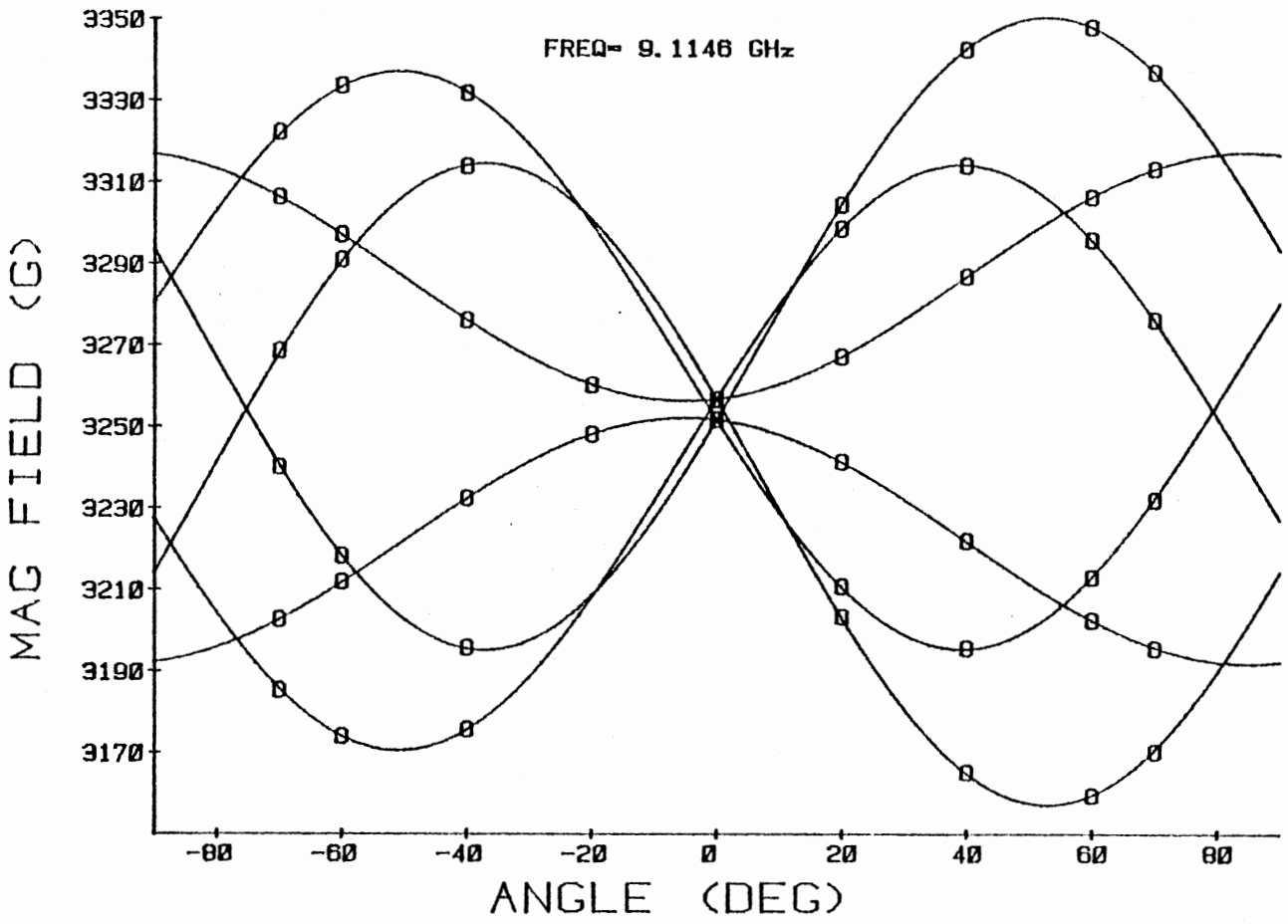

Figure 12. The Angular Variation for the E_1'' Center (Primary Lines)

TABLE IX

ORIGINAL DATA FOR THE PRIMARY LINES OF THE E_3'' CENTER

Angle	Uncorrected Field in Gauss	Corrected Field in Gauss	Calculated Field in Gauss	Microwave Frequency in GHZ
-70°	3237.64	3238.08	3238.07	9.1151368
(-69.70°)	3241.92	3242.36	3242.35	9.1151351
	3243.01	3243.45	3243.46	9.1151352
	3267.06	3267.51	3267.49	9.1151350
	3267.96	3268.41	3268.00	9.1151314
	3270.63	3271.08	3271.04	9.1151312
-60°	3232.27	3232.80	3232.71	9.1144975
(-59.76°)	3241.27	3241.80	3241.73	9.1144960
	3243.45	3243.98	3243.95	9.1144937
	3265.97	3266.51	3266.48	9.1144928
	3268.04	3268.58	3268.55	9.1144930
	3275.15	3275.69	3275.64	9.1144890
-40°	3228.14	3228.51	3228.52	9.1145589
(-39.86)	3243.89	3244.26	3244.28	9.1145555
	3250.14	3250.51	3250.51	9.1145517
	3259.47	3259.85	3259.85	9.1145490
	3265.12	3265.50	3265.50	9.1145455
	3279.24	3279.62	3279.63	9.1145440
-20°	3233.23	3233.53	3233.60	9.1145947
(-19.92)	3251.27	3251.57	3251.61	9.1145912
	3252.49	3252.79	3252.85	9.1145895
	3256.10	3256.40	3256.44	9.1145866
	3257.87	3258.17	3258.21	9.1145856
	3274.48	3274.78	3274.82	9.1145860
0°	3245.26	3245.56	3245.61	9.1146003
	3263.13	3263.43	3263.47	9.1145986
$+20^{\circ}$	3237.92	3238.26	3238.24	9.1152095
(19.94°)	3244.52	3244.86	3244.85	9.1152064
	3250.75	3251.09	3251.05	9.1152061
	3258.93	3259.27	3259.23	9.1152086
	3263.74	3264.08	3264.05	9.1152097
	3271.13	3271.48	3271.44	9.1152085
$+40^{\circ}$	3237.02	3237.40	3237.40	9.1150955
(39.88°)	3242.66	3243.04	3242.98	9.1150984
	3248.93	3249.31	3249.31	9.1150985
	3258.98	3259.37	3259.33	9.1151017
	3267.41	3267.80	3267.73	9.1151006
	3272.31	3272.70	3272.67	9.1151078

TABLE IX (Continued)

Angle	Uncorrected Field in Gauss	Corrected Field in Gauss	Calculated Field in Gauss	Microwave Frequency in GHZ
$+60^{\circ}$	3242.88	3243.21	3243.24	9.1149813
(59.76°)	3243.27	3243.60	3243.68	9.1149801
	3251.34	3251.67	3251.76	9.1149804
	3256.73	3257.06	3257.14	9.1149771
	3266.42	3266.75	3266.85	9.1149781
	3267.03	3267.36	3267.40	9.1149777
$+70^{\circ}$	3246.24	3246.52	3246.63	9.1149604
(69.76°)	3247.53	3247.81	3247.97	9.1149618
	3248.29	3248.57	3248.72	9.1149609
	3260.80	3261.08	3261.24	9.1149582
	3261.55	3261.83	3262.01	9.1149617
	3263.40	3263.68	3263.79	9.1149601

TABLE X

SPIN-HAMILTONIAN PARAMETERS FOR THE E_3'' CENTER AS DETERMINED AT ROOM TEMPERATURE

		θ	ϕ
g_x	2.0004	83.6°	78.9°
g_y	2.0005	47.4°	343.0°
g_z	2.0013	136.7°	355.8°
D_x	-25.0 MHZ	50.0°	335.4°
D_y	-25.2 MHZ	79.3°	236.3°
D_z	+50.2 MHZ	138.0°	314.3°

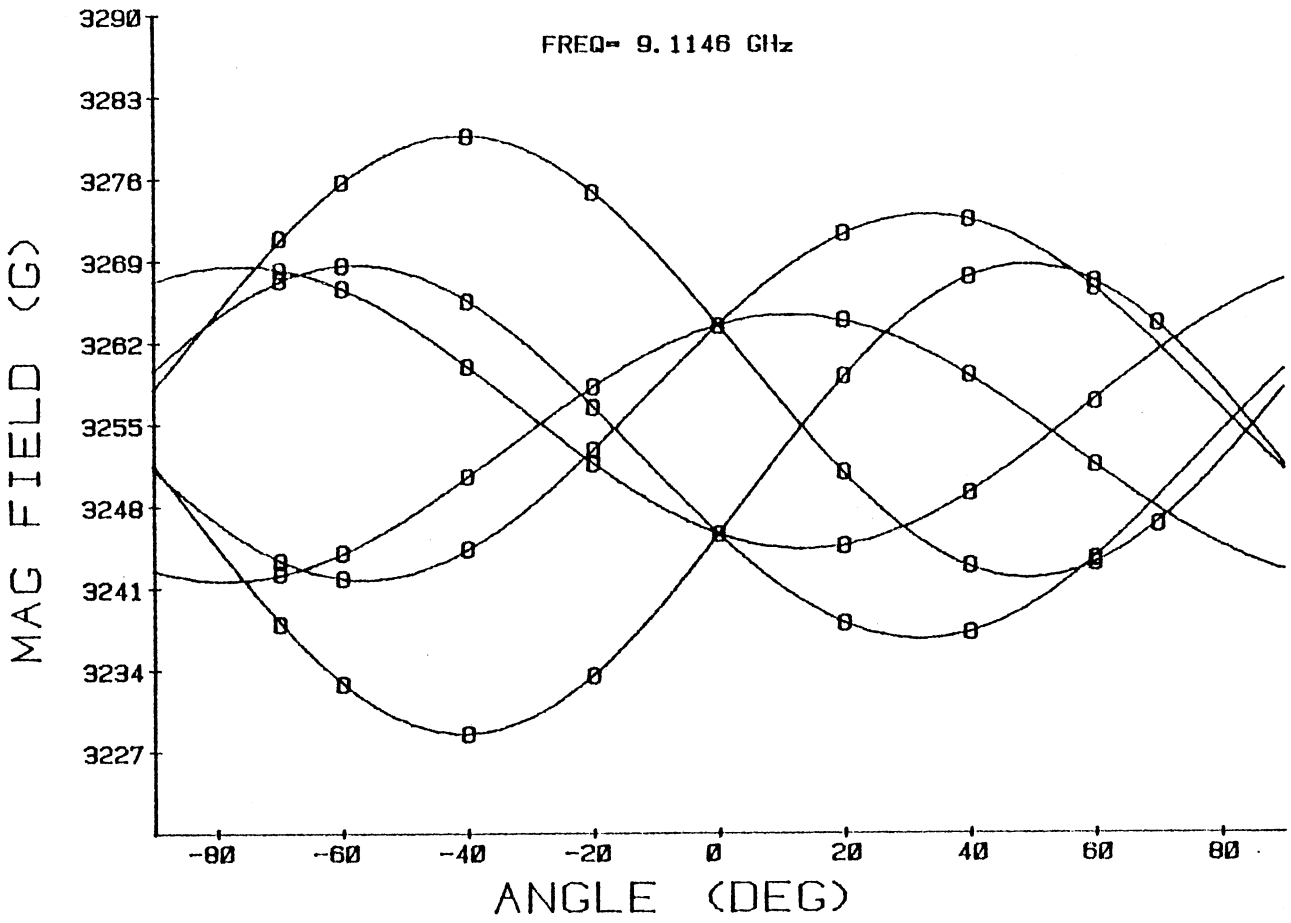

Figure 13. The Angular Variation for the E''_3 Center (Primary Lines)

CHAPTER V

HYPERFINE RESULTS FOR THE E_1'' CENTER

When samples WEA-1 or SQA-10 were electron irradiated at 300K and then irradiated at low temperature (77K), additional weak ESR lines were observed, four on the low field side and four on the high field side of the main line spectrum for each of the E" centers when the magnetic field is along the c-axis of the crystal. These lines are shown in Figures 14 and 15. This means that there are four pairs of these smaller-intensity lines for each defect and they are approximately centered on the two primary lines for each center. These widely-split pairs of lines have been assigned to hyperfine interactions of each triplet center with two inequivalent ^{29}Si nuclei (I = 1/2 and 4.7% natural abundance).

The magnetic field values for the hyperfine lines corresponding to the E_1'' center when the field is parallel to the c-axis are given in Table XI along with the assignments to specific nuclei. The fine structure line splittings of the two hyperfine doublets on the low field side of the main spectrum are 4.90G and 4.30G, whereas the similar splittings of the two hyperfine doublets on the high field side are 13.12G and 12.75G. The separation between the doublets on the low and high field side are 202.23G and 195.82G for nucleus 1 and 2, respectively. All the ESR spectra were recorded with the 100 kHz modulation "in-phase" and with higher microwave power and gain, which is quite different from the conditions found to optimize the primary lines.

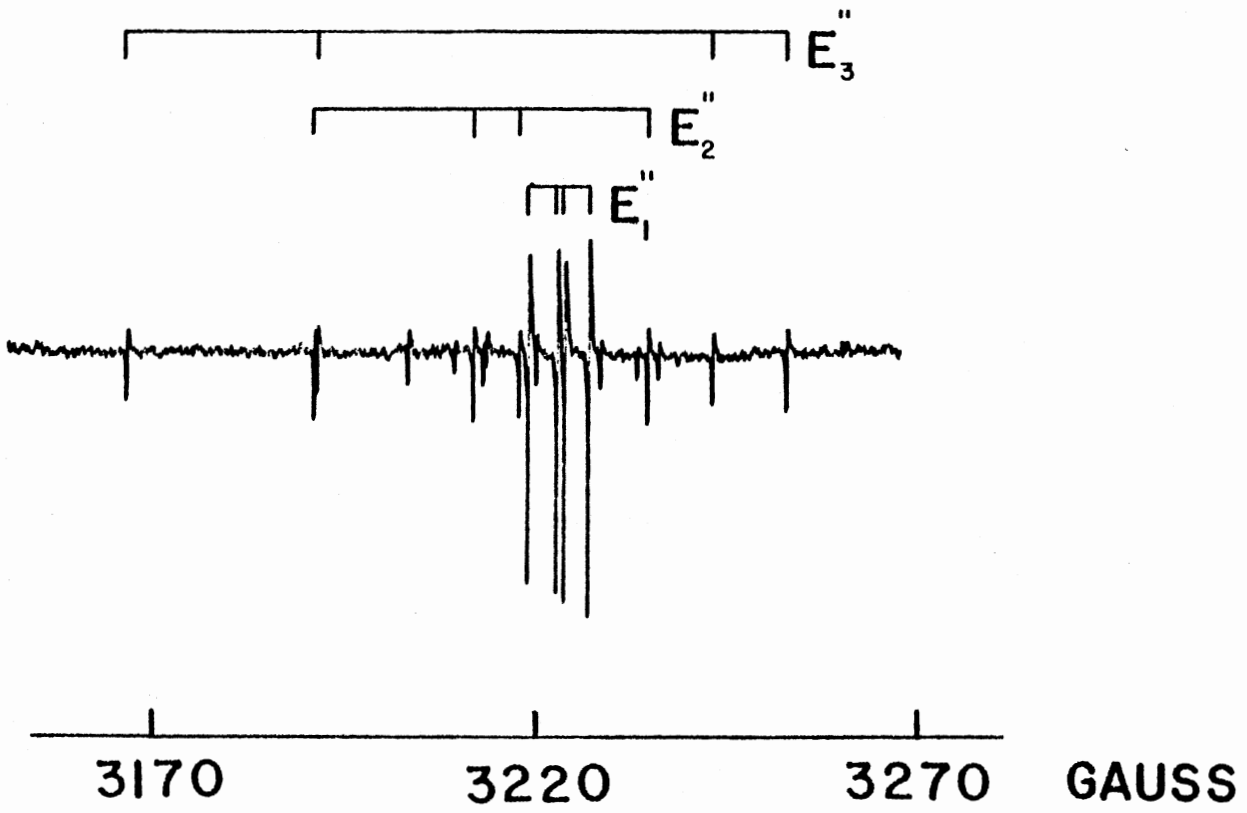

Figure 14. Low-field ^{29}Si Hyperfine Spectrum for the E" Centers at 300K When $\vec{H}$ is Along the C-axis. The Microwave Frequency is 9.31412 GHZ

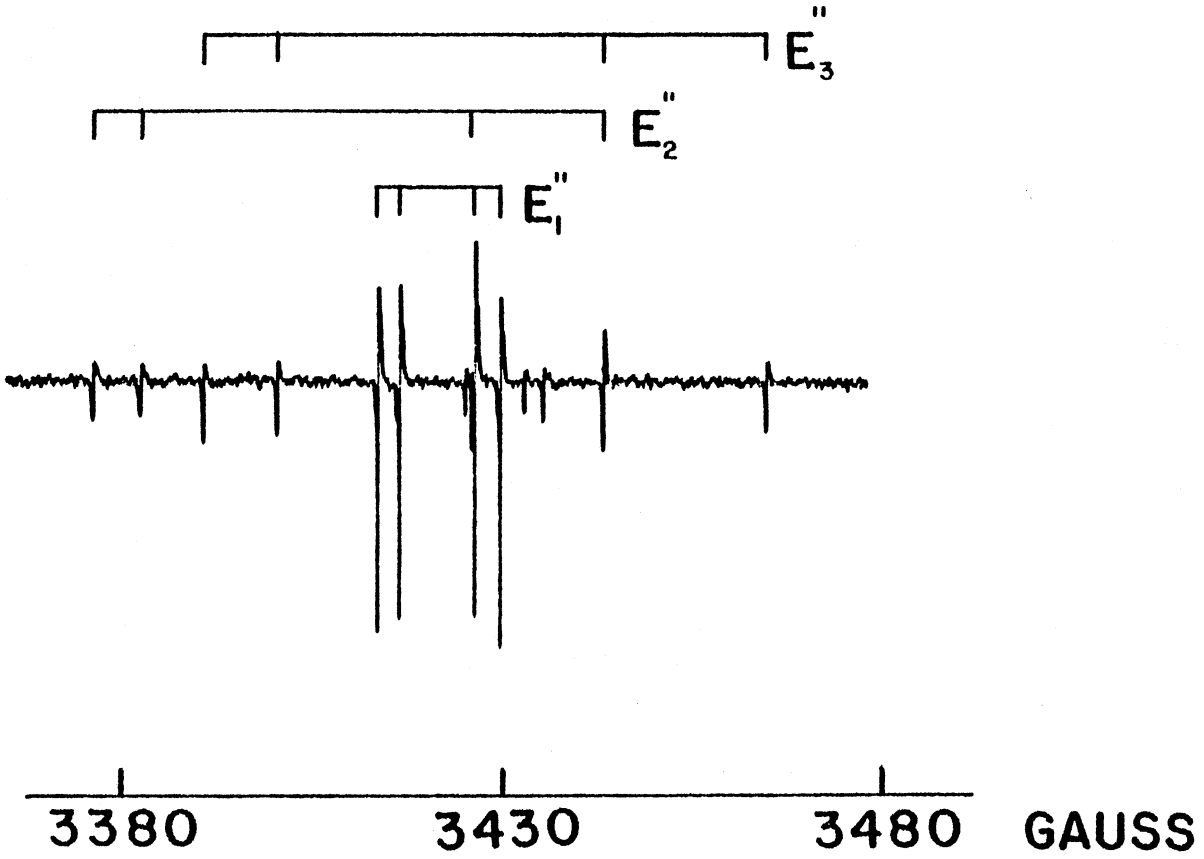

Figure 15. High-field ^{29}Si Hyperfine Spectrum for the E" Centers at 300K When $\vec{H}$ is Along the C-axis. The Microwave Frequency is 9.31412 GHZ

TABLE XI

MAGNETIC FIELD POSITIONS OF THE PRIMARY DOUBLET AND THE EIGHT ^{29}Si HYPERFINE LINES FOR THE E_1'' CENTER. THE MAGNETIC FIELD VALUES ARE IN GAUSS AND THE MICROWAVE FREQUENCY IS 9.3165 GHZ

Primary Lines:	3323.74	3328.75
Hyperfine Lines:		
Nucleus 1	3219.43, 3224.25	3417.56, 3430.75
Nucleus 2	3223.18, 3227.44	3414.75, 3427.54

An angular-dependence study of the E_1'' center ^{29}Si hyperfine lines for rotation in the plane perpendicular to the X(or $\vec{a}$) axis was done at 300K. The interactions with the two nuclei proved to be similar and it was very difficult to determine to which nucleus a particular hyperfine line should be assigned. In order to distinguish between lines resulting from the two different nuclei, data was taken for every one-tenth of a degree of rotation of the magnetic field up to fifteen degrees on each side of the c-axis. Although very tedious and time-consuming, this helped considerably in making proper line assignments and for later use in the computer program to determine hyperfine matrix principal values and directions for two ^{29}Si nuclei. The angular dependence for -15° to $+15^{\circ}$ rotation of the magnetic field are shown in Figures 16 and 17 for the low and high field sides. The solid and dashed lines represent the calculated angular dependence for nucleus 1 and 2, respectively, using parameters determined later in this chapter, whereas the O's represent the measured field values at five degree intervals.

ESR spectra for the angles beyond fifteen degrees on each side of the c-axis were obtained by rotating the sample in the Varian Cavity (instead of rotating the magnetic field and keeping the sample fixed as in the -15° to $+15^{\circ}$ case). Normally, the samples were not cut with perfect x-plane ends and the rotating mechanism could not maintain the sample properly in the plane at all angles; therefore, the following procedure was used. First, the sample was placed at an approximate angle setting, making sure that the magnetic field was perpendicular to the two-fold (a) axis. [The approximate settings of the angles were -30°, -48°, and -70° on one side and 30°, 40°, 60° and 75° on the other side of the c-axis.] Then, at each approximate angle setting, the values of the magnetic field and the microwave frequency were recorded

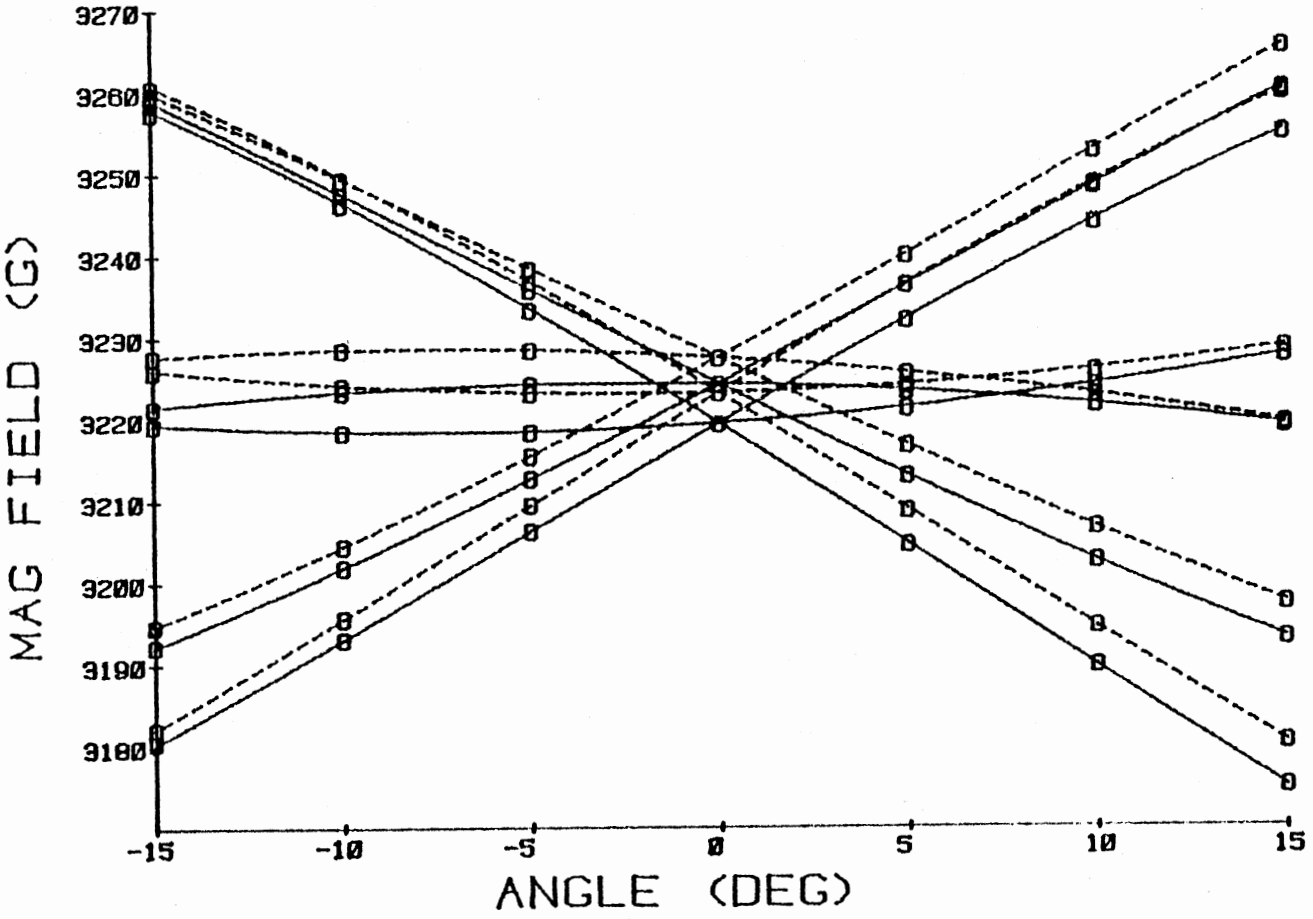

Figure 16. Calculated Low-field ^{29}Si Hyperfine Angular Dependence of the E_1'' Center for Rotation of the Magnetic Field From -15° to +15° in the X-plane. The O's Represent Experimentally Measured Field Values. The Solid Curve Corresponds to Nucleus 1 and the Dashed Curve Corresponds to Nucleus 2

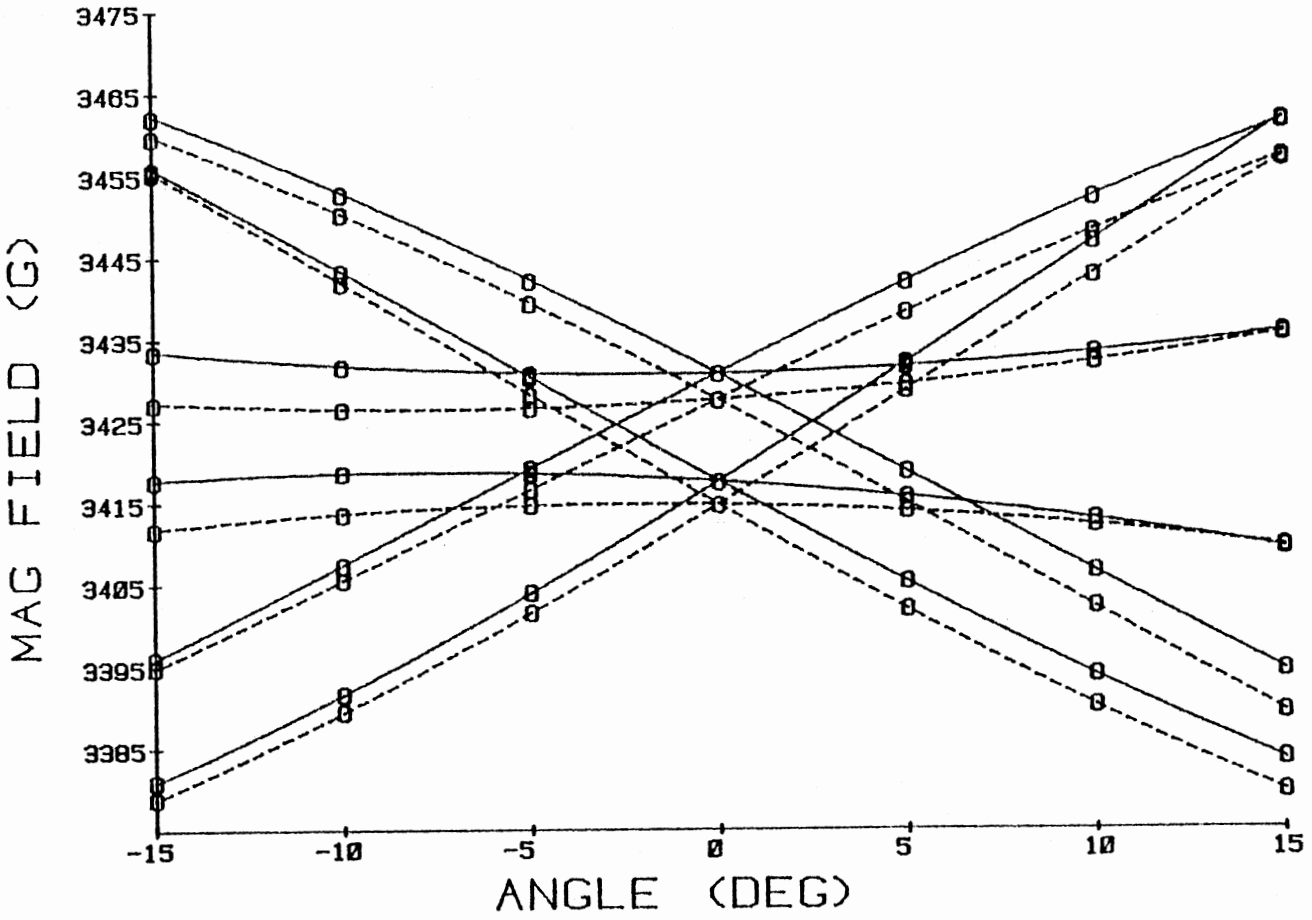

Figure 17. Calculated High-field ^{29}Si Hyperfine Angular Dependence of the E_1'' Center for Rotation of the Magnetic Field From -15^{o} to $+15^{o}$ in the X-plane. The O's Represent Experimentally Measured Field Values. The Solid Curve Corresponds to Nucleus 1 and the Dashed Curve Corresponds to Nucleus 2

recorded for each of the main line and hyperfine line positions. This set of raw data for the various approximate angles is listed in Appendix C. Also, ESR spectra were recorded at several in-between angles to follow the different hyperfine lines as they shifted positions.

Since the angles at which the hyperfine data were taken were known to be slightly in error, a separate computer program making use of the previously determined $\vec{g}$ and $\vec{D}$ matrix parameters was designed to correct the values of these angles. The best set of values for the $\vec{g}$ and $\vec{D}$ matrices for the E_1'' center, listed in Table VIII, was given to the line position program. The separations within pairs of fine-structure-split lines in the primary spectrum were used as experimental data. For a particular angular setting, the experimental fine-structure separations (DF) were compared to the calculated separations (DFC) and the value of SUM

$$SUM = \sum_{K=1}^{3} [DFC(k) - DF(k)]^2$$

was evaluated. Then the value of the angle was increased by a specified increment and the value of SUM was calculated again. The new value of SUM was compared with the previous value and the smaller of the two was retained along with the corresponding angle. If the new value of SUM was greater than the previous value, then the angle was decreased by twice the specified increment and another new value of SUM was calculated and compared to the previous value. Using this iteration scheme, the minimum value of SUM and the corresponding angle were obtained. This process was repeated for each of the other approximate angles. The best values of the angles obtained from this program were used in analyzing the hyperfine data, i.e., to evaluate the $\vec{A}_{^{29}Si_I}$ and $\vec{A}_{^{29}Si_{II}}$ matrices.

Two programs, quite similar to the ones discussed in Chapter IV, were written to analyze the hyperfine data. These are listed in Appendix D and E. The first program predicts the line positions given a set of parameters and a microwave frequency. The fitting program (second program) was modified to allow analyzing the hyperfine data in a slightly different fashion, as discussed below.

Best values of the $\vec{g}$ and $\vec{D}$ matrices were provided as non-varying parameters and initial parameters for the $\vec{A}$ matrix were chosen. Instead of individual line-position field values, experimental differences in the field values for each particular site were provided along with the average frequency for a particular angle. The magnetic field values associated with different ESR resonance lines were predicted by an iteration scheme. An initial value of the magnetic field, H, was assigned. For each angle, there were four transitions according to the spin selection rules $\Delta M_S = \pm 1$, $\Delta M_I = 0$. These possible four transitions are shown in Figure 7. The 6x6 spin-Hamiltonian matrix shown in Table IV was diagonalized and six energy eigenvalues D(I) given in order of ascending value were obtained. The four transitions are given by

$$h\nu_1 = D(4) - D(1)$$

$$h\nu_2 = D(6) - D(4)$$

$$h\nu_3 = D(5) - D(3)$$

$$h\nu_4 = D(3) - D(2)$$

The assigned field value was then varied and the microwave frequency corresponding to a particular transition was recalculated and compared with the experimental microwave frequency. If the calculated microwave frequency was within 0.1 MHz of the experimental frequency, then the microwave frequency for the other 3 transitions were calculated by a similar iteration. The differences were calculated for each angle for the dif-

ferent sites as follows:

$$DFC(MM,1) = HF(3) - HF(2)$$

$$DFC(MM,2) = HF(4) - HF(1)$$

Since the initial parameters for the A tensor were not necessarily the correct ones, the calculated differences were not the same as the experimental values DF(MM,1) and DF(MM,2). Therefore, a quantity called SUM

$$SUM = \sum_{MM=1}^{62} [(DFC(MM,1) - DF(MM,1))^2 + (DFC(MM,2) - DF(MM,2))^2]$$

was calculated. Then the value of SUM was minimized by the iteration technique discussed in Chapter IV until any variation in parameters failed to lower the value of the SUM. It was necessary for us to use the differences in field values, instead of individual line positions, since the corrections to the magnetic field were not measured because of the obstacles involved in placing the standard $MgO:Cr^{3+}$ sample in the cavity at the same position as the quartz sample. This procedure of minimizing the SUM in the above-discussed program does not in anyway hinder us in obtaining the best set of parameters since each individual line would have to be corrected by an almost identical amount for a particular angle, and this correction is not necessary if differences are used.

Tables XII and XIII lists the experimentally measured and calculated differences for nucleus 1 and 2, respectively. A fairly good agreement is obtained between the measured and calculated differences using the best set of parameters listed in Table XIV. The calculated angular dependence for the low and high field side are shown in Figures

TABLE XII

HYPERFINE DATA FOR NUCLEUS 1 IN THE E_1'' CENTER

Angle	Measured Differences in Gauss	Calculated Differences in Gauss
-70° (-70.27°)	199.22	199.02
	217.02	216.80
	201.4	202.30
	218.57	219.48
	196.71	196.71
	211.32	211.35
-48° (-49°)	202.08	201.92
	----	218.87
	192.14	192.69
	206.42	206.98
	198.63	198.69
	214.98	215.05
-30° (-30.45°)	200.43	200.39
	218.14	218.17
	188.05	188.29
	201.71	201.95
	198.14	198.20
	215.49	215.61
-15° (-14.92°)	197.01	196.94
	215.53	215.55
	188.68	188.67
	204.54	204.51
	196.2	196.19
	214.02	214.05
-10° (-9.95°)	195.8	195.70
	214.3	214.3
	189.93	189.72
	206.53	206.45
	195.35	195.30
	213.27	213.24
-5° (-4.96°)	191.37	191.28
	208.82	208.75

TABLE XII (Continued)

Angle	Measured Differences in Gauss	Calculated Differences in Gauss
0°	193.3	193.28
	211.37	211.30
$+5^{\circ}$	192.26	192.17
(4.98°)	209.72	209.67
	195.66	195.66
	214.02	214.04
	192.3	192.21
	210.3	210.23
$+10^{\circ}$	191.28	191.19
(9.93°)	208.08	208.02
	198.32	198.34
	216.7	216.79
	191.27	191.16
	209.2	209.13
$+15^{\circ}$	190.42	190.37
(14.95)	206.45	206.39
	201.21	201.30
	219.35	219.53
	190.45	190.15
	208.09	208.02
$+30^{\circ}$	188.78	188.67
(29.71°)	202.64	202.55
	209.99	210.38
	226.26	226.67
	187.99	187.84
	205.06	204.94
$+43^{\circ}$	188.03	187.93
(43.09°)	201.55	201.46
	187.08	186.96
	203.14	203.02
$+75^{\circ}$	190.48	190.19
(75.02°)	208.2	207.99

TABLE XII (Continued)

Angle	Measured Differences in Gauss	Calculated Differences in Gauss
	190.36	190.29
	203.3	203.69

TABLE XIII

HYPERFINE DATA FOR NUCLEUS 2 IN THE E_1'' CENTER

Angle	Measured Differences in Gauss	Calculated Differences in Gauss
-70°	212.02	211.76
(-70.27°)	226.73	226.54
	182.93	183.26
	199.64	199.97
	181.86	181.91
	195.35	195.39
-48°	211.9	211.71
(-49°)	221.91	225.77
	181.05	181.25
	194.41	194.61
	179.92	181.01
	195.43	195.53
-30°	204.45	204.42
(-30.45°)	220.1	220.07
	181.98	182.08
	194.8	194.89
	181.22	181.34
	197.96	198.10
-15°	194.59	195.38
(-14.92°)	212.62	212.60
	184.06	184.04
	199.88	199.00
	184.07	184.11
	201.2	201.24
-10°	192.41	192.48
(-9.95°)	209.9	209.88
	185.03	184.95
	200.94	200.75
	185.17	185.16
	202.31	202.30

TABLE XIII (Continued)

Angle	Measured Differences in Gauss	Calculated Differences in Gauss
-5° (4.96°)	186.11	186.05
	202.6	202.55
0°	187.3	187.27
	204.35	204.33
$+5^{\circ}$ (4.98°)	185.17	185.13
	201.78	201.71
	----	----
	206.05	206.02
	188.33	188.37
	205.3	205.25
$+10^{\circ}$ (9.93°)	183.43	183.40
	199.34	199.32
	189.99	190.00
	207.56	207.60
	189.26	189.19
	206.12	206.05
$+15^{\circ}$ (14.95°)	182.12	182.13
	196.99	197.23
	191.65	191.45
	208.89	208.98
	189.91	190.02
	206.81	206.73
$+30^{\circ}$ (29.71°)	181.09	181.10
	194.01	193.99
	195.21	195.41
	211.49	211.68
	----	191.76
	207.84	207.72
$+43^{\circ}$ (43.09°)	183.23	183.22
	195.87	195.84
	192.22	192.14
	207.35	207.24

TABLE XIII (Continued)

Angle	Measured Differences in Gauss	Calculated Differences in Gauss
$+75^{\circ}$	196.87	196.64
(75.02°)	213.15	212.93
	188.87	188.53
	202.96	201.41

TABLE XIV

^{29}Si HYPERFINE PARAMETERS FOR NUCLEUS 1 AND NUCLEUS 2 IN THE E_1'' CENTER

		θ	ϕ
A_{x_1}	-544.6 MHZ	95.9°	359.5°
A_{y_1}	-546.6 MHZ	152.2°	100.1°
A_{z_1}	-637.1 MHZ	63.0°	86.5°
A_{x_2}	-526.6 MHZ	79.2°	300.5°
A_{y_2}	-525.6 MHZ	148.7°	12.2°
A_{z_2}	-616.1 MHZ	61.0°	36.5°

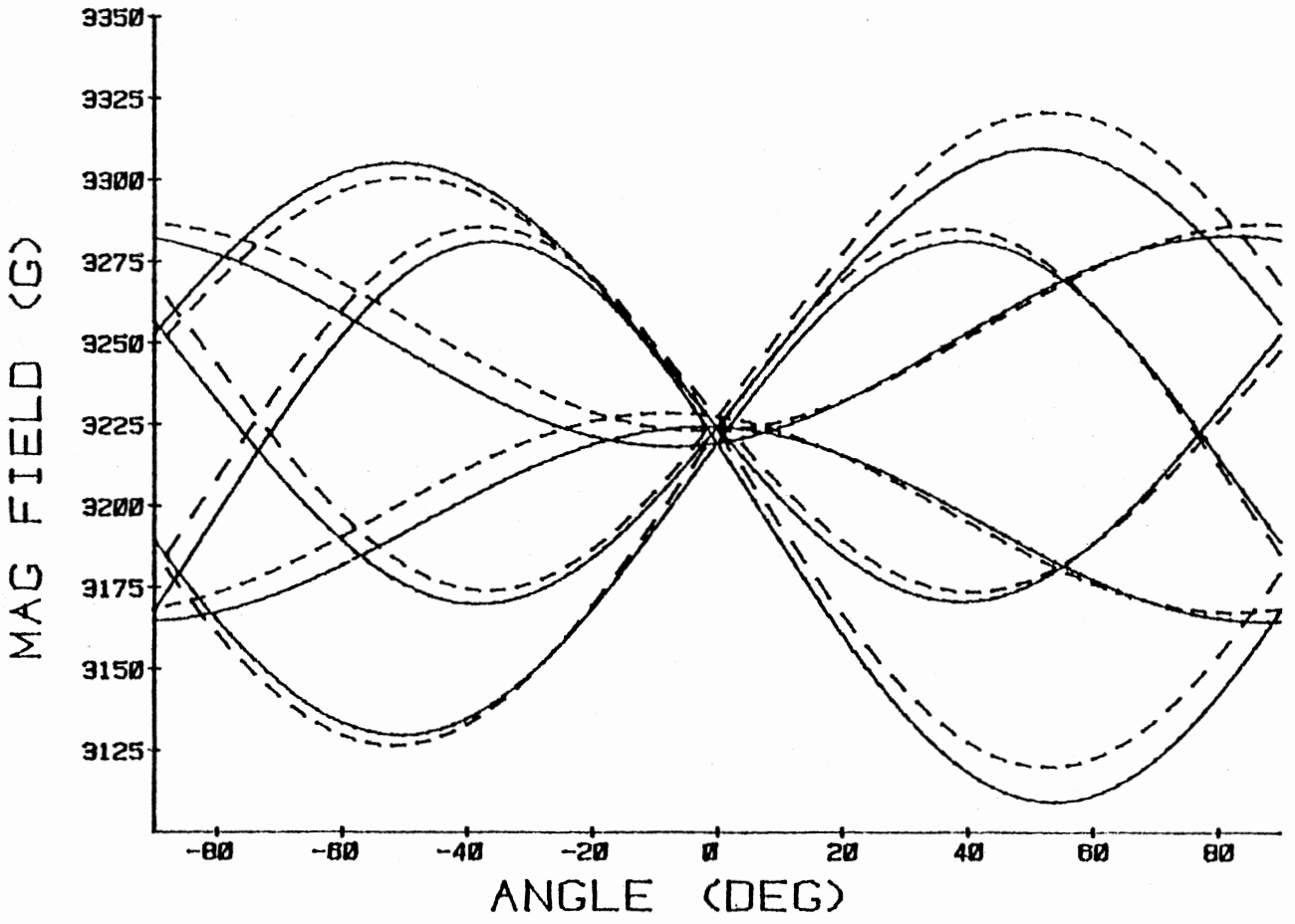

Figure 18. Calculated Low-field ^{29}Si Hyperfine Angular Dependence of the E_1'' Center for Rotation of the Magnetic Field in the X-plane. The Solid Curve Corresponds to Nucleus 1 and the Dashed Curve Corresponds to Nucleus 2. The Microwave Frequency is

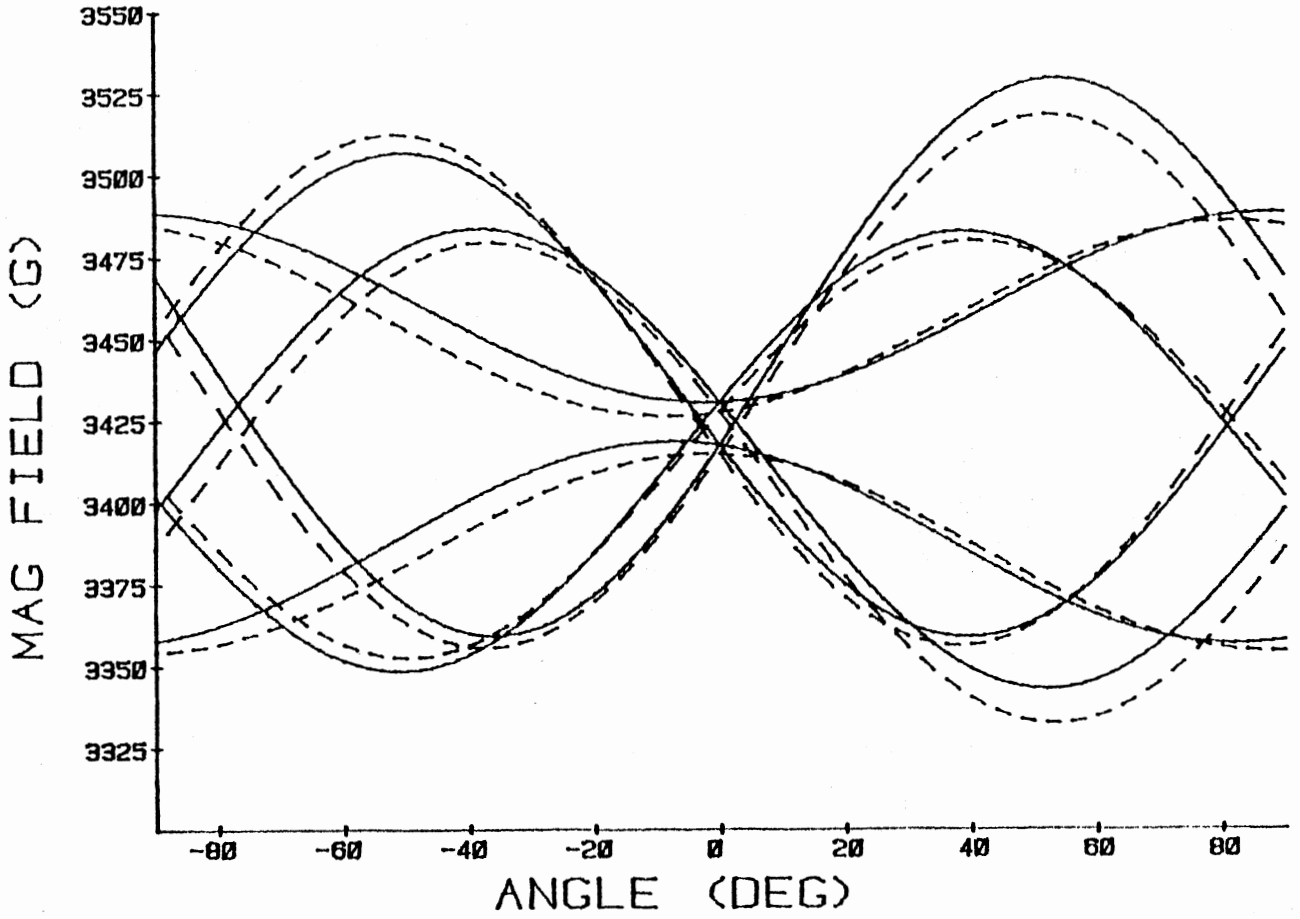

Figure 19. Calculated High-field ^{29}Si Hyperfine Angular Dependence of the E_1'' Center for Rotation of the Magnetic Field in the X-Plane. The Solid Curve Corresponds to Nucleus 1 and the Dashed Curve Corresponds to Nucleus 2. The Microwave Frequency is

18 and 19, respectively. The solid lines represent nucleus 1 and the dashed lines represent nucleus 2.

CHAPTER VI

DISCUSSION

It is concluded from the experimental results that the E" centers are S = 1 spin systems, interacting with two almost equivalent ^{29}Si nuclei with nuclear spin I = 1/2. The $\vec{g}$, $\vec{D}$ and $\vec{A}$ matrices have been determined for the E''_1 center and the $\vec{g}$ and $\vec{D}$ matrices for the E''_3 centers. Since the ESR spectra of the E" centers could be observed only if the sample had been irradiated at 300K prior to 77K irradiation, further detailed growth and pulse anneal studies not reported in this dissertation were performed by Dr. Robert B. Bossoli and the present author. It was possible to produce only very small concentrations of these E" centers in hydrogen-swept quartz crystals.

A variable-temperature electron irradiation between 77K and 300K of an as-grown Premium Q quartz sample was performed where each irradiation was followed by a short 77K irradiation. It was observed that the 77K irradiation by itself will not produce the E" centers unless the sample has previously received an electron irradiation above 200K. This is the temperature at which the alkali interstitial ions become mobile under electron irradiation, as reported by Markes and Halliburton in the ESR studies of the $[Al_{e+}]^{o}$ centers in quartz (25). Since the E" centers have not been observed in Sawyer-swept Premium Q samples, it suggests that alkalis (Na^{+},Li^{+}) must be present in the quartz samples and must be removed from the Al^{3+} substitutional ions

(by the above-200K irradiation) in order for the E" centers to be formed. No hyperfine ESR lines due to alkalis (Na is 100% abundant and Li is 93% abundant, both with nuclear spin I = 3/2) were observed for the E" centers even though the ESR linewidth is less than 0.05 gauss. Thus far, it has been impossible to determine the precise role of the alkalis in the formation or stabilization of the E" centers.

It has also been observed that if we keep a sample, which has E" centers, at 300K for a few days then the E_1'' and E_3'' centers slowly convert into E_1' centers, whereas the E_2'' centers convert into the E_2' and the E_4' centers. This conversion suggest a correlation between the S = 1 spin systems and the S = 1/2 spin systems. But, during pulse anneal studies, it was observed that the E_2'' centers decay at $40^{\circ}C$ while the E_1'' and E_3'' centers decay at $90^{\circ}C$ and none of the E' (S = 1/2) centers seem to grow in while the E" centers are decaying. The concentration of the E" centers is approximately the same as the concentration of the E_1' center obtained after a $350^{\circ}C$ anneal. The conversion of E" to E' centers seems to be a complicated process. And the dynamics of this process are not yet understood well.

A simple way to look at the S = 1 centers is that there are two S = 1/2 centers at a distance r from each other. An approximation to the value of r can be made by examining the D matrix. The electron dipole-electron dipole contribution to $\vec{D}$ is given by

$$\vec{D} = (g^2\beta^2/2) \begin{bmatrix} \left\langle \frac{r^2-3x^2}{5} \right\rangle & \left\langle - \frac{3xy}{5} \right\rangle & \left\langle - \frac{3xz}{5} \right\rangle \\ \left\langle - \frac{3xy}{5} \right\rangle & \left\langle \frac{r^2-3y^2}{5} \right\rangle & \left\langle - \frac{3yz}{5} \right\rangle \\ \left\langle - \frac{3xz}{r^5} \right\rangle & \left\langle - \frac{iyz}{r^5} \right\rangle & \left\langle \frac{r^2-3z^2}{r^5} \right\rangle \end{bmatrix} r$$

where x, y, and z are the components of the position vector r between the two electrons. The integrals are over the spatial distribution of the electron. In the point dipole approximation we have

$$D = -(3/2)D_{zz} = (3/4)g^2\beta^2(3\cos^2\theta - 1)\left\langle \frac{1}{R^3} \right\rangle$$

from which we get the value R, the separation of the electrons: by using the value of D obtained from fitting the spin-Hamiltonian:

$$R = 4.85\text{Å} \text{ at room temperature for the } E_1'' \text{ center}$$

$$R = 8.03\text{Å} \text{ at room temperature for the } E_3'' \text{ center}$$

Taking into account the value of R and the principal directions of $\vec{g}$, $\vec{D}$, $\vec{A}_{^{29}Si_1}$, and $\vec{A}_{^{29}Si_2}$, a plausible model for the E_1'' center is shown in Figure 20. It is suggested that two oxygens and a silicon are missing from the cluster and the two electrons are in the sp^3 hybrid orbitals extending from Si(1) and Si(2). The separation between Si(1) and Si(2) is 5.78Å as reported in Table III. Each hybrid orbital extends approximately 0.6Å out from the silicon. Taking this extension of sp^3 hybrid orbitals into account, the separation between the two unpaired electrons is 4.58Å. This separation is about 5% from the predicted separation 4.85Å. This discrepancy could be explained by taking into consideration the relaxation effects associated with the lattice. The possible model proposed for the E_1'' center has a net charge of -2. Numerical values of the different principle axes directions and Si-O and Si-Si directions are presented in Table XV for comparison.

The precursor of this center could possibly consist of the two oxygen and one silicon vacancies with charge compensating impurities

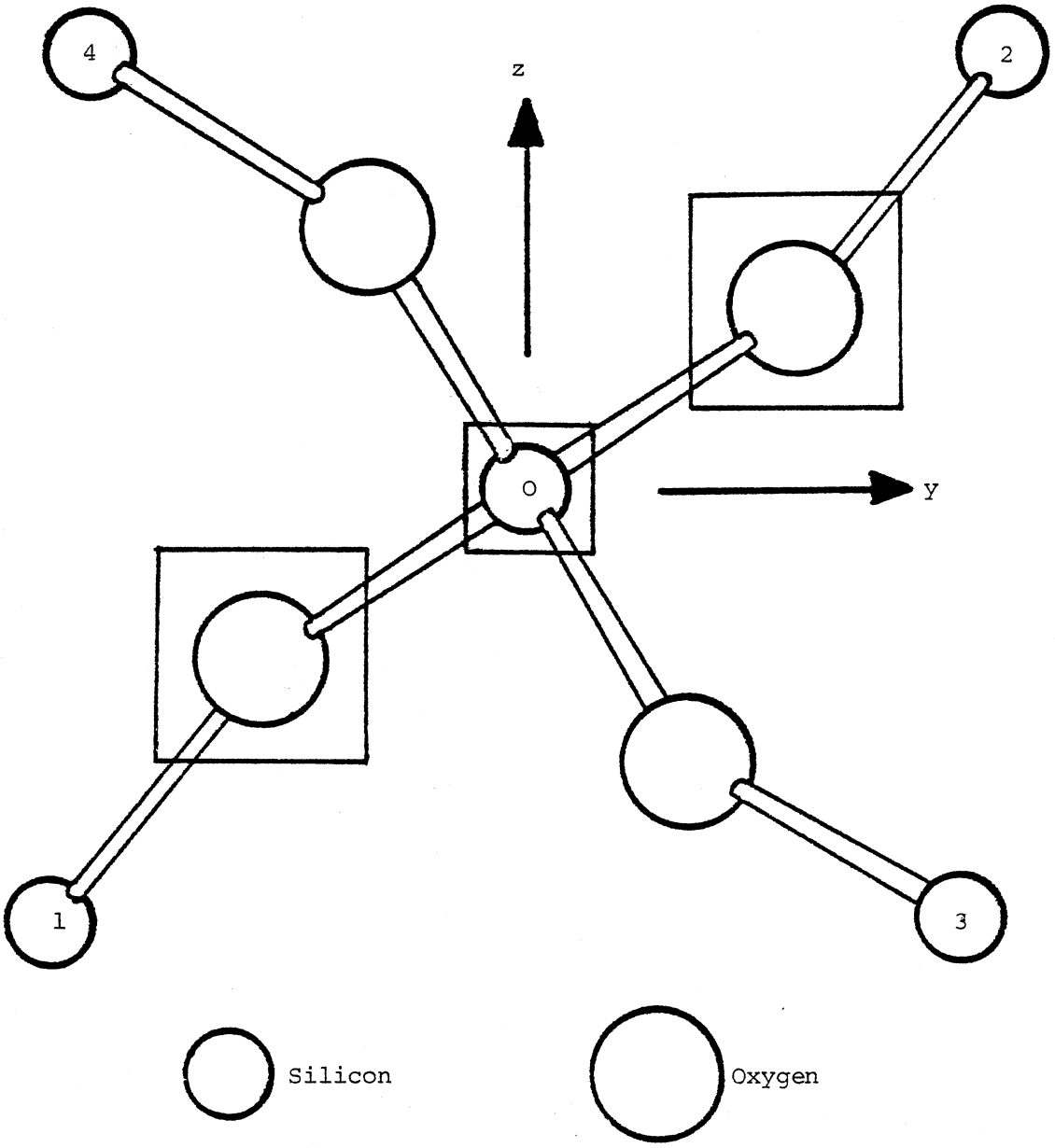

Figure 20. Proposed Model for the E_1'' Center. One Electron is Located on Si(1) and the Other is Located on Si(2)

TABLE XV

SUMMARY OF DISTANCES AND DIRECTIONS FOR VARIOUS SILICON-SILICON AND SILICON-OXYGEN PAIRS IN QUARTZ, AND COMPARISON WITH Z-COMPONENT DIRECTIONS OF THE SPIN HAMILTONIAN MATRICES OF THE E_1'' CENTER

Atoms	Distance	θ	ϕ
Si(1)-Si(2)	5.7764Å	51.39	90.0°
Si(1)-Si(O)	3.0585Å	53.9°	65.97°
Si(1)-Ox[1,O]	1.61221Å	43.99°	86.28°
Ox[2,O]-Si(2)	1.61221Å	43.99°	93.71°
Ox[1,O]-Si(2)	4.1853Å	54.3°	91.2°
Si(1)-Ox[2,O]	4.185Å	54.26°	88.77°

	θ	ϕ
g_z	57.77°	61.9°
D_z	56.05	63.5°
A_{1_z}	63.0°	86.5°
A_{2_z}	61.0°	36.5°

nearby. It has been observed by Sibley, et al. (26) that two infrared bands, at 3367 cm^{-1} and 3306 cm^{-1}, appear with irradiation at temperatures above 180K, which is the same temperature reported by Markes and Halliburton (20) for movement of alkalis away from Al^{3+} ions. Kats (27) has postulated that these two infrared bands are due to OH^- ions in the vicinity of Al^{3+} ions, with no alkali ions nearby. This model can be explained in the following manner. Alkali ions near Al^{3+} ions are moved away by irradiation above 180K and are replaced by H^+ ions or holes trapped in the non-bonding orbitals of neighboring oxygen ions. We have observed that it is very difficult to form the E" centers in hydrogen-swept quartz crystals. Thus it is not possible to form the E" centers unless one is able to move hydrogen in the crystal. This fact along with the appearance of the two Al-OH^- infrared bands for irradiations above 180K suggests that the protons may be somehow associated with the precursors of the E" center. A variety of such models are conceivable.

A similar type of model is reasonable for the E_3'' center except for the fact that the two unpaired electrons are separated by 8.033Å. For this center also there are two slightly inequivalent ^{29}Si nuclei giving rise to hyperfine ESR spectra. Since the concentration of this center is almost one third that of the E_1'' center it was not possible to collect experimental data for evaluating the $\vec{A}_{^{29}Si}$ matrices. A plausible model for the E_3'' center is shown in Figure 21 taking into account the separation between the two dipoles and the z-components directions for the $\vec{g}$ and $\vec{D}$ matrices.

It has also been observed in our study that the separation of the c-axis primary lines of the E_1'' center increases from 5.00G at room

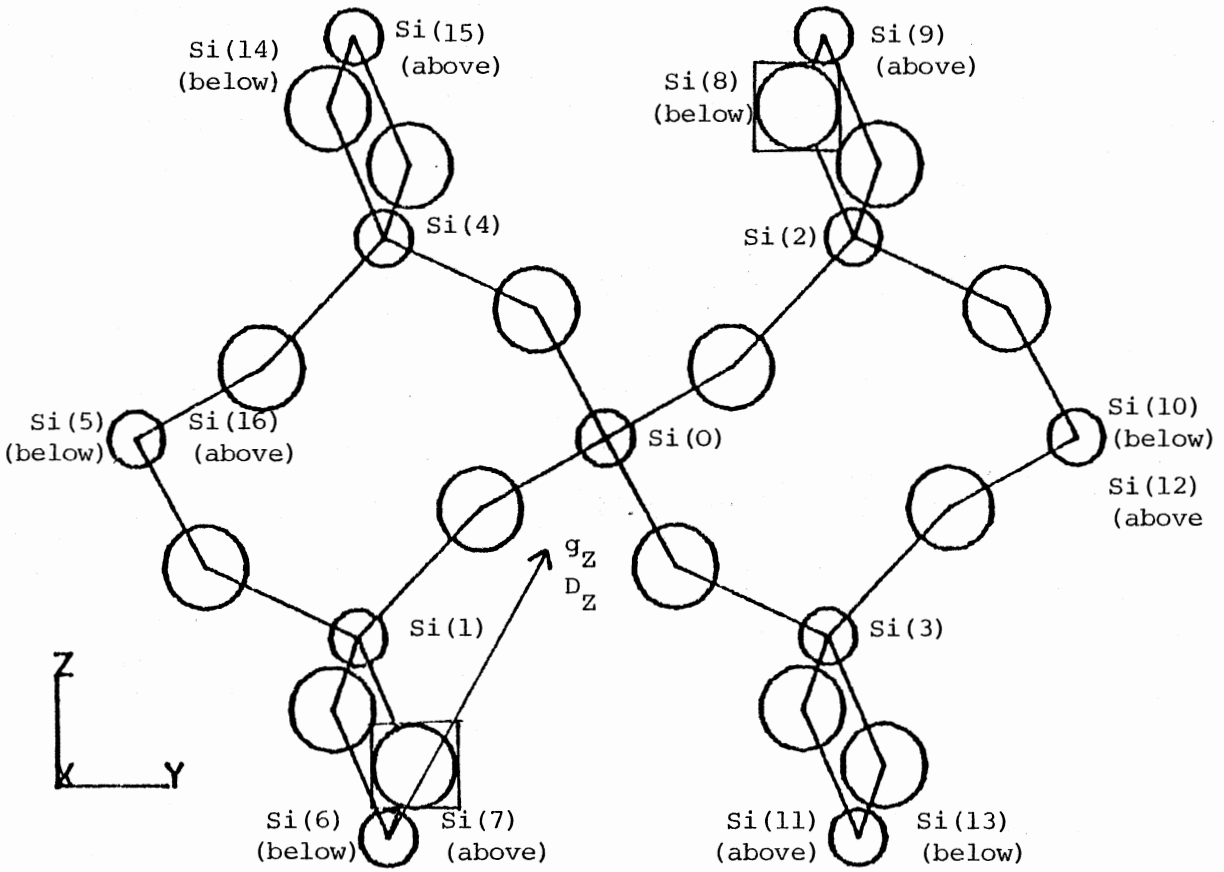

Figure 21. Proposed Model for the E_3'' Center

temperature to approximately 7.40G at about 90K. Hence, calculations of the principal values and directions for the $\vec{g}$, $\vec{D}$ and $\vec{A}$ matrices at 90K will enable one to shed more light on the defect structure and associated relaxation effects of the lattice. The correlation of the ESR results for the E_1'' centers with known results for the E' (S = 1/2) and $[Al_{e+}]$ centers will help to determine the role of the E" centers in the overall response of high-quality quartz to radiation.

REFERENCES

1. Fowler, W. B., Physics of Color Centers (Academic Press, New York, 1968).

2. Henderson, B. and J. E. Wertz, Defects in Alkaline-Earth Oxides

3. Zavoisky, E., Fiz. Zh. 9, 211, 245 (1945).

4. Abragam, A. and B. Bleaney, Electron Paramagnetic Resonance of Transition Ions (Clarendon Press, Oxford, 1970).

5. Wertz, J. E. and J. R. Bolton, Electron Spin Resonance; Elementary Theory and Practical Applications (McGraw-Hill Book Company, 1972).

6. Pake, G. E. and T. L. Estle, The Physical Principles of Electron Paramagnetic Resonance (Second Edition, W. A. Benjamin, Inc., 1973).

7. Poole, C. P., Jr., Electron Spin Resonance (John Wiley and Sons, 1967).

8. Weeks, R. A., J. Appl. Phys. 27, 1376 (1956).

9. Weeks, R. A. and C. M. Nelson, J. Am. Ceram. Soc. 43, 399 (1960).

10. Silsbee, R. H., J. Appl. Phys. 32, 1459 (1961).

11. Feigl, F. J., W. B. Fowler and K. L. Yip, Solid State Commun. 14, 225 (1974).

12. Yip, K. L. and W. B. Fowler, Phys. Rev. B11, 2327 (1975).

13. Weeks, R. A., Phys. Rev. 130, 570 (1963).

14. Castle, J. G., Jr., D. W. Feldman, D. G. Klemens, and R. A. Weeks, Phys. Rev. 130, 577 (1963).

15. Feigl, F. J., J. H. Anderson, J. Phys. Chem. Solids 31, 575 (1970).

16. Isoya, J., J. A. Weil and L. E. Halliburton, J. Chem. Physics 74, 5436 (1981).

17. Weeks, R. A. and M. M. Abraham, Solid State Division Annual Progress Report, Oak Ridge National Laboratory, USA, p. 36 (1964).

18. Weeks, R. A. and M. M. Abraham, Bull. Am. Phys. Soc. 10, 374 (1965).

19. Solntsoev, V. P., R. I. Mashkovtsev and M. Ya. Schlerbakova, J. Structural Chem. 18, 578 (1977), translated from Zhurnal Strukturnoi Khimii, 18, 729 (1977).

20. Megaw, H. D. Crystal Structures: A Working Approach (W. B. Saunders Co., 1973).

21. Cohen, A. J. and G. G. Summer, Amer. Min. 43, 58 (1958).

22. Wyckoff, R. W. G., Crystal Structures, Second Edition, Vol. 1 (1963).

23. Lepage, Y. and G. Donnay, Acta Crysta. B 32, 2456 (1976).

24. Nuttal, R. H. D., Ph.D. Dissertation, University of Saskatchewan.

25. Markes, M. and L. E. Halliburton, J. Appl. Phys. 50, 8172 (1979).

26. Sibley, W. A., J. J. Martin, M. C. Wintersgill and J. D. Brown, J. of Appl. Physics 50, 5449 (1979).

27. Kats, A. Phillips Res. Rep. 17, 133 (1962).

APPENDIX A

LISTING OF THE LINE POSITION PROGRAM

FOR AN S=1 SPIN SYSTEM

```
//U12105A  JOB (77777,448-70-3751),'JANI',CLASS=K,TIME=(2,00),
// MSGCLASS=X,NOTIFY=U12105A
/*PASSWORD ?
//   EXEC  FORTGCLG
//FORT.SYSIN DD *
      IMPLICIT  REAL * 8 (A-H,O-Z)
      REAL * 8 AR(3,3),AI(3,3),E(3),E2(3),TAL(2,3),D(3),HF(3),P(12),
     CG(3,3),H(3,3),RM(3,3),R2(3,3),R3(3,3),RT(3,3),TG(3,3),TH(3,3),
     CR(3,3)
C     THE PARAMETERS FOR THE G TENSOR ARE 1-GX, 2-GY, 3-GZ, 4-THETA,
C     5-PHI, 6-PSI.  THE PARAMETERS FOR THE FINE-STRUCTURE TENSOR ARE
C     7-DX, 8-DY, 9-DZ,10-THETA, 11-PHI, 12-PSI.
C
      P(1)=2.00041D+00
      P(2)=2.00062D+00
      P(3)=2.001387D+00
      P(4)=57.77D+00
      P(5)=31.92D+00
      P(6)=92.13D+00
      P(7)=109.955D+00
      P(8)=117.601D+00
      P(9)=-227.557D+00
      P(10)=56.05D+00
      P(11)=33.48D+00
      P(12)=95.16D+00
      WRITE(6,10) (P(I),I=1,12)
   10 FORMAT (12F10.5)
      B=9.27410D+00/6.6262D+00
      FREQ=9.1146D+03
      N=3
      NM=3
      NN=1
      ALPHA= 0.0D+00
      BETA= -90.0D+00
C
C           CHANGE ANGLES IN DEGREES TO RADIANS.
C
      DO  91  L=1,3
      P(L+3)=P(L+3)*(3.141590D+00/1.8D+02)
   91 P(L+9)=P(L+9)*(3.141590D+00/1.8D+02)
C
C           SET UP ROTATION MATRICES G(3,3), H(3,3),
C           RM(3,3).
C
      AG=DSIN(P(4))
      AAG=DCOS(P(4))
      CG=DSIN(P(5))
      CCG=DCOS(P(5))
      FG=DSIN(P(6))
      FFG=DCOS(P(6))
      AH=DSIN(P(10))
      AAH=DCOS(P(10))
      CH=DSIN(P(11))
      CCH=DCOS(P(11))
      FH=DSIN(P(12))
      FFH=DCOS(P(12))
      CO=DCOS(2.094395D+00)
      SI=DSIN(2.094395D+00)
      G(1,1)=FFG*CCG-AAG*CG*FG
      G(1,2)=FFG*CG+AAG*CCG*FG
      G(1,3)=FG*AG
      G(2,1)=-FG*CCG-AAG*CG*FFG
      G(2,2)=-FG*CG+AAG*CCG*FFG
      G(2,3)=FFG*AG
```

```
      G(3,1)=AG*CG
      G(3,2)=-AG*CCG
      G(3,3)=AAG
      H(1,1)=FFH*CCH-AAH*CH*FH
      H(1,2)=FFH*CH+AAH*CCH*FH
      H(1,3)=FH*AH
      H(2,1)=-FH*CCH-AAH*CH*FFH
      H(2,2)=-FH*CH+AAH*CCH*FFH
      H(2,3)=FFH*AH
      H(3,1)=AH*CH
      H(3,2)=-AH*CCH
      H(3,3)=AAH
   20 ALPHAR=ALPHA*(3.14159D+00/1.80D+02)
      BETAR=BETA*(3.14159D+00/1.8D+02)
      WRITE(6,30) ALPHA, BETA
   30 FORMAT('0',2F15.3)
C
C           SET UP MAGNETIC FIELD ROTATION MATRIX RM(3,3).
C
      RM(1,1)=DCOS(ALPHAR)
      RM(1,2)=-DSIN(ALPHAR)*DSIN(BETAR)
      RM(1,3)=DSIN(ALPHAR)*DCOS(BETAR)
      RM(2,1)=0.0D+00
      RM(2,2)=DCOS(BETAR)
      RM(2,3)=DSIN(BETAR)
      RM(3,1)=-DSIN(ALPHAR)
      RM(3,2)=-DCOS(ALPHAR)*DSIN(BETAR)
      RM(3,3)=DCOS(ALPHAR)*DCOS(BETAR)
      K = 1
   40 GO TO (50,50,50,60,60,60),K
   50 R2(1,1)=1.0D+00
      R2(1,2)=0.0D+00
      R2(1,3)=0.0D+00
      R2(2,1)=0.0D+00
      R2(2,2)=1.0D+00
      R2(2,3)=0.0D+00
      R2(3,1)=0.0D+00
      R2(3,2)=0.0D+00
      R2(3,3)=1.0D+00
      GO TO (70,80,90),K
   60 R2(1,1)=1.0D+00
      R2(1,2)=0.0D+00
      R2(1,3)=0.0D+00
      R2(2,1)=0.0D+00
      R2(2,2)=-1.0D+00
      R2(2,3)=0.0D+00
      R2(3,1)=0.0D+00
      R2(3,2)=0.0D+00
      R2(3,3)=-1.0D+00
      KK = K-3
      GO TO (70,80,90),KK
   70 R3(1,1)=1.0D+00
      R3(1,2)=0.0D+00
      R3(1,3)=0.0D+00
      R3(2,1)=0.0D+00
      R3(2,2)=1.0D+00
      R3(2,3)=0.0D+00
      R3(3,1)=0.0D+00
      R3(3,2)=0.0D+00
      R3(3,3)=1.0D+00
      GO TO 100
   80 R3(1,1)=CO
      R3(1,2)=SI
      R3(1,3)=0.0D+00
      R3(2,1)=-SI
      R3(2,2)=CO
```

```
      R3(2,3)=0.0D+00
      R3(3,1)=0.0D+00
      R3(3,2)=0.0D+00
      R3(3,3)=1.0D+00
      GO TO 100
   90 R3(1,1)=CO
      R3(1,2)=-SI
      R3(1,3)=0.0D+00
      R3(2,1)=SI
      R3(2,2)=CO
      R3(2,3)=0.0D+00
      R3(3,1)=0.0D+00
      R3(3,2)=0.0D+00
      R3(3,3)=1.0D+00
  100 DO 110 L=1,3
      DO 110 M=1,3
  110 RT(L,M)=R2(L,1)*R3(1,M)+R2(L,2)*R3(2,M)+R2(L,3)*R3(3,M)
      DO 120 L=1,3
      DO 120 M=1,3
  120 R(L,M)=RT(L,1)*RM(1,M)+RT(L,2)*RM(2,M)+RT(L,3)*RM(3,M)
      DO 130 L=1,3
      DO 130 M=1,3
      TG(L,M)=G(L,1)*R(1,M)+G(L,2)*R(2,M)+G(L,3)*R(3,M)
  130 TH(L,M)=H(L,1)*R(1,M)+H(L,2)*R(2,M)+H(L,3)*R(3,M)
      I=1
  140 HH=4.00D+03
  150 W1=8*HH*(P(1)*TG(1,1)*TG(1,3)+P(2)*TG(2,1)*TG(2,3)+P(3)*TG(3,1)*
     CTG(3,3))
      W2=8*HH*(P(1)*TG(1,2)*TG(1,3)+P(2)*TG(2,2)*TG(2,3)+P(3)*TG(3,2)*
     CTG(3,3))
      W3=8*HH*(P(1)*TG(1,3)*TG(1,3)+P(2)*TG(2,3)*TG(2,3)+P(3)*TG(3,3)*
     CTG(3,3))
      W4=P(7)*TH(1,1)*TH(1,1)+P(8)*TH(2,1)*TH(2,1)+P(9)*TH(3,1)*TH(3,1)
      W5=P(7)*TH(1,2)*TH(1,2)+P(8)*TH(2,2)*TH(2,2)+P(9)*TH(3,2)*TH(3,2)
      W6=P(7)*TH(1,3)*TH(1,3)+P(8)*TH(2,3)*TH(2,3)+P(9)*TH(3,3)*TH(3,3)
      W7=P(7)*TH(1,2)*TH(1,1)+P(8)*TH(2,2)*TH(2,1)+P(9)*TH(3,2)*TH(3,1)
      W8=P(7)*TH(1,1)*TH(1,3)+P(8)*TH(2,1)*TH(2,3)+P(9)*TH(3,1)*TH(3,3)
      W9  =P(7)*TH(1,3)*TH(1,2)+P(8)*TH(2,3)*TH(2,2)+P(9)*TH(3,3)*
     CTH(3,2)
      Q1R=W1/2.0D+00
      Q1I= W2/2.0D+00
      Q2R=(W4-W5)/4.0D+00
      Q2I=W7/2.0D+00
      Q3R=(W4+W5)/4.0D+00
      Q4R=W8/2.0D+00
      Q4I=W9/2.0D+00
      DO 160 L=1,3
      DO 160 M=1,3
      AR(L,M)= 0.0D+00
  160 AI(L,M)= 0.0D+00
C
C           SET UP REAL AND IMAGINARY MATRIX ELEMENTS
C           AR(3,3), AI(3,3).
C
      AR(1,1)=W3+W6+2*Q3R
      AR(2,1)=(Q1R+Q4R)*DSQRT(2.0D+00)
      AI(2,1)=(Q1I+Q4I)*DSQRT(2.0D+00)
      AR(2,2)=4*Q3R
      AR(3,1)=2*Q2R
      AI(3,1)=2*Q2I
      AR(3,2)=(Q1R-Q4R)*DSQRT(2.0D+00)
      AI(3,2)=(Q1I-Q4I)*DSQRT(2.0D+00)
      AR(3,3)=W6-W3+(2*Q3R)
C
C           DIAGONALIZE SPIN-ENERGY MATRIX.
C
```

```
      CALL   HTRIDI  (NM,N,AR,AI,D,E,E2,TAU)
      CALL   IMTQL1  (N,D,E,IERR)
      GO TO (170,180),I
  170 FREQ=D(2)-D(1)
      GO TO 210
  180 FREQ=D(3)-D(2)
  210 IF(CABS(FREQQ-FREQ)-1.00-03)220,220,230
  220 HF(I)=HH
      GO TO 240
  230 HH=HH*(FREQQ/FREQ)
      GO TO 150
  240 IF(I-2)250,260,260
  250 I=I+1
      GO TO 140
  260 DIFF=DABS(HF(1)-HF(2))
      WRITE(6,270)  (HF(I),I=1,2),DIFF
  270 FORMAT(3F20.4)
      IF(K-3)280,290,290
  280 K=K+1
      GO TO 40
  290 BETA=BETA+10.0D+00
      IF(BETA-91.0D+00)20,300,300
  300 WRITE(6,310) (P(I),I=1,12)
  310 FORMAT('0',12F10.5)
      STOP
      END
//LKED.SSP DD DSNAME=OSU.ACT12105.ESPLIB,DISP=SHR
//
```

APPENDIX B

LISTING OF THE FITTING PROGRAM

FOR AN S=1 SPIN SYSTEM

```
//U12105A  JOB (?????,448-70-3751),'JANI',CLASS=K,TIME=(4,00),
//  MSGCLASS=X,NOTIFY=U12105A
/*PASS#GRD ?
//   EXEC  FORTGCLG
//FORT.SYSIN DD *
C
C           THIS PROGRAM FITS SPIN-HAMILTONIAN
C           TO ESR DATA FOR S=1 DEFECT.
C
      IMPLICIT  REAL * 8 (A-H,O-Z)
      REAL * 8 AR(3,3),AI(3,3),E(3),E2(3),TAU(2,3),D(3),HF(3),P(20),
     CG(3,3),H(3,3),RM(3,3),R2(3,3),R3(3,3),RT(3,3),TG(3,3),TH(3,3),
     CR(3,3),FREQ1(46),FREQQ(46)
C     THE PARAMETERS FOR THE G TENSOR ARE 1-GX, 2-GY, 3-GZ, 4-THETA,
C     5-PHI, 6-PSI.  THE PARAMETERS FOR THE FINE-STRUCTURE TENSOR ARE
C     7-D, 8-E, 9-THETA, 10-PHI, 11-PSI, 12-19 REPRESENT ANGLES
C     BETWEEN THE MAGNETIC FIELD AND THE C-AXIS OF CRYSTAL.
C
      P(1)=2.00041D+00
      P(2)=2.00062D+00
      P(3)=2.001385D+00
      P(4)=87.75D+00
      P(5)=32.00+00
      P(6)=92.1D+00
      P(7)=341.355D+00
      P(8)=3.8D+00
      P(9)=56.05D+00
      P(10)=33.5D+00
      P(11)=85.1D+00
      P(12)=69.76D+00
      P(13)=59.76D+00
      P(14)=39.88D+00
      P(15)=19.94D+00
      P(16)=-19.94D+00
      P(17)=-39.86D+00
      P(18)=-59.78D+00
      P(19)=-69.72D+00
      B=9.2741D+00/6.6262D+00
      N=3
      NN=3
      ALPHA= 0.0D+00
C
C           CHANGE ANGLES IN DEGREES TO RADIANS.
C
      DO  91  L=1,3
      P(L+3)=P(L+3)*(3.141590D+00/1.8D+02)
   91 P(L+9)=P(L+9)*(3.141590D+00/1.8D+02)
      DO 11 M=1,8
   11 P(M+12)=P(M+12)*(3.141590D+00/1.8D+02)
      WRITE(6,10) (P(I),I=1,20)
   10 FORMAT (6F10.5)
   92 DO 93 LL=1,19
   94 K1=1
   95 MM=1
   96 GO TO (351,352,353,354,355,356,357,358,359,360,361,362,
     C363,364,365,366,367,368,369,370,371,372,373,374,375,376,377,378,
     C379,380,381,382,383,384,385,386,387,388,389,390,391,392,393,
     C394,395,396),MM
C
  351 MM=3276.40D+00
      BETAR=P(12)
      K=1
      I=1
      FREQQ(1)=9.114954D+03
```

```
      GO TO 97
  352 HH=3232.106D+00
      I=2
      FREQQ(2)=9.1149549D+03
      GO TO 97
  353 HH=3170.36D+00
      K=2
      I=1
      FREQQ(3)=9.1149567D+03
      GO TO 97
  354 HH=3337.14D+00
      I=2
      FREQQ(4)=9.1149541D+03
      GO TO 97
  355 HH=3312.39D+00
      K=3
      I=1
      FREQQ(5)=9.1149530+03
      GO TO 97
  356 HH=3195.71D+00
      I=2
      FREQQ(6)=9.1149560+03
      GO TO 97
C
C
  357 HH=3236.06D+00
      BETAR=P(13)
      K=1
      I=1
      FREQQ(7)=9.1149937D+03
      GO TO 97
  358 HH=3213.13D+00
      I=2
      FREQQ(8)=9.1150D+03
      GO TO 97
  359 HH=3159.53D+00
      K=2
      I=1
      FREQQ(9)=9.1150115D+03
      GO TO 97
  360 HH=3348.16D+00
      I=2
      FREQQ(10)=9.1149850+03
      GO TO 97
  361 HH=3306.57D+00
      K=3
      I=1
      FREQQ(11)=9.1149901D+03
      GO TO 97
  362 HH=3202.59D+00
      I=2
      FREQQ(12)=9.1150053D+03
      GO TO 97
C
C
  363 HH=3314.24D+00
      BETAR=P(14)
      K=1
      I=1
      FREQQ(13)=9.1151003D+03
      GO TO 97
  364 HH=3195.84D+00
      I=2
      FREQQ(14)=9.1151183D+03
      GO TO 97
  365 HH=3185.32D+00
```

```
      K=2
      I=1
      FREQQ(15)=9.1151215D+03
      GO TO 97
  366 HH=3342.74D+00
      I=2
      FREQQ(16)=9.1150987D+03
      GO TO 97
  367 HH=3287.03D+00
      K=3
      I=1
      FREQQ(17)=9.1151012D+03
      GO TO 97
  368 HH=3222.13D+00
      I=2
      FREQQ(18)=9.1151099D+03
      GO TO 97
C
C
  369 HH=3238.77D+00
      BETAR=P(15)
      K=1
      I=1
      FREQQ(19)=9.1152169D+03
      GO TO 97
  370 HH=3211.05D+00
      I=2
      FREQQ(20)=9.1152218D+03
      GO TO 97
  371 HH=3203.60+00
      K=2
      I=1
      FREQQ(21)=9.1152273D+03
      GO TO 97
  372 HH=3304.70D+00
      I=2
      FREQQ(22)=9.1152178D+03
      GO TO 97
  373 HH=3267.46D+00
      K=3
      I=1
      FREQQ(23)=9.1152201D+03
      GO TO 97
  374 HH=3241.58D+00
      I=2
      FREQQ(24)=9.1152240D+03
      GO TO 97
C
C
  375 HH=3256.69D+00
      BETAR=0.0D+00
      K=2
      I=1
      FREQQ(25)=9.1146013D+03
      GO TO 97
  376 HH=3251.68D+00
      I=2
      FREQQ(26)=9.1146035D+03
      GO TO 97
C
C
  377 HH=3260.21D+00
      BETAR=P(16)
      K=3
      I=1
      FREQQ(27)=9.1145946D+03
```

```
      GO TO 97
  378 HH=3248.140+00
      I=2
      FREQQ(28)=9.1145552D+03
      GO TO 97
C
C
  379 HH=3175.730+00
      BETAR=P(17)
      K=1
      I=1
      FREQQ(29)=9.1145659D+03
      GO TO 97
  380 HH=3331.740+00
      I=2
      FREQQ(30)=9.1145571D+03
      GO TO 97
  381 HH=3313.860+00
      K=2
      I=1
      FREQQ(31)=9.1145558D+03
      GO TO 97
  382 HH=3195.750+00
      I=2
      FREQQ(32)=9.1145661D+03
      GO TO 97
  383 HH=3276.120+00
      K=3
      I=1
      FREQQ(33)=9.1145617D+03
      GO TO 97
  384 HH=3232.380+00
      I=2
      FREQQ(34)=9.1145609D+03
      GO TO 97
C
C
  385 HH=3173.940+00
      BETAR=P(18)
      K=1
      I=1
      FREQQ(35)=9.1145077D+03
      GO TO 97
  386 HH=3333.590+00
      I=2
      FREQQ(36)=9.1144997D+03
      GO TO 97
  387 HH=3290.680+00
      K=2
      I=1
      FREQQ(37)=9.1145014D+03
      GO TO 97
  388 HH=3218.240+00
      I=2
      FREQQ(38)=9.1145014D+03
      GO TO 97
  389 HH=3297.090+00
      K=3
      I=1
      FREQQ(39)=9.1145016D+03
      GO TO 97
  390 HH=3211.240+00
      I=2
      FREQQ(40)=9.1145029D+03
      GO TO 97
C
```

```
C
  391 HH=3135.51D+00
      BETAR=P(19)
      K=1
      I=1
      FREQQ(41)=9.1151497D+03
      GO TO 97
  392 HH=3322.34D+00
      I=2
      FREQQ(42)=9.1151377D+03
      GO TO 97
  393 HH=3268.68D+00
      K=2
      I=1
      FREQQ(43)=9.1151423D+03
      GO TO 97
  394 HH=3240.25D+00
      I=2
      FREQQ(44)=9.1151460+03
      GO TO 97
  395 HH=3306.50D+00
      K=3
      I=1
      FREQQ(45)=9.1151389D+03
      GO TO 97
  396 HH=3202.90D+00
      I=2
      FREQQ(46)=9.1151451D+03
C
C          SET UP ROTATION MATRICES G(3,3), F(3,3), RM(3,3).
C
   97 AG=DSIN(P(4))
      AAG=DCOS(P(4))
      CG=DSIN(P(5))
      CCG=DCOS(P(5))
      FG=DSIN(P(6))
      FFG=DCOS(P(6))
      AH=DSIN(P(10))
      AAH=DCOS(P(10))
      CH=DSIN(P(11))
      CCH=DCOS(P(11))
      FH=DSIN(P(12))
      FFH=DCOS(P(12))
      CC=DCOS(2.094395D+00)
      SI=DSIN(2.094395D+00)
      G(1,1)=FFG*CCG-AAG*CG*FG
      G(1,2)=FFG*CG+AAG*CCG*FG
      G(1,3)=FG*AG
      G(2,1)=-FG*CCG-AAG*CG*FFG
      G(2,2)=-FG*CG+AAG*CCG*FFG
      G(2,3)=FFG*AG
      G(3,1)=AG*CG
      G(3,2)=-AG*CCG
      G(3,3)=AAG
      H(1,1)=FFH*CCH-AAH*CH*FH
      H(1,2)=FFH*CH+AAH*CCH*FH
      H(1,3)=FH*AH
      H(2,1)=-FH*CCH-AAH*CH*FFH
      H(2,2)=-FH*CH+AAH*CCH*FFH
      H(2,3)=FFH*AH
      H(3,1)=AH*CH
      H(3,2)=-AH*CCH
      H(3,3)=AAH
   20 ALPHAR=ALPHA*(3.14159D+00/1.80D+02)
C
C          SET UP MAGNETIC FIELD ROTATION MATRIX RM(3,3).
```

```
C
      RM(1,1)=DCOS(ALPHAR)
      RM(1,2)=-DSIN(ALPHAR)*DSIN(BETAR)
      RM(1,3)=DSIN(ALPHAR)*DCOS(BETAR)
      RM(2,1)=0.0D+00
      RM(2,2)=DCOS(BETAR)
      RM(2,3)=DSIN(BETAR)
      RM(3,1)=-DSIN(ALPHAR)
      RM(3,2)=-DCOS(ALPHAR)*DSIN(BETAR)
      RM(3,3)=DCOS(ALPHAR)*DCOS(BETAR)
   40 GO TO (50,50,50,60,60,60),K
   50 R2(1,1)=1.0D+00
      R2(1,2)=0.0D+00
      R2(1,3)=0.0D+00
      R2(2,1)=0.0D+00
      R2(2,2)=1.0D+00
      R2(2,3)=0.0D+00
      R2(3,1)=0.0D+00
      R2(3,2)=0.0D+00
      R2(3,3)=1.0D+00
      GO TO (70,80,90),K
   60 R2(1,1)=1.0D+00
      R2(1,2)=0.0D+00
      R2(1,3)=0.0D+00
      R2(2,1)=0.0D+00
      R2(2,2)=-1.0D+00
      R2(2,3)=0.0D+00
      R2(3,1)=0.0D+00
      R2(3,2)=0.0D+00
      R2(3,3)=-1.0D+00
      KK = K-3
      GO TO (70,80,90),KK
   70 R3(1,1)=1.0D+00
      R3(1,2)=0.0D+00
      R3(1,3)=0.0D+00
      R3(2,1)=0.0D+00
      R3(2,2)=1.0D+00
      R3(2,3)=0.0D+00
      R3(3,1)=0.0D+00
      R3(3,2)=0.0D+00
      R3(3,3)=1.0D+00
      GO TO 100
   80 R3(1,1)=CO
      R3(1,2)=SI
      R3(1,3)=0.0D+00
      R3(2,1)=-SI
      R3(2,2)=CO
      R3(2,3)=0.0D+00
      R3(3,1)=0.0D+00
      R3(3,2)=0.0D+00
      R3(3,3)=1.0D+00
      GO TO 100
   90 R3(1,1)=CO
      R3(1,2)=-SI
      R3(1,3)=0.0D+00
      R3(2,1)=SI
      R3(2,2)=CO
      R3(2,3)=0.0D+00
      R3(3,1)=0.0D+00
      R3(3,2)=0.0D+00
      R3(3,3)=1.0D+00
  100 DO 110 L=1,3
      DO 110 M=1,3
  110 RT(L,M)=R2(L,1)*R3(1,M)+R2(L,2)*R3(2,M)+R2(L,3)*R3(3,M)
      DO 120 L=1,3
      DO 120 M=1,3
```

```
  120 R(L,M)=RT(L,1)*RM(1,M)+RT(L,2)*RM(2,M)+RT(L,3)*RM(3,M)
      DO 130 L=1,3
      DO 130 M=1,3
      TG(L,M)=G(L,1)*R(1,M)+G(L,2)*R(2,M)+G(L,3)*R(3,M)
  130 TH(L,M)=H(L,1)*R(1,M)+H(L,2)*R(2,M)+H(L,3)*R(3,M)
      DX=P(7)/3.0D+00-P(8)
      DY=P(7)/3.0D+00+P(8)
      DZ=-2.0D+00*P(7)/3.0D+00
  150 W1=8*HH*(P(1)*TG(1,1)*TG(1,3)+P(2)*TG(2,1)*TG(2,3)+P(3)*TG(3,1)*
     CTG(3,3))
      W2=8*HH*(P(1)*TG(1,2)*TG(1,3)+P(2)*TG(2,2)*TG(2,3)+P(3)*TG(3,2)*
     CTG(3,3))
      W3=8*HH*(P(1)*TG(1,3)*TG(1,3)+P(2)*TG(2,3)*TG(2,3)+P(3)*TG(3,3)*
     CTG(3,3))
      W4=DX*TH(1,1)*TH(1,1)+DY*TH(2,1)*TH(2,1)+DZ*TH(3,1)*TH(3,1)
      W5=DX*TH(1,2)*TH(1,2)+DY*TH(2,2)*TH(2,2)+DZ*TH(3,2)*TH(3,2)
      W6=DX*TH(1,3)*TH(1,3)+DY*TH(2,3)*TH(2,3)+DZ*TH(3,3)*TH(3,3)
      W7=DX*TH(1,2)*TH(1,1)+DY*TH(2,2)*TH(2,1)+DZ*TH(3,2)*TH(3,1)
      W8=DX*TH(1,1)*TH(1,3)+DY*TH(2,1)*TH(2,3)+DZ*TH(3,1)*TH(3,3)
      W9=DX*TH(1,3)*TH(1,2)+DY*TH(2,3)*TH(2,2)+DZ*TH(3,3)*TH(3,2)
      Q1R=W1/2.0D+00
      Q1I= W2/2.0D+00
      Q2R=(W4-W5)/4.0D+00
      Q2I=W7/2.0D+00
      Q3R=(W4+W5)/4.0D+00
      Q4R=W8/2.0D+00
      Q4I=W9/2.0D+00
      DO 160 L=1,3
      DO 160 M=1,3
      AR(L,M)= 0.0D+00
C
C             SET UP REAL AND IMAGINARY MATRIX
C             ELEMENTS  AR(3,3),AI(3,3).
C
  160 AI(L,M)= 0.0D+00
      AR(1,1)=W3+W6+2*Q3R
      AR(2,1)=(Q1R+C4R)*DSQRT(2.0D+00)
      AI(2,1)=(Q1I+C4I)*DSQRT(2.0D+00)
      AR(2,2)=4*Q3R
      AR(3,1)=2*Q2R
      AI(3,1)=2*Q2I
      AR(3,2)=(Q1R-C4R)*DSQRT(2.0D+00)
      AI(3,2)=(Q1I-C4I)*DSQRT(2.0D+00)
      AR(3,3)=W6-W3+(2*Q3R)
C
C             DIAGONALIZE SPIN-ENERGY MATRIX A(3,3).
C
      CALL  HTRIDI (NM,N,AR,AI,D,E,E2,TAU)
      CALL  IMTQL1  (N,D,E,IERR)
      GO TO (170,180),I
  170 FREQ=D(2)-D(1)
      GO TO 210
  180 FREQ=D(3)-D(2)
  210 FREQ1(MM)=FREQ
      MM=MM+1
      IF(MM-46)96,96,399
  399 SUM=0.0D+00
      DO 400 MM=1,46
  400 SUM=SUM+(FREQ1(MM)-FREQC(MM))**2
      GO TO (401,408,410),K1
  401 SUM2=SUM
      IF(LL-1)402,402,403
  402 SUM1=SUM
  403 GO TO (404,404,404,405,405,405,456,457,405,405,405,
     C        406,406,406,406,406,406,406,406),LL
  404 PP=1.0D-06
```

```
      GO TO 407
  405 PP=0.02D+00*(3.14159D+00/180.0D+00)
      GO TO 407
  406 PP=0.01D+00
      GO TO 407
  457 PP=0.001D+00
      GO TO 407
  406 PP=0.02D+00*(3.14159D+00/180.0D+00)
  407 P(LL)=P(LL)+PP
      K1=K1+1
      GO TO 95
  408 IF(SUM-SUM2)93,409,409
  409 P(LL)=P(LL)-2.0D+00*PP
      K1=K1+1
      GO TO 95
  410 IF(SUM-SUM1)93,411,411
  411 P(LL)=P(LL)+PP
   95 CONTINUE
      IF(SUM-SUM2)412,413,413
  412 SUM2=SUM
  413 CONTINUE
      WRITE(6,420)SUM2
  420 FORMAT(' SUM2 EQUALS',F12.3)
      WRITE(6,430) (P(I),I=1,20)
  430 FORMAT('0',6F12.6)
      IF(SUM1-SUM2)450,450,92
  450 CONTINUE
      DO 451 L=1,3
      P(L+3)=P(L+3)*(180.0D+00/3.14159D+00)
  451 P(L+8)=P(L+8)*(180.0D+00/3.14159D+00)
      DO  452  M=1,8
  452 P(M+11)=P(M+11)*(180.0D+00/3.14159D+00)
      WRITE(6,452)
  452 FORMAT(1H0,32H THE FINAL SET OF PARAMETERS IS )
      WRITE(6,430) (P(I),I=1,19)
      DX=P(7)/3.0D+00-P(8)
      DY=P(7)/3.0D+00+P(8)
      DZ=-2.0D+00*P(7)/3.0D+00
      WRITE(6,500)DX,DY,DZ
  500 FORMAT(1H ,'DX= ',F15.6,'DY= ',F15.6,'DZ= ',F15.6)
      STOP
      END
//LKED.SSP DD DSNAME=CSU.ACT12105.ESPLIB,DISP=SHR
//
```

APPENDIX C

INITIAL DATA FOR ^{29}Si HYPERFINE INTERACTION OF THE E'_1 CENTER

Nucleus 1

	Low Field		High Field	
Angle	Magnetic Field in Gauss	Microwave Frequency in GHz	Magnetic Field in Gauss	Microwave Frequency in GHz
-70°	3163.58*	9.3657049	3380.60*	9.3657625
	3190.57	9.3657064	3387.28	9.3657957
	3227.43*	9.3657087	3428.83*	9.3658104
	3243.60	9.3657107	3462.17*	9.3658222
	3286.78	9.3657127	3498.1	9.3658355
	3308.08	9.3657149	3507.37	9.3658410
-48°	3139.84*	9.3448948	3352.59*	9.3449090
	3185.12	9.3448952	3377.26	9.3449114
	3202.96	9.3448960	3401.59	9.3449126
	3256.59	9.3448976	3471.57	9.3449143
	3282.56	9.3448987	3488.98	9.3449157
	3314.86*	9.3449003	3516.94*	9.3449164
-30°	3150.54	9.3255709	3363.88	9.3255487
	3175.83	9.3255934	3368.68	9.3255472
	3214.34	9.3255884	3412.48	9.3255418
	3231.21	9.3255844	3446.70	9.3255368
	3282.50	9.3255818	3489.21	9.3255340
	3291.67	9.3255771	3492.1	9.3255325
-15°	3180.32	9.3161709	3380.85	9.3161746
	3192.17	9.3161707	3395.85	9.3161746
	3219.2	9.3161712	3417.56	9.3161743
	3221.36	9.3161715	3433.22	9.3161740
	3257.39	9.3161712	3455.56	9.3161740
	3258.55	9.3161726	3461.93	9.3161742
-10°	3193.0	9.3161886	3391.59	9.3161842
	3201.76	9.3161890	3407.30	9.3161827
	3218.23	9.3161896	3418.48	9.3161819
	3223.13	9.3161899	3431.50	9.3161821
	3246.05	9.3161905	3443.04	9.3161811
	3247.24	9.3161907	3452.58	9.3161800
-5°	3206.16*	9.3162544	3403.93	9.3162780
	3212.56	9.3162517	3418.43*	9.3162745
	3218.27*	9.3162497	3419.03*	9.3162735
	3224.07*	9.3162483	3430.16*	9.3162697
	3233.18	9.3162473	3430.6*	9.3162686
	3235.62*	9.3162467	3442.0	9.3162661
0°	3219.2	9.3163091	3417.4	9.3162963
	3224.1	9.3163066	3430.57	9.3162945

Nucleus 1 (Continued)

Angle	Low Field Magnetic Field in Gauss	Low Field Microwave Frequency in GHz	High Field Magnetic Field in Gauss	High Field Microwave Frequency in GHz
+5°	3202.23	9.3096972	3402.87	9.3096862
	3210.61	9.3096964	3413.22	9.3096838
	3218.81	9.3096957	3416.25	9.3096830
	3220.92	9.3096951	3429.11	9.3096810
	3229.65	9.3096942	3429.51	9.3096805
	3233.85	9.3096941	3439.37	9.3096799
+10°	3187.38	9.3096663	3391.50	9.3096596
	3200.22	9.3096657	3404.08	9.3096593
	3219.20	9.3096651	3410.47	9.3096588
	3221.57	9.3096646	3430.77	9.3096585
	3241.53	9.3096637	3444.20	9.3096579
	3245.88	9.3096634	3449.61	9.3096576
+15°	3172.59	9.3096562	3381.18	9.3096570
	3190.76	9.3096564	3391.94	9.3096571
	3216.65	9.3096570	3406.90	9.3096577
	3225.16	9.3096573	3433.25	9.3096580
	3252.41	9.3096576	3458.86	9.3096608
	3257.82	9.3096577	3459.03	9.3096611
+30°	3156.55	9.3715455	3382.62	9.3715419
	3193.84	9.3715442	3382.81	9.3715421
	3227.25	9.3715428	3415.24	9.3715423
	3261.49	9.3715421	3466.55	9.3715425
	3296.70	9.3715419	3499.34	9.3715432
	3310.23	9.3715418	3520.22	9.3715434
+43°	3122.61*	9.3377248	3359.16*	9.3377396
	3178.96	9.3377258	3366.99	9.3377401
	3201.66	9.3377271	3388.74	9.3377400
	3264.36	9.3377279	3467.50	9.3377398
	3288.23	9.3377281	3489.78	9.3377396
	3309.62*	9.3377290	3530.92*	9.3377400
+75°	3152.59*	9.3754087	3378.69*	9.3754035
	3188.33	9.3754090	3391.11	9.3754024
	3238.75	9.3754088	3429.23	9.3754018
	3249.40	9.3754087	3457.60	9.3754004
	3303.43	9.3754081	3506.73	9.3753982
	3304.44*	9.3754075	3527.21*	9.3753965

*These values were not used in the fitting procedure to determine the hyperfine matrix parameters.

Nucleus 2

Angle	Low Field: Magnetic Field in Gauss	Low Field: Microwave Frequency in GHz	High Field: Magnetic Field in Gauss	High Field: Microwave Frequency in GHz
-70°	3159.23	9.3657035	3379.91	9.3657729
	3198.05	9.3657077	3385.96	9.3657839
	3236.66*	9.3657096	3419.59*	9.3658035
	3253.14*	9.3657120	3452.78*	9.3658156
	3294.88	9.3657133	3490.23	9.3658156
	3302.21	9.3657143	3514.23	9.3658464
-48°	3136.82*	9.3448946	3358.73*	9.3449086
	3190.77	9.3448958	3371.82	9.3449107
	3212.32	9.3448965	3392.24	9.3449118
	3266.43	9.3448984	3461.86	9.3449136
	3288.76	9.3448991	3483.17	9.3449152
	3310.41*	9.3448997	3522.31	9.3449170
-30°	3149.94	9.3255721	3361.02	9.3255509
	3179.04	9.3255909	3370.04	9.3255453
	3222.83	9.3255863	3404.05	9.3255434
	3240.07	9.3255831	3438.03	9.3255401
	3286.23	9.3255806	3481.03	9.3255353
	3290.02	9.3255784	3494.47	9.3255311
-15°	3182.1	9.3161706	3378.73	9.3161748
	3194.67	9.3161709	3394.72	9.3161746
	3225.78	9.3161717	3411.59	9.3161746
	3227.52	9.3161712	3426.98	9.3161743
	3259.59	9.3161727	3455.03	9.3161739
	3260.44	9.3161722	3459.47	9.3161741
-10°	3195.51	9.3161888	3389.39	9.3161847
	3204.36	9.3161893	3405.41	9.3161837
	3223.91	9.3161901	3413.50	9.3161823
	3228.33	9.3161902	3426.22	9.3161814
	3249.08	9.3161916	3441.64	9.3161819
	3249.20	9.3161917	3450.02	9.3161807
-5°	3209.32*	9.3162530	3401.50	9.3162795
	3215.39	9.3162504	3414.52*	9.3162770
	3222.99*	9.3162490	3416.43*	9.3162757
	3228.28*	9.3162476	3426.34*	9.3162723
	3236.57	9.3162463	3427.99*	9.3162707
	3238.20*	9.3162459	3439.17	9.3162670
0°	3223.00	9.3163076	3414.60	9.3162972
	3227.30	9.3163059	3427.35	9.3162954

Nucleus 2 (Continued)

	Low Field		High Field	
Angle	Magnetic Field in Gauss	Microwave Frequency in GHz	Magnetic Field in Gauss	Microwave Frequency in GHz
+5°	3206.46	9.3096967	3399.49	9.3096869
	3214.32	9.3096959	3411.45	9.3096854
	3221.61	9.3096946	3412.51	9.3096844
	3223.12	9.3096945	3426.14	9.3096822
	3233.85	9.3096941	3426.91	9.3096814
	3237.52	9.3096441	3435.63	9.3096801
+10°	3192.18	9.3096660	3387.72	9.3096599
	3204.29	9.3096653	3399.74	9.3096594
	3220.44	9.3096647	3409.70	9.3096591
	3223.43	9.3096638	3409.70	9.3096591
	3246.14	9.3096629	3440.18	9.3096582
	3250.19	9.3096626	3445.48	9.3096576
+15°	3178.02	9.3096562	3377.18	9.3096565
	3195.06	9.3096567	3386.91	9.3096572
	3216.99	9.3096573	3406.90	9.3096575
	3226.16	9.3096575	3432.97	9.3096581
	3257.25	9.3096577	3454.24	9.3096581
	3262.85	9.3096575	3454.50	9.3096579
+30°	3164.06	9.3715450	3375.55	9.3715417
	3197.84	9.3715437	3378.93	9.3715417
	3225.62*	9.3715433	----- *	------
	3260.52*	9.3715426	3468.36*	9.3715426
	3301.26	9.3715418	3495.27	9.3715426
	3317.66	9.3715415	3512.87	9.3715431
+43°	3131.96*	9.3377253	3353.42*	9.3377391
	3181.55	9.3377262	3364.78	9.3377400
	3199.42	9.3377268	3391.64	9.3377400
	3262.70	9.3377274	3470.05	9.3377398
	3291.35	9.3377284	3487.23	9.3377394
	3314.58*	9.3377293	3521.26*	9.3377397
+75°	3164.40*	9.3754088	3378.18*	9.3754042
	3189.31*	9.3754088	3385.57*	9.3754029
	3235.92	9.3754088	3432.79	9.3754008
	3247.37	9.3754088	3460.52	9.3753999
	3302.96*	9.3754085	3505.92*	9.3753992
	3309.62*	9.3754069	3514.70*	9.3753972

*These values were not used in the fitting procedure to determine the hyperfine matrix parameters.

APPENDIX D

LISTING OF THE LINE POSITION PROGRAM FOR

S=1, I=½ SPIN SYSTEM

```
//U12105A  JOB (?????,443-70-3751),'JANI',CLASS=A,TIME=(0,40),
// MSGCLASS=X,NOTIFY=U12105A
/*PASSWORD ?
//  EXEC  FORTGCLG
//FORT.SYSIN DD *
      IMPLICIT  REAL * 8 (A-H,O-Z)
      REAL * 8 AR(6,6),AI(6,6),E(6),E2(6),TAU(2,6),C(6),HF(6),P(18),
     CG(3,3),H(3,3),RM(3,3),R2(3,3),R3(3,3),RT(3,3),TG(3,3),TH(3,3),
     CR(3,3),Z(3,3),TZ(3,3)
C
C
C     THE PARAMETERS FOR THE G TENSOR ARE 1-GX, 2-GY, 3-GZ, 4-THETA,
C     5-PHI, 6-PSI.  THE PARAMETERS FOR THE FINE-STRUCTURE TENSOR ARE
C     7-DX, 8-DY, 9-DZ, 10-THETA, 11-PHI, 12-PSI.  THE PARAMETERS FOR
C     THE HYPERFINE TENSOR ARE 13-AX, 14-AY, 15-AZ, 16-THETA, 17-PHI,
C     AND 18-PSI.
C
C
      P(1)=2.00041D+00
      P(2)=2.00062D+00
      P(3)=2.0013870D+00
      P(4)=37.77D+00
      P(5)=31.92D+00
      P(6)=92.18D+00
      P(7)=109.955D+00
      P(8)=117.601D+00
      P(9)=-227.557D+00
      P(10)=56.05D+00
      P(11)=33.48D+00
      P(12)=65.16D+00
      P(13)=-542.6D+00
      P(14)=-545.6D+00
      P(15)=-643.1D+00
      P(16)=63.00+00
      P(17)=56.5D+00
      P(18)=195.66D+00
C
C          OUTPUT GIVEN SET OF PARAMETERS.
C
      WRITE(6,10) (P(I),I=1,18)
   10 FORMAT (1H ,6F10.5)
      B=9.2741D+00/6.6262D+00
      GAN=-6.458D-04
      FREQQ=9.3163D+03
      N=6
      NM=6
      NN=1
      ALPHA= 0.0D+00
      BETA=-90.0D+00
C
C          CHANGE ANGLES IN DEGREES TO RADIANS.
C
      DO  91  L=1,3
      P(L+3)=P(L+3)*(3.141590D+00/1.8D+02)
      P(L+9)=P(L+9)*(3.141590D+00/1.8D+02)
   91 P(L+15)=P(L+15)*(3.141590D+00/1.8D+02)
C
C          SET UP ROTATION MATRICES G(3,3), H(3,3), RM(3,3).
C
      AG=DSIN(P(4))
      AAG=DCOS(P(4))
      CG=DSIN(P(5))
      CCG=DCOS(P(5))
      FG=DSIN(P(6))
```

```
      FFG=DCOS(P(6))
      AH=DSIN(P(10))
      AAH=DCOS(P(10))
      CH=DSIN(P(11))
      CCH=DCOS(P(11))
      FH=DSIN(P(12))
      FFH=DCOS(P(12))
      AZ=DSIN(P(16))
      AAZ=DCOS(P(16))
      CZ=DSIN(P(17))
      CCZ=DCOS(P(17))
      FZ=DSIN(P(18))
      FFZ=DCOS(P(18))
      CG=DCOS(2.094395D+00)
      SI=DSIN(2.094395D+00)
      G(1,1)=FFG*CCG-AAG*CG*FG
      G(1,2)=FFG*CG+AAG*CCG*FG
      G(1,3)=FG*AG
      G(2,1)=-FG*CCG-AAG*CG*FFG
      G(2,2)=-FG*CG+AAG*CCG*FFG
      G(2,3)=FFG*AG
      G(3,1)=AG*CG
      G(3,2)=-AG*CCG
      G(3,3)=AAG
      H(1,1)=FFH*CCH-AAH*CH*FH
      H(1,2)=FFH*CH+AAH*CCH*FH
      H(1,3)=FH*AH
      H(2,1)=-FH*CCH-AAH*CH*FFH
      H(2,2)=-FH*CH+AAH*CCH*FFH
      H(2,3)=FFH*AH
      H(3,1)=AH*CH
      H(3,2)=-AH*CCH
      H(3,3)=AAH
      Z(1,1)=FFZ*CCZ-AAZ*CZ*FZ
      Z(1,2)=FFZ*CZ+AAZ*CCZ*FZ
      Z(1,3)=FZ*AZ
      Z(2,1)=-FZ*CCZ-AAZ*CZ*FFZ
      Z(2,2)=-FZ*CZ+AAZ*CCZ*FFZ
      Z(2,3)=FFZ*AZ
      Z(3,1)=AZ*CZ
      Z(3,2)=-AZ*CCZ
      Z(3,3)=AAZ
   20 ALPHAR=ALPHA*(3.14159D+00/1.80+02)
      BETAR=BETA*(3.14159D+00/1.8D+02)
      WRITE(6,30) ALPHA, BETA
   30 FORMAT('0',2F15.3)
C
C       SET UP MAGNETIC FIELD ROTATION MATRIX RM(3,3).
C
      RM(1,1)=DCOS(ALPHAR)
      RM(1,2)=-DSIN(ALPHAR)*DSIN(BETAR)
      RM(1,3)=DSIN(ALPHAR)*DCOS(BETAR)
      RM(2,1)=0.0D+00
      RM(2,2)=DCOS(BETAR)
      RM(2,3)=DSIN(BETAR)
      RM(3,1)=-DSIN(ALPHAR)
      RM(3,2)=-DCOS(ALPHAR)*DSIN(BETAR)
      RM(3,3)=DCOS(ALPHAR)*DCOS(BETAR)
      K = 1
      GO TO (50,50,50,60,60,60),K
   50 R2(1,1)=1.0D+00
      R2(1,2)=0.0D+00
      R2(1,3)=0.0D+00
      R2(2,1)=0.0D+00
      R2(2,2)=1.0D+00
      R2(2,3)=0.0D+00
```

```
      R2(3,1)=0.0D+00
      R2(3,2)=0.0D+00
      R2(3,3)=1.0D+00
      GO TO (70,80,90),K
   60 R2(1,1)=1.0D+00
      R2(1,2)=0.0D+00
      R2(1,3)=0.0D+00
      R2(2,1)=0.0D+00
      R2(2,2)=-1.0D+00
      R2(2,3)=0.0D+00
      R2(3,1)=0.0D+00
      R2(3,2)=0.0D+00
      R2(3,3)=-1.0D+00
      KK = K-3
      GO TO (70,80,90),KK
   70 R3(1,1)=1.0D+00
      R3(1,2)=0.0D+00
      R3(1,3)=0.0D+00
      R3(2,1)=0.0D+00
      R3(2,2)=1.0D+00
      R3(2,3)=0.0D+00
      R3(3,1)=0.0D+00
      R3(3,2)=0.0D+00
      R3(3,3)=1.0D+00
      GO TO 100
   80 R3(1,1)=CO
      R3(1,2)=SI
      R3(1,3)=0.0D+00
      R3(2,1)=-SI
      R3(2,2)=CO
      R3(2,3)=0.0D+00
      R3(3,1)=0.0D+00
      R3(3,2)=0.0D+00
      R3(3,3)=1.0D+00
      GO TO 100
   90 R3(1,1)=CO
      R3(1,2)=-SI
      R3(1,3)=0.0D+00
      R3(2,1)=SI
      R3(2,2)=CO
      R3(2,3)=0.0D+00
      R3(3,1)=0.0D+00
      R3(3,2)=0.0D+00
      R3(3,3)=1.0D+00
  100 DO 110 L=1,3
      DO 110 M=1,3
  110 RT(L,M)=R2(L,1)*R3(1,M)+R2(L,2)*R3(2,M)+R2(L,3)*R3(3,M)
      DO 120 L=1,3
      DO 120 M=1,3
  120 R(L,M)=RT(L,1)*RM(1,M)+RT(L,2)*RM(2,M)+RT(L,3)*RM(3,M)
      DO 130 L=1,3
      DO 130 M=1,3
      TG(L,M)=G(L,1)*R(1,M)+G(L,2)*R(2,M)+G(L,3)*R(3,M)
      TH(L,M)=H(L,1)*R(1,M)+H(L,2)*R(2,M)+H(L,3)*R(3,M)
  130 TZ(L,M)=Z(L,1)*R(1,M)+Z(L,2)*R(2,M)+Z(L,3)*R(3,M)
      I=1
  140 HH=4.0D+03
  150 A1=8*HH*(P(1)*TG(1,1)*TG(1,3)+P(2)*TG(2,1)*TG(2,3)+P(3)*TG(3,1)*
     CTG(3,3))
      A2=8*HH*(P(1)*TG(1,2)*TG(1,3)+P(2)*TG(2,2)*TG(2,3)+P(3)*TG(3,2)*
     CTG(3,3))
      A3=8*HH*(P(1)*TG(1,3)*TG(1,3)+P(2)*TG(2,3)*TG(2,3)+P(3)*TG(3,3)*
     CTG(3,3))
      A4=P(7)*TH(1,1)*TH(1,1)+P(8)*TH(2,1)*TH(2,1)+P(9)*TH(3,1)*TH(3,1)
      A5=P(7)*TH(1,2)*TH(1,2)+P(8)*TH(2,2)*TH(2,2)+P(9)*TH(3,2)*TH(3,2)
      A6=P(7)*TH(1,3)*TH(1,3)+P(8)*TH(2,3)*TH(2,3)+P(9)*TH(3,3)*TH(3,3)
```

```
      W7=P(7)*TH(1,2)*TH(1,1)+P(8)*TH(2,2)*TH(2,1)+P(9)*TH(3,2)*TH(3,1)
      W8=P(7)*TH(1,1)*TH(1,3)+P(8)*TH(2,1)*TH(2,3)+P(9)*TH(3,1)*TH(3,3)
      W9=P(7)*TH(1,3)*TH(1,2)+P(8)*TH(2,3)*TH(2,2)+P(9)*TH(3,3)*
     CTH(3,2)
      W10=P(13)*TZ(1,1)*TZ(1,1)+P(14)*TZ(2,1)*TZ(2,1)+P(15)*TZ(3,1)
     C*TZ(3,1)
      W11=P(13)*TZ(1,1)*TZ(1,2)+P(14)*TZ(2,1)*TZ(2,2)+
     CP(15)*TZ(3,1)*TZ(3,2)
      W12=P(13)*TZ(1,1)*TZ(1,3)+P(14)*TZ(2,1)*TZ(2,3)+
     CP(15)*TZ(3,1)*TZ(3,3)
      W13=P(13)*TZ(1,2)*TZ(1,2)+P(14)*TZ(2,2)*TZ(2,2)+
     CP(15)*TZ(3,2)*TZ(3,2)
      W14=P(13)*TZ(1,2)*TZ(1,3)+P(14)*TZ(2,2)*TZ(2,3)+
     CP(15)*TZ(3,2)*TZ(3,3)
      W15=P(13)*TZ(1,3)*TZ(1,3)+P(14)*TZ(2,3)*TZ(2,3)+
     CP(15)*TZ(3,3)*TZ(3,3)
      Q1R=W1/2.0D+00
      Q1I= W2/2.0D+00
      Q2R=(W4-W5)/4.0D+00
      Q2I=W7/2.0D+00
      Q3R=(W4+W5)/4.0D+00
      Q4R=W8/2.0D+00
      Q4I=W9/2.0D+00
      Q5R=(W10-W13)/4.0D+00
      Q5I=W11/2.0D+00
      Q6R=(W10+W13)/4.0D+00
      Q7R=W12/2.0D+00
      Q7I=W14/2.0D+00
      DO 100 L=1,6
      DO 100 M=1,6
      AR(L,M)= 0.0D+00
  100 AI(L,M)= 0.0D+00
C
C        SET UP SPIN-HAMILTONIAN REAL AND IMAGINARY MATRIX
C        ELEMENTS AR(6,6), AI(6,6).
C
      AR(1,1)=W3+W6+W15/2.0D+00+2.0D+00*Q3R-(GBN*HH)/2.0D+00
      AR(2,2)=W3+W6-W15/2.0D+00+2.0D+00*Q3R+(GBN*HH)/2.0D+00
      AR(3,3)=4.0D+00*Q3R-(GBN*HH)/2.0D+00
      AR(4,4)=4.0D+00*Q3R+(GBN*HH)/2.0D+00
      AR(5,5)=W6-W3-W15/2.0D+00+2.0D+00*Q3R-(GBN*HH)/2.0D+00
      AR(6,6)=W6-W3+W15/2.0D+00+2.0D+00*Q3R+(GBN*HH)/2.0D+00
      AR(2,1)=Q7R
      AI(2,1)=Q7I
      AR(3,1)=(Q1R+Q4R)*DSQRT(2.0D+00)+Q7R/DSQRT(2.0D+00)
      AI(3,1)=(Q1I+Q4I)*DSQRT(2.0D+00)+Q7I/DSQRT(2.0D+00)
      AR(3,2)=Q6R*DSQRT(2.0D+00)
      AR(4,1)=Q5R*DSQRT(2.0D+00)
      AI(4,1)=Q5I*DSQRT(2.0D+00)
      AR(4,2)=(Q1R+Q4R)*DSQRT(2.0D+00)-Q7R/DSQRT(2.0D+00)
      AI(4,2)=(Q1I+Q4I)*DSQRT(2.0D+00)-Q7I/DSQRT(2.0D+00)
      AR(5,1)=2.0D+00*Q2R
      AI(5,1)=2.0D+00*Q2I
      AR(5,3)=(Q1R-Q4R)*DSQRT(2.0D+00)+Q7R/DSQRT(2.0D+00)
      AI(5,3)=(Q1I-Q4I)*DSQRT(2.0D+00)+Q7I/DSQRT(2.0D+00)
      AR(5,4)=DSQRT(2.0D+00)*Q6R
      AR(6,2)=2.0D+00*Q2R
      AI(6,2)=2.0D+00*Q2I
      AR(6,3)=DSQRT(2.0D+00)*Q5R
      AI(6,3)=DSQRT(2.0D+00)*Q5I
      AR(6,4)=(Q1R-Q4R)*DSQRT(2.0D+00)-Q7R/DSQRT(2.0D+00)
      AI(6,4)=(Q1I-Q4I)*DSQRT(2.0D+00)-Q7I/DSQRT(2.0D+00)
      AR(6,5)=-Q7R
      AI(6,5)=-Q7I
C
C            DIAGONALIZE SPIN-ENERGY MATRIX A(6,6).
```

```
C
      CALL  HTRIDI (NM,N,AP,AI,D,E,E2,TAU)
      CALL  IMTQL1  (N,C,E,IERR)
      GO TO (170,180,190,200),I
  170 FREQ=D(4)-D(1)
      GO TO 210
  180 FREQ=D(6)-D(4)
      GO TO 210
  190 FREQ=D(5)-D(3)
      GO TO 210
  200 FREQ=D(3)-D(2)
  210 IF(DABS(FREQO-FREQ)-1.0D-01)220,220,230
  220 HF(I)=HH
      GO TO 240
  230 HH=HH*(FREQO/FREQ)
      GO TO 150
  240 IF(I-4)250,260,260
  250 I=I+1
      GO TO 140
  260 DIFF1=CABS(HF(3)-HF(2))
      DIFF2=CABS(HF(4)-HF(1))
      WRITE(6,270) (HF(I),I=1,4),DIFF1,DIFF2
  270 FORMAT(6F20.4)
      IF(K-3)280,290,290
  280 K=K+1
      GO TO 40
  290 BETA=BETA+10.0D+00
      IF(BETA-91.0D+00)20,300,300
  300 WRITE(6,310) (P(I),I=1,18)
  310 FORMAT('0',6F10.5)
      STOP
      END
//GO.SSP DD DSNAME=OSU.ACT12105.ESRLIB,DISP=SHR
//
```

APPENDIX E

LISTING OF THE FITTING PROGRAM FOR AN S=1, I=½ SPIN SYSTEM

```
//U12105A  JOB (?????,448-70-3751),'JANI',CLASS=L,TIME=(10,00),
// MSGCLASS=X,NOTIFY=U12105A
/*PASSWORD ?
//  EXEC  FORTGCLG
//FORT.SYSIN DD *
      IMPLICIT  REAL * 8 (A-H,O-Z)
      REAL * 8 AR(6,6),AI(6,6),E(6),E2(6),TAU(2,6),D(6),HF(6),P(18),
     CG(3,3),H(3,3),RM(3,3),R2(3,3),R3(3,3),RT(3,3),TG(3,3),TH(3,3),
     CR(3,3),Z(3,3),TZ(3,3),FREQQ(34),DF(34,2),DFC(34,2)
C
C
C     THE PARAMETERS FOR THE G TENSOR ARE 1-GX, 2-GY, 3-GZ, 4-THETA,
C     5-PHI, 6-PSI.  THE PARAMETERS FOR THE FINE-STRUCTURE TENSOR ARE
C     7-DX, 8-DY, 9-DZ, 10-THETA, 11-PHI, 12-PSI.THE PARAMETERS
C     FOR HYPERFINE MATRIX ARE 13-AX, 14-AY, 15-AZ, 16-THETA,
C     17-PHI, 18-PSI.
C
C
      P(1)=2.00041D+00
      P(2)=2.00062D+00
      P(3)=2.0013870D+00
      P(4)=57.77D+00
      P(5)=31.92D+00
      P(6)=92.18D+00
      P(7)=109.955D+00
      P(8)=117.601D+00
      P(9)=-227.557D+00
      P(10)=56.05D+00
      P(11)=33.48D+00
      P(12)=85.16D+00
      P(13)=-545.6D+00
      P(14)=-545.6D+00
      P(15)=-638.1D+00
      P(16)=63.0D+00
      P(17)=55.5D+00
      P(18)=193.66D+00
      WRITE(6,10) (P(I),I=1,18)
   10 FORMAT (1H ,6F10.5)
      B=9.2741D+00/6.6262D+00
      GBN=-8.458D-04
      N=6
      NM=6
      ALPHA= 0.0D+00
      DO  91  L=1,3
      P(L+3)=P(L+3)*(3.14159D+00/1.8D+02)
      P(L+9)=P(L+9)*(3.14159D+00/1.8D+02)
   91 P(L+15)=P(L+15)*(3.14159D+00/1.8D+02)
   92 DO 93 LL=13,18
   94 K1=1
   95 MM=1
   96 GO TO (351,352,353,354,355,356,357,358,359,360,
     C        361,362,363,364,365,366,367,368,369,370,
     C        371,372,373,374,375,376,377,378,379,380,
     C        381),MM
C
C          INPUT EXPERIMENTAL DATA IN THE FORM OF DIFFERENCES
C          BETWEEN DIFFERENT FIELD VALUES RATHER THAN PARICULAR
C          MAGNETIC FIELD VALUES SINCE THE CORRECTIONS WERE
C          NOT OBTAINED FOR INDIVIDUAL LINE POSITIONS.
C
  351 BETA=14.95D+00
      DF(1,1)=190.42D+00
      DF(1,2)=206.45D+00
      K=1
```

```
      FREQQ(1)=9.3096578D+03
      GO TO 97
  352 DF(2,1)=201.21D+00
      DF(2,2)=219.35D+00
      K=2
      FREQQ(2)=FREQQ(1)
      GO TO 97
  353 DF(3,1)=190.25D+00
      DF(3,2)=208.09D+00
      K=3
      FREQQ(3)=FREQQ(1)
      GO TO 97
  354 BETA=9.93D+00
      DF(4,1)=191.28D+00
      DF(4,2)=208.08D+00
      K=1
      FREQQ(4)=9.3096617D+03
      GO TO 97
  355 DF(5,1)=198.32D+00
      DF(5,2)=216.7D+00
      K=2
      FREQQ(5)=FREQQ(4)
      GO TO 97
  356 DF(6,1)=191.27D+00
      DF(6,2)=209.2D+00
      K=3
      FREQQ(6)=FREQQ(4)
      GO TO 97
  357 BETA=4.98D+00
      DF(7,1)=192.26D+00
      DF(7,2)=209.72D+00
      K=1
      FREQQ(7)=9.3096889D+03
      GO TO 97
  358 DF(8,1)=195.56D+00
      DF(8,2)=214.02D+00
      K=2
      FREQQ(8)=FREQQ(7)
      GO TO 97
  359 DF(9,1)=192.3D+00
      DF(9,2)=210.3D+00
      K=3
      FREQQ(9)=FREQQ(7)
      GO TO 97
  360 BETA=0.0D+00
      DF(10,1)=193.3D+00
      DF(10,2)=211.37D+00
      K=2
      FREQQ(10)=9.3163016D+03
      GO TO 97
  361 BETA=-4.96D+00
      DF(11,1)=191.37D+00
      DF(11,2)=208.82D+00
      K=2
      FREQQ(11)=9.3162607D+03
      GO TO 97
  362 BETA=-9.95D+00
      DF(12,1)=195.8D+00
      DF(12,2)=214.3D+00
      K=1
      FREQQ(12)=9.3161859D+03
      GO TO 97
  363 DF(13,1)=189.83D+00
      DF(13,2)=206.53D+00
      K=2
      FREQQ(13)=FREQQ(12)
```

```
      GO TO 97
  364 DF(14,1)=195.35D+00
      DF(14,2)=213.27D+00
      K=3
      FREQQ(14)=FREQQ(12)
      GO TO 97
  365 BETA=-14.92D+00
      DF(15,1)=197.01D+00
      DF(15,2)=215.53D+00
      K=1
      FREQQ(15)=9.3161728D+03
      GO TO 97
  366 DF(16,1)=188.68D+00
      DF(16,2)=204.54D+00
      K=2
      FREQQ(16)=FREQQ(15)
      GO TO 97
  367 DF(17,1)=196.2D+00
      DF(17,2)=214.02D+00
      K=3
      FREQQ(17)=FREQQ(15)
      GO TO 97
  368 BETA=-30.45D+00
      DF(18,1)=188.05D+00
      DF(18,2)=201.71D+00
      K=2
      FREQQ(18)=9.3255614D+03
      GO TO 97
  369 DF(19,1)=198.14D+00
      DF(19,2)=215.49D+00
      K=3
      FREQQ(19)=FREQQ(18)
      GO TO 97
  370 DF(20,1)=200.43D+00
      DF(20,2)=218.14D+00
      K=1
      FREQQ(20)=FREQQ(18)
      GO TO 97
  371 BETA=-49.0D+00
      DF(21,1)=192.14D+00
      DF(21,2)=206.42D+00
      K=2
      FREQQ(21)=9.3449051D+03
      GO TO 97
  372 DF(22,1)=198.63D+00
      DF(22,2)=214.98D+00
      K=3
      FREQQ(22)=FREQQ(21)
      GO TO 97
  373 BETA=-70.27D+00
      DF(23,1)=199.22D+00
      DF(23,2)=217.02D+00
      K=1
      FREQQ(23)=9.3657553D+03
      GO TO 97
  374 DF(24,1)=196.71D+00
      DF(24,2)=211.32D+00
      FREQQ(24)=FREQQ(23)
      K=3
      GO TO 97
  375 BETA=29.71D+00
      DF(25,1)=188.78D+00
      DF(25,2)=202.64D+00
      K=1
      FREQQ(25)=9.3715411D+03
      GO TO 97
```

```
376 BETA=29.71D+00
    DF(26,1)=187.99D+00
    DF(26,2)=205.06D+00
    K=3
    FREQQ(26)=9.371541D+03
    GO TO 97
377 BETA=43.09D+00
    DF(27,1)=188.03D+00
    DF(27,2)=201.55D+00
    K=1
    FREQQ(27)=9.3377335D+03
    GO TO 97
378 DF(28,1)=187.08D+00
    DF(28,2)=203.14D+00
    K=3
    FREQQ(28)=FREQQ(27)
    GO TO 97
379 BETA=75.02D+00
    DF(29,1)=190.48D+00
    DF(29,2)=208.2D+00
    K=1
    FREQQ(29)=9.3754045D+03
    GO TO 97
380 DF(30,1)=190.36D+00
    DF(30,2)=203.3D+00
    K=3
    FREQQ(30)=FREQQ(29)
    GO TO 97
381 BETA=29.71D+00
    DF(31,1)=209.99D+00
    DF(31,2)=226.26D+00
    K=2
    FREQQ(31)=9.371541D+03
 97 AG=DSIN(P(4))
    AAG=DCOS(P(4))
    CG=DSIN(P(5))
    CCG=DCOS(P(5))
    FG=DSIN(P(6))
    FFG=DCOS(P(6))
    AH=DSIN(P(10))
    AAH=DCOS(P(10))
    CH=DSIN(P(11))
    CCH=DCOS(P(11))
    FH=DSIN(P(12))
    FFH=DCOS(P(12))
    AZ=DSIN(P(16))
    AAZ=DCOS(P(16))
    CZ=DSIN(P(17))
    CCZ=DCOS(P(17))
    FZ=DSIN(P(18))
    FFZ=DCOS(P(18))
    CO=DCOS(2.094395D+00)
    SI=DSIN(2.094395D+00)
    G(1,1)=FFG*CCG-AAG*CG*FG
    G(1,2)=FFG*CG+AAG*CCG*FG
    G(1,3)=FG*AG
    G(2,1)=-FG*CCG-AAG*CG*FFG
    G(2,2)=-FG*CG+AAG*CCG*FFG
    G(2,3)=FFG*AG
    G(3,1)=AG*CG
    G(3,2)=-AG*CCG
    G(3,3)=AAG
    H(1,1)=FFH*CCH-AAH*CH*FH
    H(1,2)=FFH*CH+AAH*CCH*FH
    H(1,3)=FH*AH
    H(2,1)=-FH*CCH-AAH*CH*FFH
```

```
      H(2,2)=-FH*CH+AAH*CCH*FFH
      H(2,3)=FFH*AH
      H(3,1)=AH*CH
      H(3,2)=-AH*CCH
      H(3,3)=AAH
      Z(1,1)=FFZ*CCZ-AAZ*CZ*FZ
      Z(1,2)=FFZ*CZ+AAZ*CCZ*FZ
      Z(1,3)=FZ*AZ
      Z(2,1)=-FZ*CCZ-AAZ*CZ*FFZ
      Z(2,2)=-FZ*CZ+AAZ*CCZ*FFZ
      Z(2,3)=FFZ*AZ
      Z(3,1)=AZ*CZ
      Z(3,2)=-AZ*CCZ
      Z(3,3)=AAZ
   20 ALPHAR=ALPHA*(3.14159D+00/1.8D+02)
      BETAR=BETA*(3.14159D+00/1.8D+02)
      RM(1,1)=DCOS(ALPHAR)
      RM(1,2)=-DSIN(ALPHAR)*DSIN(BETAR)
      RM(1,3)=DSIN(ALPHAR)*DCOS(BETAR)
      RM(2,1)=0.0D+00
      RM(2,2)=DCOS(BETAR)
      RM(2,3)=DSIN(BETAR)
      RM(3,1)=-DSIN(ALPHAR)
      RM(3,2)=-DCOS(ALPHAR)*DSIN(BETAR)
      RM(3,3)=DCOS(ALPHAR)*DCOS(BETAR)
   40 GO TO (50,50,50,60,60,60),K
   50 R2(1,1)=1.0D+00
      R2(1,2)=0.0D+00
      R2(1,3)=0.0D+00
      R2(2,1)=0.0D+00
      R2(2,2)=1.0D+00
      R2(2,3)=0.0D+00
      R2(3,1)=0.0D+00
      R2(3,2)=0.0D+00
      R2(3,3)=1.0D+00
      GO TO (70,80,90),K
   60 R2(1,1)=1.0D+00
      R2(1,2)=0.0D+00
      R2(1,3)=0.0D+00
      R2(2,1)=0.0D+00
      R2(2,2)=-1.0D+00
      R2(2,3)=0.0D+00
      R2(3,1)=0.0D+00
      R2(3,2)=0.0D+00
      R2(3,3)=-1.0D+00
      KK = K-3
      GO TO (70,80,90),KK
   70 R3(1,1)=1.0D+00
      R3(1,2)=0.0D+00
      R3(1,3)=0.0D+00
      R3(2,1)=0.0D+00
      R3(2,2)=1.0D+00
      R3(2,3)=0.0D+00
      R3(3,1)=0.0D+00
      R3(3,2)=0.0D+00
      R3(3,3)=1.0D+00
      GO TO 100
   80 R3(1,1)=CO
      R3(1,2)=SI
      R3(1,3)=0.0D+00
      R3(2,1)=-SI
      R3(2,2)=CO
      R3(2,3)=0.0D+00
      R3(3,1)=0.0D+00
      R3(3,2)=0.0D+00
      R3(3,3)=1.0D+00
```

```
      GO TO 100
   90 R3(1,1)=CO
      R3(1,2)=-SI
      R3(1,3)=0.0D+00
      R3(2,1)=SI
      R3(2,2)=CO
      R3(2,3)=0.0D+00
      R3(3,1)=0.0D+00
      R3(3,2)=0.0D+00
      R3(3,3)=1.0D+00
  100 DO 110 L=1,3
      DO 110 M=1,3
  110 RT(L,M)=R2(L,1)*R3(1,M)+R2(L,2)*R3(2,M)+R2(L,3)*R3(3,M)
      DO 120 L=1,3
      DO 120 M=1,3
  120 R(L,M)=RT(L,1)*RM(1,M)+RT(L,2)*RM(2,M)+RT(L,3)*RM(3,M)
      DO 130 L=1,3
      DO 130 M=1,3
      TG(L,M)=G(L,1)*R(1,M)+G(L,2)*R(2,M)+G(L,3)*R(3,M)
      TH(L,M)=H(L,1)*R(1,M)+H(L,2)*R(2,M)+H(L,3)*R(3,M)
  130 TZ(L,M)=Z(L,1)*R(1,M)+Z(L,2)*R(2,M)+Z(L,3)*R(3,M)
      I=1
  140 HH=3.50D+03
  150 W1=8*HH*(P(1)*TG(1,1)*TG(1,3)+P(2)*TG(2,1)*TG(2,3)+P(3)*TG(3,1)*
     CTG(3,3))
      W2=8*HH*(P(1)*TG(1,2)*TG(1,3)+P(2)*TG(2,2)*TG(2,3)+P(3)*TG(3,2)*
     CTG(3,3))
      W3=8*HH*(P(1)*TG(1,3)*TG(1,3)+P(2)*TG(2,3)*TG(2,3)+P(3)*TG(3,3)*
     CTG(3,3))
      W4=P(7)*TH(1,1)*TH(1,1)+P(8)*TH(2,1)*TH(2,1)+P(9)*TH(3,1)*TH(3,1)
      W5=P(7)*TH(1,2)*TH(1,2)+P(8)*TH(2,2)*TH(2,2)+P(9)*TH(3,2)*TH(3,2)
      W6=P(7)*TH(1,3)*TH(1,3)+P(8)*TH(2,3)*TH(2,3)+P(9)*TH(3,3)*TH(3,3)
      W7=P(7)*TH(1,2)*TH(1,1)+P(8)*TH(2,2)*TH(2,1)+P(9)*TH(3,2)*TH(3,1)
      W8=P(7)*TH(1,1)*TH(1,3)+P(8)*TH(2,1)*TH(2,3)+P(9)*TH(3,1)*TH(3,3)
      W9  =P(7)*TH(1,3)*TH(1,2)+P(8)*TH(2,3)*TH(2,2)+P(9)*TH(3,3)*
     CTH(3,2)
      W10=P(13)*TZ(1,1)*TZ(1,1)+P(14)*TZ(2,1)*TZ(2,1)+P(15)*TZ(3,1)
     C*TZ(3,1)
      W11=P(13)*TZ(1,1)*TZ(1,2)+P(14)*TZ(2,1)*TZ(2,2)+
     CP(15)*TZ(3,1)*TZ(3,2)
      W12=P(13)*TZ(1,1)*TZ(1,3)+P(14)*TZ(2,1)*TZ(2,3)+
     CP(15)*TZ(3,1)*TZ(3,3)
      W13=P(13)*TZ(1,2)*TZ(1,2)+P(14)*TZ(2,2)*TZ(2,2)+
     CP(15)*TZ(3,2)*TZ(3,2)
      W14=P(13)*TZ(1,2)*TZ(1,3)+P(14)*TZ(2,2)*TZ(2,3)+
     CP(15)*TZ(3,2)*TZ(3,3)
      W15=P(13)*TZ(1,3)*TZ(1,3)+P(14)*TZ(2,3)*TZ(2,3)+
     CP(15)*TZ(3,3)*TZ(3,3)
      Q1R=W1/2.0D+00
      Q1I= W2/2.0D+00
      Q2R=(W4-W5)/4.0D+00
      Q2I=W7/2.0D+00
      Q3R=(W4+W5)/4.0D+00
      Q4R=W8/2.0D+00
      Q4I=W9/2.0D+00
      Q5R=(W10-W13)/4.0D+00
      Q5I=W11/2.0D+00
      Q6R=(W10+W13)/4.0D+00
      Q7R=W12/2.0D+00
      Q7I=W14/2.0D+00
      DO 160 L=1,6
      DO 160 M=1,6
      AR(L,M)= 0.0D+00
  160 AI(L,M)= 0.0D+00
```

```
      AR(1,1)=W3+W6+W15/2.0D+00+2.0D+00*Q3R-(GBN*HH)/2.0D+00
      AR(2,2)=W3+W6-W15/2.0D+00+2.0D+00*Q3R+(GBN*HH)/2.0D+00
      AR(3,3)=4.0D+00*Q3R-(GBN*HH)/2.0D+00
      AR(4,4)=4.0D+00*Q3R+(GBN*HH)/2.0D+00
      AR(5,5)=W6-W3-W15/2.0D+00+2.0D+00*Q3R-(GBN*HH)/2.0D+00
      AR(6,6)=W6-W3+W15/2.0D+00+2.0D+00*Q3R+(GBN*HH)/2.0D+00
      AR(2,1)=Q7R
      AI(2,1)=Q7I
      AR(3,1)=(Q1R+Q4R)*DSQRT(2.0D+00)+Q7R/DSQRT(2.0D+00)
      AI(3,1)=(Q1I+Q4I)*DSQRT(2.0D+00)+Q7I/DSQRT(2.0D+00)
      AR(3,2)=Q6R*DSQRT(2.0D+00)
      AR(4,1)=Q5R*DSQRT(2.0D+00)
      AI(4,1)=Q5I*DSQRT(2.0D+00)
      AR(4,2)=(Q1R+Q4R)*DSQRT(2.0D+00)-Q7R/DSQRT(2.0D+00)
      AI(4,2)=(Q1I+Q4I)*DSQRT(2.0D+00)-Q7I/DSQRT(2.0D+00)
      AR(5,1)=2.0D+00*Q2R
      AI(5,1)=2.0D+00*Q2I
      AR(5,3)=(Q1R-Q4R)*DSQRT(2.0D+00)+Q7R/DSQRT(2.0D+00)
      AI(5,3)=(Q1I-Q4I)*DSQRT(2.0D+00)+Q7I/DSQRT(2.0D+00)
      AR(5,4)=DSQRT(2.0D+00)*Q6R
      AR(6,2)=2.0D+00*Q2R
      AI(6,2)=2.0D+00*Q2I
      AR(6,3)=DSQRT(2.0D+00)*Q5R
      AI(6,3)=DSQRT(2.0D+00)*Q5I
      AR(6,4)=(Q1R-Q4R)*DSQRT(2.0D+00)-Q7R/DSQRT(2.0D+00)
      AI(6,4)=(Q1I-Q4I)*DSQRT(2.0D+00)-Q7I/DSQRT(2.0D+00)
      AR(6,5)=-Q7R
      AI(6,5)=-Q7I
C
C       DIAGONALIZE SPIN-ENERGY MATRIX A(6,6).
C
      CALL  HTRIDI (NM,N,AR,AI,D,E,E2,TAU)
      CALL  IMTQL1  (N,D,E,IERR)
      GO TO (170,180,190,200),I
  170 FREQ=D(4)-D(1)
      GO TO 210
  180 FREQ=D(6)-D(4)
      GO TO 210
  190 FREQ=D(5)-D(3)
      GO TO 210
  200 FREQ=D(3)-D(2)
  210 IF(DABS(FREQQ(MM)-FREQ)-1.0D-01)220,220,230
  220 HF(I) =HH
      GO TO 240
  230 HH= HH* (FREQQ(MM)/FREQ)
      GO TO 150
  240 IF(I-4) 250,250,260
  250 I=I+1
      GO TO 140
  260 CONTINUE
      DFC(MM,1)=(HF(3)-HF(2))
      DFC(MM,2)=(HF(4)-HF(1))
      MM=MM+1
      IF(MM-31)96,96,399
  399 SUM=0.0D+00
      DO 400 MM=1,31
  400 SUM=SUM+(DFC(MM,1)-DF(MM,1))**2+(DFC(MM,2)-DF(MM,2))**2
      GO TO (401,408,410),K1
  401 SUM2=SUM
      IF(LL-13)402,402,403
  402 SUM1=SUM
  403 LLL=LL-12
      GO TO (404,404,404,405,405,405),LLL
  404 PP=1.0D+00
```

```
      GO TO 407
  405 PP=1.0D+00*(3.14159D+00/180.0D+00)
  407 P(LL)=P(LL)+PP
      K1=K1+1
      GO TO 95
  408 IF(SUM-SUM2)93,409,409
  409 P(LL)=P(LL)-2.0D+00*PP
      K1=K1+1
      GO TO 95
  410 IF(SUM-SUM2)93,411,411
  411 P(LL)=P(LL)+PP
   93 CONTINUE
      IF(SUM-SUM2)412,412,413
  412 SUM2=SUM
  413 CONTINUE
      WRITE(6,420)SUM2
  420 FORMAT('  SUM2 EQUALS ',F12.3)
      WRITE(6,430)  (P(I),I=1,18)
  430 FORMAT('0',6F12.6)
      IF(SUM1-SUM2)450,450,92
  450 CONTINUE
      DO 451 L=1,3
      P(L+3)=P(L+3)*(180.0D+00/3.14159D+00)
      P(L+9)=P(L+9)*(180.0D+00/3.14159D+00)
  451 P(L+15)=P(L+15)*(180.0D+00/3.14159D+00)
      WRITE(6,452)
  452 FORMAT(1H0,' THE FINAL SET OF PARAMETERS IS ')
      WRITE(6,430) (P(I),I=1,18)
      STOP
      END
//LKED.SSP DD DSNAME=OSU.ACT12105.ESRLIB,DISP=SHR
//
```

VITA

Mahendrakumar G. Jani

Candidate for the Degree of

Doctor of Philosophy

Thesis: RADIATION EFFECTS IN CRYSTALLINE SiO_2: STRUCTURE OF THE E" CENTERS

Major Field: Physics

Personal Data: Born at Kanpur, Uttar Pradesh, India, August 28, 1954, the son of Gunvantrai and Manglagauri Jani.

Education: Graduated from Sainik School, Balachadi, India, in 1970, received Bachelor of Science degree in 1976 from Gujarat University, received Master of Science degree from Oklahoma State University, Stillwater, Oklahoma in May, 1979; completed requirements for the degree of Doctor of Philosophy at Oklahoma State University, Stillwater, Oklahoma, in May, 1982.

Experience: Graduate Teaching and Research Assistant, Oklahoma State University, Stillwater, Oklahoma, 1976-1981.